STRUCTURAL SYSTEMATICS OF HALOGENATED BENZAMIDES

Niall Hehir B.Sc.

Thesis Submitted for Award of

Doctor of Philosophy

School of Chemical Sciences

Dublin City University

Research Supervisor:

Dr. John Gallagher

January 2017

Declaration

I hereby certify that this material, which I now submit for assessment on the programme of study leading to the award of Doctor of Philosophy is entirely my own work, and that I have exercised reasonable care to ensure that the work is original, and does not to the best of my knowledge breach any law of copyright, and has not been taken from the work of others save and to the extent that such work has been cited and acknowledged within the text of my work.

Signed: _____

ID No.: _____

Date: _____

For Mam

ACKNOWLEDGEMENTS

I would like to take this opportunity to thank everyone in my life that helped to motivate and assist me during my years in DCU.

Firstly, I'd like to thank my supervisor, Dr John F. Gallagher, whose patience and guidance went above and beyond what was required. He helped grow my love of all things Science, and for that I am extremely grateful.

I'd also like to thank all the staff and students I had the pleasure of working beside. Their insight and different points of view were invaluable to me during the tough times, especially during chromatography. A special thank you must go to Pavle Mocilac, whose direction and work ethic during the first year of my PhD. gave me a goal to reach towards, as well as all my 4^{th} year students, who allowed me to progress as both a teacher and a scientist with their help and questions.

Thank you to the Meath VEC, without their assistance I never could have followed my dream and continued to study this field that I find so captivating.

Without my friends Eoin, Andy, Bryan and Killian and my little brother Paul, this thesis and my life would be in a much worse state. Thank you for all the laughs, pints and help over the years.

Last but not least, I'd like to thank my parents, Anna and Sean, without whom I wouldn't be here. Mam, without your love and constant support, I have no idea where I'd be. Thank you for your constant optimism and belief in me.

I would like to thank Meath V.E.C. for funding this PhD.

Table of Contents:

List of Figures

Abbreviations (in alphabetical order)

% w/v	Percentage weight per volume
^{13}C-NMR	Carbon 13 nuclear magnetic resonance
^{19}F	Fluorine 19
^{1}H-NMR	Proton nuclear magnetic resonance
2-AP	2-aminopyridine
4-AP	4-aminopyridine
ADP	Adenosine diphosphate
ATP	Adenosine triphosphate
BBB	Blood brain barrier
BHAT	β-Blocker Heart Attack
BK	Channels of big conductance
CAN	Chemically modified nucleic acids
CAST	Cardiac Arrhythmia Suppression Trial
$CDCl_3$	Deuterated chloroform
CIS	Clinically Isolated Syndrome' or CIS.
CMC	Comprehensive Medicinal Chemistry
CNS	Central nervous system
CPP	Cell penetrating peptides
CSD	Cambridge Structural Database
DCC	Dicyclohexylcarbodiimide
DCM	Dichloromethane

DMAP	4-(Dimethylamino) pyridine
DMSO	Dimethyl sulfoxide
EAE	Experimental autoimmune encephalomyelitis
EDC	1-Ethyl-3-(3-dimethylaminopropyl) carbodiimide
FDA	Food and Drug Administration
GA	Glatiramer acetate
HCl	Hydrochloric acid
HERG	Ether-à-go-go related gene
HOBt	1-hydroxy-1H-benzotriazole
IC_{50}	Half maximal inhibitory concentration
IK	Channels of intermediate conductance
IR	Infrared
K_{Ca}	Calcium activated potassium channels
K_{ir}	Inwardly rectifying potassium channels
Kir6.2	Inwardly rectifying potassium channel 6.2
K_v	Voltage-gated potassium channels
LiCl	Lithium chloride
M.p	Melting point
MOG	Myelin oligodendrocyte glycoprotein
mRNA	Messenger Ribonucleic acid
MS	Multiple Sclerosis
NMR	Nuclear magnetic resonance
NOE	Nuclear Overhauser effect
pK_a	acid dissociation constant

PML	Progressive multifocal leukoencephalopathy
PPMS	Primary Progressive MS
Pyr	Pyridine
Pyrm	Pyrimidine
Pyrz	Pyrazine
RBF	Round bottomed flask
RNA	Ribonucleic acid
RRMS	relapsing – remitting MS
SAR	Structure-Activity Relationship
SK	Small conductance
SPMS	Secondary Progressive MS
SUR1	Sulfonylurea receptor 1
TEA	Triethylamine
TLC	Thin layer chromatography
δ^+	Partial positive charge
σ	sigma

ABSTRACT

Niall Hehir PhD. Thesis

Structural Systematics of Halogenated Benzamides

This PhD. Thesis, entitled "Structural Systematics of Halogenated Benzamides", describes the synthesis, characterisation and analysis of a series of 3×3 isomer grids. A range of *bromo*- and *iodo*- substituted compounds based on both the benzamide and carboxamide backbones were synthesised and fully characterised by ^{1}H NMR, ATR-IR and X-ray crystallography. The goal of this work was to explore the effect of different functional groups and their position on small drug-like molecules and analyse the trends noted in the compounds, including the formation of an imide moiety, following placement of the pyridine nitrogen and bromine moiety in close proximity in the *ortho*- position.

Further work was carried out on the benzamide backbone, with two isomer grids synthesised in which the positions of both a difluoro- and methyl moiety were varied and trends in ^{1}H NMR, ^{19}F NMR and solid state structure were analysed and rationalised. This data allowed us to observe how the addition and position of various functional groups drive or inhibit the formation of mixed amide/imide (foldamer) structures.

A number of modifications to the benzamide backbone were carried out, with a carbamate based alternative being the primary backbone investigated. The reactions, combined with the previous data gathered from the isomer grid analysis, allowed us to rationalise an approach using the most suitable compounds from our earlier work to synthesise larger conformationally constrained foldamers.

Using this information, compounds with a mixed imide/amide backbone were synthesised and a number of interesting variations on the basic 2:1 fluoro aminopyridine: pyridinedicarbonyl structural motif found in the earlier isomer grids, were found. Compounds containing 3:2 and 4:3 ratios were synthesised and characterised fully.

CHAPTER 1

Theoretical Framework and Survey of Literature

1.1 Introduction

Nature relies on large molecules capable of taking very constrained and compact conformations to carry out their roles in myriad different roles in the body (*e.g.* proteins and RNA). These molecules carry out vital processes such as enzymatic catalysis,[1] as well as acting as immune protection in the form of antibodies.[2]

The backbones of these molecules are composed of amino acids. The basic template for an amino acid consists of an amide functional group and a carboxylic acid group along with a variable side chain depending on the specific amino acid in question.

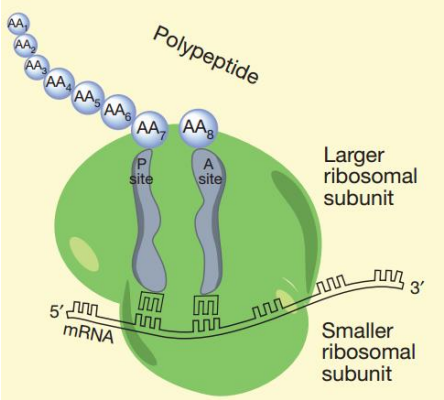

Fig 1.1: Protein Formation:[3]

With the abundance of the amide bond in biological systems, it stands to reason that a large proportion of the medicinal compounds synthesised to treat disorders in the body have amide bonds or functional groups analogous to amide bonds in their structure. According to Ghose *et al*.,[4]

"Over 25 per cent of the molecules in the Comprehensive Medicinal Chemistry (CMC) database contained a carboxamide functional group."

In the body, protein synthesis is a complex, multi-step process, involving the transcription of detail genetic information onto mRNA in the nucleus of a cell, followed by translation of said information into proteins in the ribosomes (as seen in *Fig 1.1*).[5] Amide bond formation in the laboratory has issues with adverse thermodynamic conditions, as the products when reacting amines with carboxylic acids will lean towards hydrolysis rather than the preferred formation of the amide linkage (see scheme on pg 4).[6]

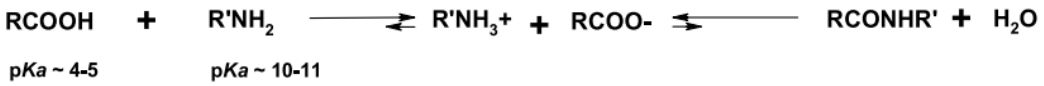

A number of different methods are currently used in the formation of amide bonds, the most common of which is the use of carbodiimides. Dicyclohexylcarbodiimide (DCC) was first discovered by Sheehan *et al*., and proceeds by the mechanism seen below in *Fig 1.2*.[7]

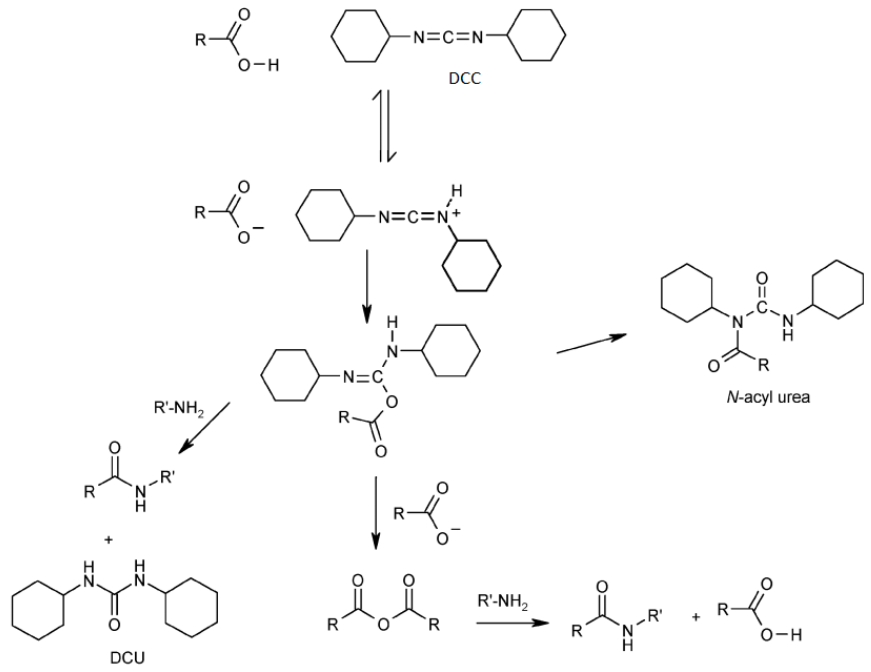

Fig 1.2: *Mechanism of action of DCC:*[8]*adapted*

In order to increase the efficacy of these carbodiimides, König *et al*. added 1-hydroxy-1H-benzotriazole (HOBt) and observed an increase in yields of the amide. Another method used in the formation of amide bonds are the use of acyl chlorides. In the presence of base (usually triethylamine or Hünigs base), the amine is reacted with an acyl chloride in dry solvent, to give the relevant amide bridge and loss of hydrochloric acid (HCl). Triethylamine is added to prevent the amine from converting to its inert salt form in the presence of the acid.

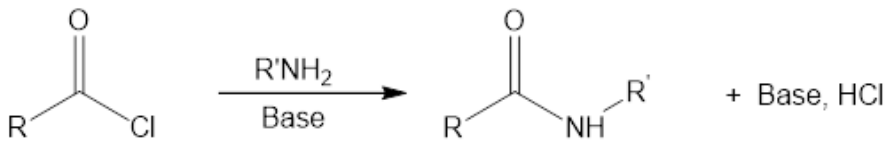

Fig 1.3: Formation of amide bonds using acyl chlorides:

The problem of hydrolysis can be avoided by the use of acyl fluorides, which tend to be more reactive than their chlorine analogues while being less water sensitive.[10] In the past few years, a number of groups have published work on the synthesis of amide bonds without the use of carbodiimides. Al-Zoubi discovered that by using *ortho*-halophenyl boronic acids, the reaction could proceed without the need for high temperature, provided no water was present.[11]

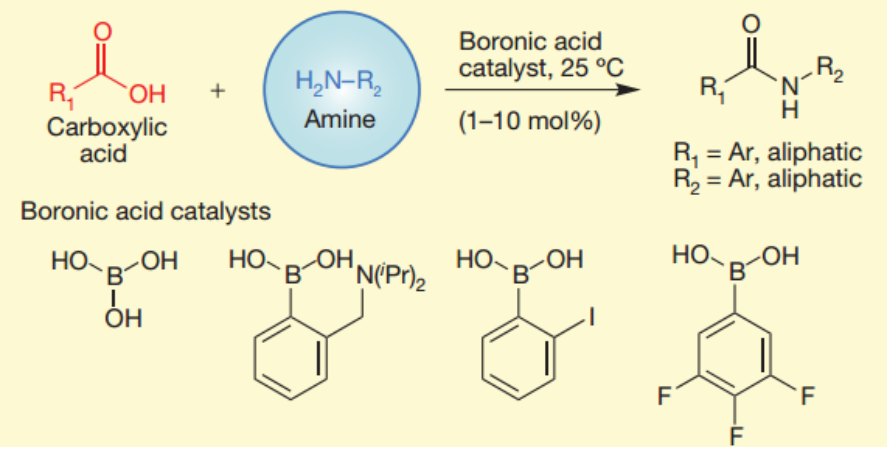

Fig 1.4: Boronic acid catalysts:[3]

Compounds containing amide linkages have been used in medicinal chemistry to treat a large number of disorders, a few of which will be discussed over the next few pages. Their efficacy relies on the fact that the body uses proteins to facilitate transport of nutrients across the cell membrane. In particular, the potassium channels on said membrane have been the target of a large number of drugs designed to emulate the correct conformation to allow for entry to the cell. The phospholipid bilayer acts as a selectively impermeable barrier to most water-soluble molecules. The protein molecules embedded in the bilayer fulfil numerous other roles for the cell, one of which is transport. Gases like O_2, and small uncharged molecules, can pass through the bilayer without the involvement of transport proteins. No energy is used as the molecules are moving from an area of high concentration to an area of low concentration.[12]

Other molecules pass through the membrane by either passive or active transport. Passive transport is the facilitated diffusion of molecules across the membrane, with the concentration gradient. If the molecule to be transported has no charge then the concentration gradient determines the speed of the transport, however if the molecule

is charged it will travel in the direction its electrochemical gradient allows it to be transported. This is merely the concentration gradient and the electrical gradient combined to give an electrochemical gradient. To move molecules against their electrochemical gradient is called active transport, and energy must be expended in doing so.[13]

Channel proteins form pores across the membrane and when said pores are open, allow the molecules to be transported and to pass through and enter the cell. The structure of channel proteins, specifically potassium channels, will be discussed in detail later in this review. Carrier proteins work by binding the molecule to be transported. The protein then *"undergoes a series of conformational changes to transfer the bound solute across the membrane"*[13] p 617.

1.1.1 Introduction to ion channels**:**

As stated previously, the cell membrane forms an impermeable barrier to most molecules. For the cell to survive, it needs to get supplied with the molecules and charged ions used in its intracellular processes. Some of these molecules are small enough to passively diffuse through the membrane, but most enter the cell through channel proteins.

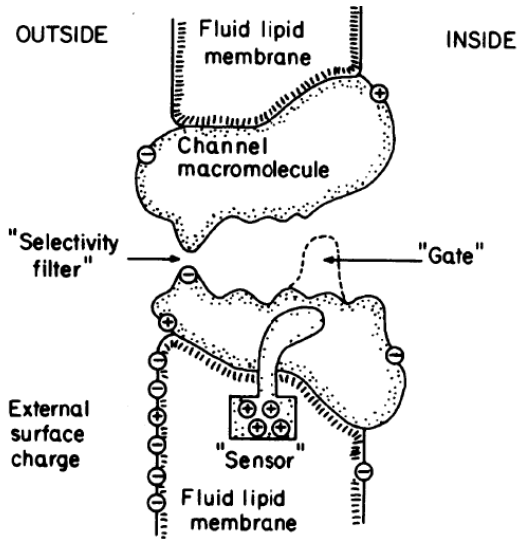

Fig 1.5: Basic structure of an ion channel:[14] *p 285*

To transport ions across the cell membrane, specific channel proteins called ion channels are needed. These channels work similarly to other transport channels; they transport ions down their electrochemical gradient. The basic structure of an ion channel can be seen above in *Fig 1.5*.

All ion channels possess the same three basic properties. The first of these properties is the conduction rates of the ions across the membrane. Ion channels transport a specific ion across the membrane at very fast rates, 10^7-10^8 ions per second.[15] Selectivity is another property all ion channels possess. Ions like potassium and calcium move through the cell membrane by passing through their respective channels. For example K^+ channels only allow the passage of potassium ions, either into or out of the cell, depending on the electrochemical gradient at the time. Another property of ion channels is gating. All ion channels are gated, meaning they can undergo a conformational change to stop the flow of ions. This gate closing can happen as a result of external stimuli, such as a change in membrane voltage or a molecule binding to the extracellular surface.[15]

1.1.2 Historical perspective

The first work done on potassium channels was carried out by Hodgkins and Huxley in 1952. Their seminal piece of work on the action potentials of giant squid axons sparked interest into exploring the mechanism of what happens during the transport of ions through the membrane. One fundamental aspect of their theory was that the axon membrane somehow changed its permeability to K^+ and Na^+ ions, but they did not yet know the mechanism of how this came about.[16] In 1955, it was found that K^+ moved through membrane by the use of a channel. Hodgkin measured the passage and flow of K^+ ions across a membrane using the isotope $^{42}K^+$. They observed that the flow in one direction was dependent on the flow in the other.[17]

Armstrong showed in 1975 that the method of K^+ transport across the membrane was carried out by some sort of pore or channel rather than a carrier protein.[18] His experiments showed that the rates of potassium transfer through the membrane of both squid axon and frog membrane was too fast to have possibly travelled through the membrane by a carrier-mediated protein. Neher *et al*. came up with a new method of accurately measuring the currents of single ion channels, which was a large improvement over previous methods.[19] In *Fig 1.6*, a diagram of 'Patch clamp recording' apparatus can be seen. VC is the standard voltage clamp setup placed within 200 Å. P is a pipette tip with a 3-5 μm opening at the tip. This opening will enclose one ion channel. V and VG are the detectors for the potential changes that occur in the pipette tip due to charge applied by voltage clamp.

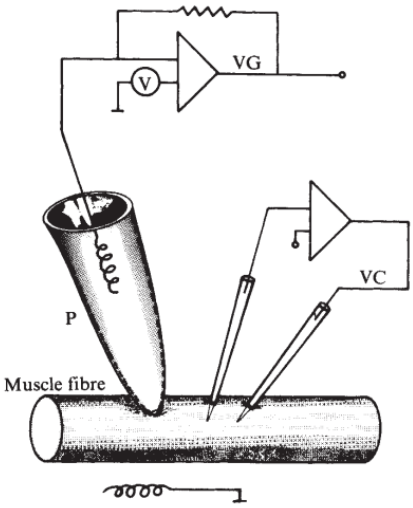

Fig 1.6: Diagram of patch-clamp recording apparatus:[19] p 800

Since the early days of ion channel research, a lot of work has been done on the amino acid sequences of these channel molecules and on the elucidation of a crystal structure. In 2003, Roderick McKinnon received a Nobel Prize in Chemistry for his work on 'structural and mechanistic studies of ion channels'. His work on the structure of a bacterial K^+ channel called KcsA from *Streptomyces lividans* allowed for much greater understanding of how K^+ channels function.[20]

1.2 Potassium Channels

Potassium channels are one of the most important ion channels as they have a role in many different processes, including hormone secretion, electrical impulse formation in neurons, and other electrically active cells.[20,21]

Potassium channels are differentiated by their mode of gating. There are three that will be discussed in this review.

1. Voltage-gated potassium channels
2. Calcium activated potassium channels
3. Inwardly rectifying potassium channels

1.2.1 Voltage-gated potassium channels

Voltage-gated potassium channels are channels that open and close in response to small changes in a cells membrane potential. Our knowledge of the structure of K_v channels is based on the work done by Nobel Prize winner Roderick McKinnon and his work on the K^+ channel KcsA. The general structure of K_v channels can be seen below in *Fig 1.7*.

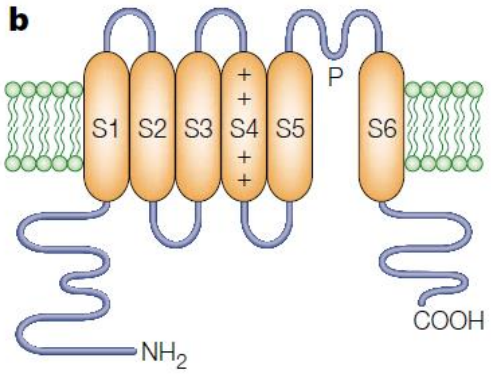

Fig 1.7: General structure of commonly occurring K_v Channels:[22] *p 116*

K^+ channels are made up of a number of sub-units, which differ depending on what type of channel it is. K_v channels consist of four sub-units. Inside each of these subunits are six transmembrane segments, labelled S1 to S6 in Fig 1.7. Cylinders in the diagram above represent helices.[23] Helices S5 and S6 assemble together with the P loop to form the pore domain. This pore domain contains the selective K^+ channel and its associated gating mechanism. Helices S1 to S4 make up what is known as the voltage-sensing domain.[23] These helices surround the pore domain and control the activation and deactivation of the gating mechanism.

1.2.2 Selectivity of the K_v Channel

In order for K^+ channels to efficiently transport potassium ions across the membrane, the channels must have selectivity for only potassium ions. This idea seems simple, but when you take into account the relative sizes of the ions in question the problem becomes much more difficult. A potassium ion has a Pauling radius of 1.33 Å whereas a sodium ion is only 0.95 Å across.[24] If K^+ channels were made by nature to exactly fit the dimensions of the potassium ion, it stands to reason that the sodium

ion would also be able to pass through into the cell. This scenario does not happen in the cells, which tells us that some sort of selectivity filter is in action in the K^+ channel, keeping the smaller sodium ion outside the cell, while allowing the potassium ion access to the intracellular environment (seen below in *Fig 1.8*).

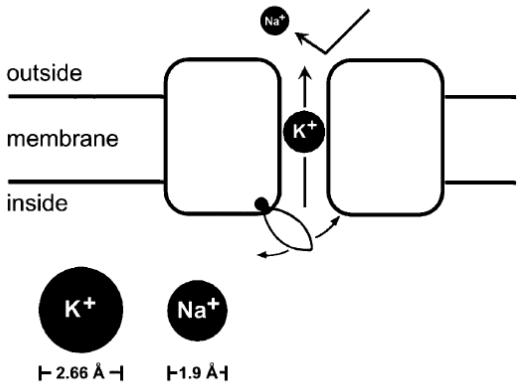

Fig 1.8: Simple diagram of the selectivity of potassium channels:[15] *p 76*

1.2.3 Mechanism of Selectivity Filter in KcsA Channel

To allow only potassium ions through the channel, something in the pore domain of the K^+ channel must be ion selective. Ion selectivity takes place along the ion pathway inside the pore. According to McKinnon, in the centre of the ion channel, there is a water filled pore about 10 Å in diameter.[15] This pore helps the potassium ions passing through to overcome the electrostatic repulsion that the ion would encounter when moving from an environment with a large amount of water present (outside the cell), to an intracellular environment with a lot less water molecules.

As the K^+ ions pass through the channel, they will lose the shell of water molecules that normally surrounds them in the body (their hydration shell).[22] This hydration shell is replaced by a series of oxygen atoms placed in the selectivity filter in the first third of the pore (as seen in *Fig 1.9*) which mimic the effects of the potassium hydration shell. By mimicking the potassium hydration shell, the selectivity filter effectively shuts out all other types of ion.

If a sodium ion tried to pass through the filter, the oxygen would not simulate its hydration shell and the forces of repulsion acting on its dehydrated form would force it out of the channel. As a K^+ ion passes through the channel, it will be bound at four specific points by a sequence of amino acids. This sequence of amino acids is called the 'signature sequence' and exists in every K^+ channel. The signature sequence allows the channel to exclusively bind and transport potassium ions. The signature sequence surrounds the potassium ion in eight oxygens, four above and four below.[22]

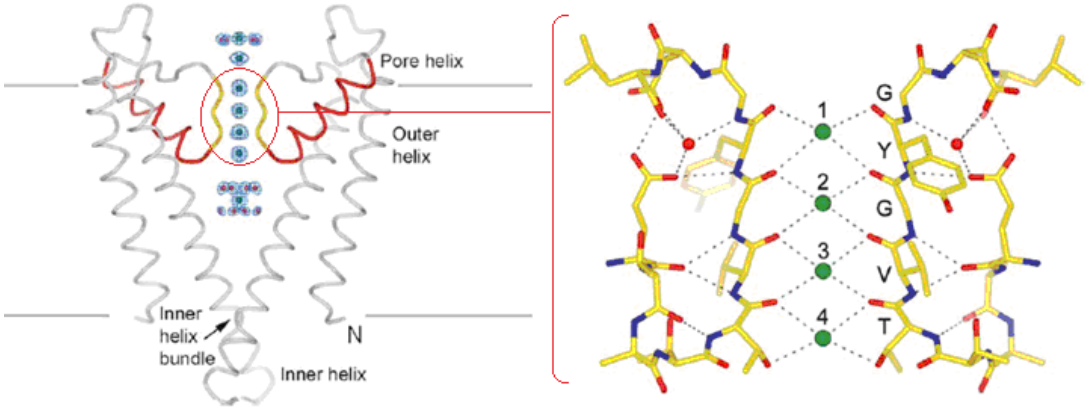

Fig 1.9: Diagram of Selectivity filter in a K^+ channel: adapted from [15] p 81-82

1.2.4 Gating in K_v channels

In voltage-gated K^+ channels, the gating mechanism is located on the intracellular side if the channel (*Fig 1.10*).[25] Hodgkin determined that channel opening/activation must be due to movement of charges in the membrane.[16] They predicted a 'gating current', a small charge movement in the membrane, which we know today, stimulates voltage-driven conformational changes.[25] The cloning of sodium channels provided more information as to what moiety changed position to close and open the gate mechanism. The earlier ideas of Armstrong theorized that the channel would contain two oppositely charged helices, which would move slightly, relative to one another, and be voltage-sensitive.[26]

What was instead found a few years later was the existence of a positively charged S4 helix. A number of research groups worked on finding out how exactly this positively charged S4 helix affected the activation and deactivation of the gating in K_v channels.

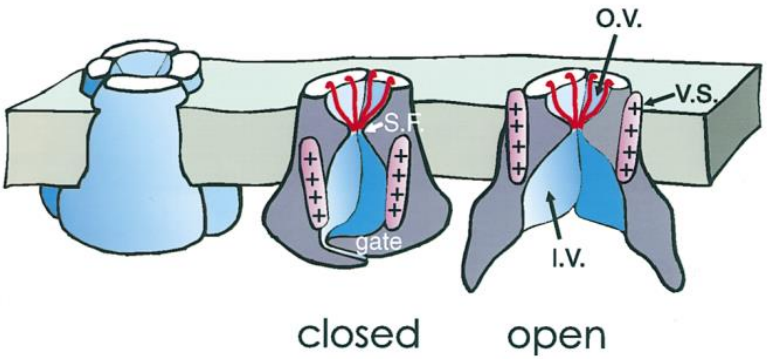

Fig 1.10: Diagram showing components of a K_v channel:[25] *p 372*

According to Armstrong and Hille (1998), it may take years until the mechanism for the movement of S4 is known. They also say that;

'*It is likely that all four S4 units must move in order to open the channel and that there are several nonconducting, partially activated states in which some but not all S4 units have moved.*'[25] p 376

1.3 Calcium activated potassium channels

The calcium ion is used in the body for activation of secondary messenger systems and gene transcription, among other things.[27] Another important role for Ca^{2+} ions is the activation of specific potassium channels in the cell. The first identification of an ion channel activated by calcium ions came in 1970 when Meech, found that a potassium channel in snail neurons activated in the presence of calcium ions.[28] Calcium activated K^+ channels come in three general forms, channels of small conductance (SK) channels of intermediate conductance (IK) and channels of big conductance (BK).[27] The BK channel was the first calcium activated channel to be cloned from *Drosophila*, and so they have been identified in a number of tissues.[29] The pore structure is similar to other potassium channels, with 6 transmembrane segments labelled S1 through S6 (*Fig 1.11*).

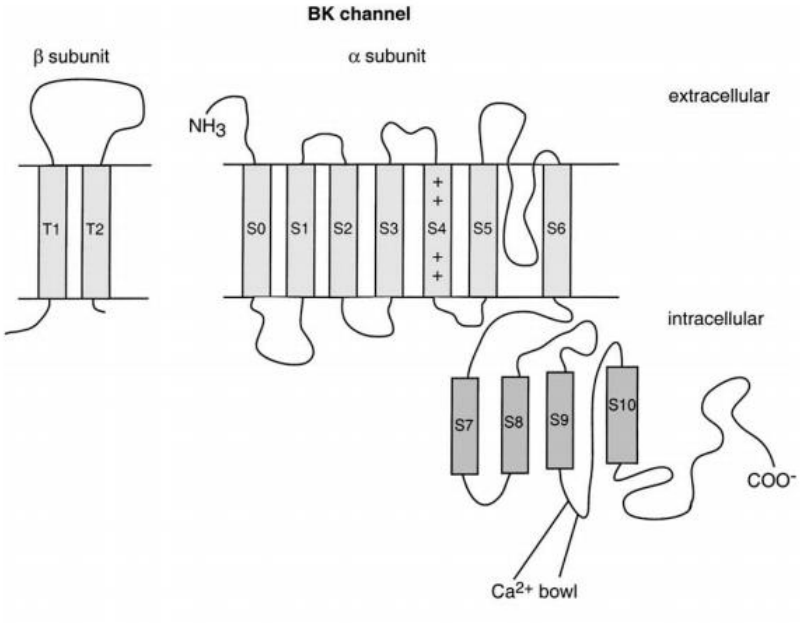

Fig 1.11: Structure of BK calcium activated K^+ channel:[27] *pg 347*

Along with the normal potassium channel transmembrane segments, an additional 4 hydrophobic segments have been identified in the intracellular environment.[30] Calcium in the cytoplasm of the cell activates the channel, but it is still unknown where exactly the calcium binds. It has been theorized that a number of negatively charged amino acids near S9 and S10 form a sort of calcium bowl that contains the binding site.[27] The β sub-unit of the BK type of calcium activating potassium channels adds diversity to the channel subtype BK. Only one α subunit has been identified and cloned, while three β subunits, β 1, β 2/3 and β 4 have been cloned so far.[31] For example, channels that contain only the α subunit, or the α subunit and β 1 subunit, have been found in muscle and produces sustained currents that do not deactivate. Channels that contain β 2/3 and an α subunit are found in the kidney, heart and brain and show fast inactivation.[27] The SK channel is found throughout the central and peripheral nervous system and follow the normal structure of potassium channels with six transmembrane segments. Indeed, because 60% of its structure is the same as a typical voltage gated K^+ channel, it has been proposed that the SK channel assembles as a tetramer, similarly to voltage gated channels do.[32] This has yet to be proven by a study however.

1.4 Inwardly rectifying potassium channels

Nichols defined inward rectification in K^+ channels as follows;[33]

'*Inward rectification means that at any given driving force (voltage), the inward flow of K^+ ions is greater than the outward flow for the opposite driving force*.' p 171

The role of inwardly rectifying K^+ channels (K_{IR} for short) in the body, depends on the degree of rectification each specific type has, i.e. how much greater the flow of potassium ions is in one direction over the other (*Fig 1.12*). Strong inwardly rectifying channels are present in skeletal tissue and have been identified in the CNS and cardiac areas.[33] K_{ATP} channels are also weakly inwardly rectifying and are found in muscle cells, brain tissue and in pancreatic β cells. Inward rectification is caused by ions present in the cytoplasm of the cell, like Mg^{2+}, and polyanilines like spermine and spermidine, which have a positive charge. These ions act to block K^+ leaving the cell at potentials above the resting potential.[34] Electrophysiological studies carried out on Mg^{2+} and the polyanilines present in the cytoplasm suggest that there is more than one binding site for these blocking ions in the K_{IR} channel. An M2 residue in $K_{IR}2.1$ has been found to be important to the Mg^{2+} block but not to the polyanilines.[35]

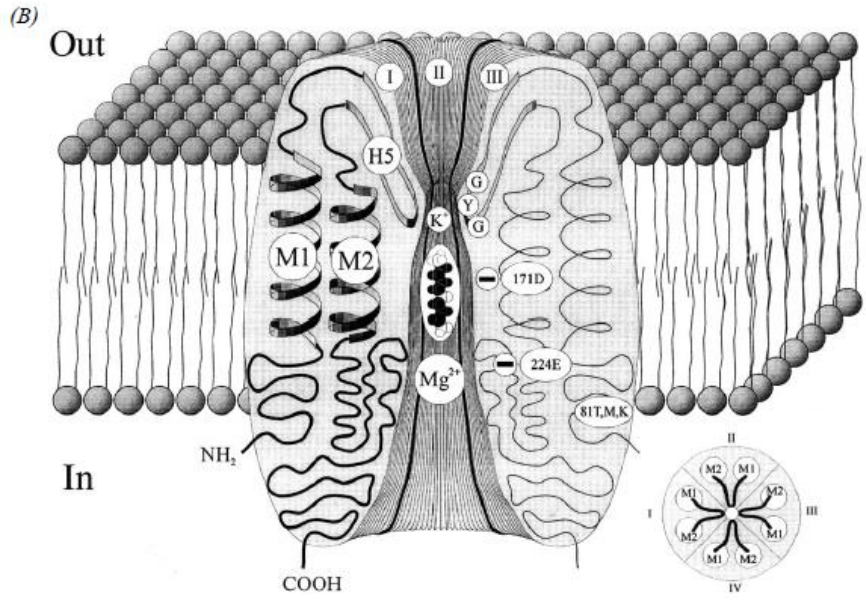

Fig 1.12: Diagram of K_{IR} channels showing major components:[33] *p 174*

1.4.1 Structure of K_{IR} channels

The crystal structure of K_{IR}Bac has helped researchers to elucidate the structure of inwardly rectifying potassium channels, by giving us a clear view of the component parts. The structure of K_{IR}Bac was first elucidated by Kuo *et al.* who crystallized in its closed state, which was unusual as all previous channels that had been successfully crystallised were in the open conformation.[36] As can be seen in *Fig 1.13*, K_{IR} channels have two transmembrane segments, labelled M1 and M2. The pore loop, labelled P, contains the signature sequence and acts as it does in all K^+ channels, as a selectivity filter.[34]

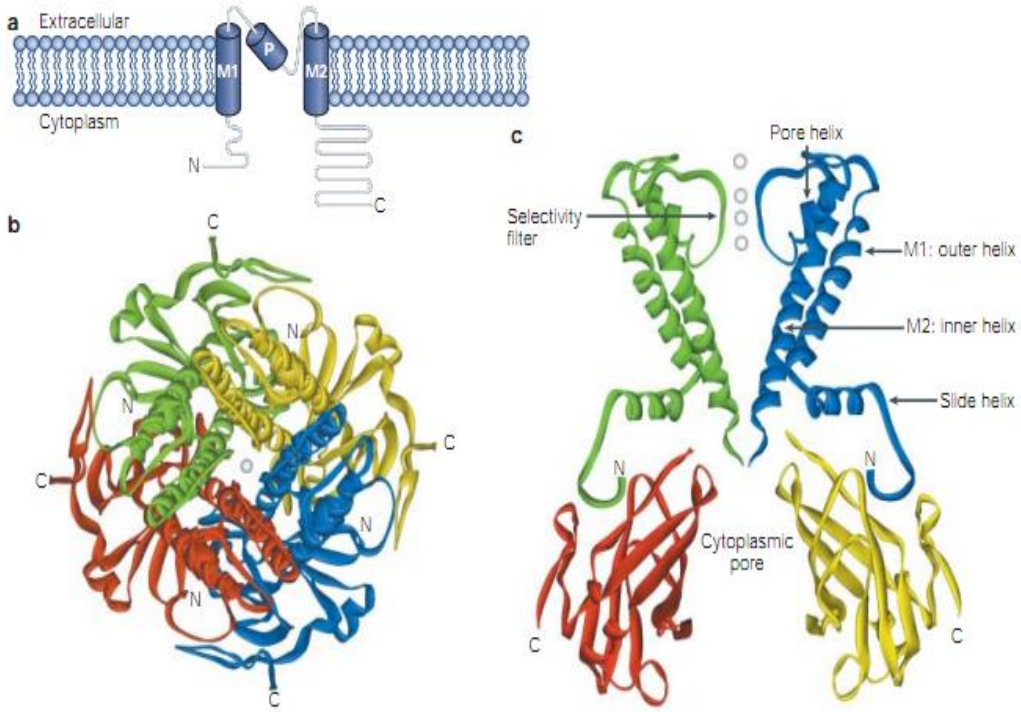

Fig 1.13: General structure of K_{IR} channels (a) along with the crystal structure of K_{IR}Bac (b) Top down and (c) transmembrane:[34] p 958

It is evident that approximately two-thirds of the amino acid sequence is on the intracellular part of the membrane. This inner protein has a role in the establishment of inward rectification, and in the attachment of ion blockers to prevent efflux of K^+ ions. There has also been evidence of binding sites on both the intracellular proteins and the transmembrane channel, on one of the M segments.[37] This theory would account for the relative speed of the activation of inward rectification in some strongly rectifying potassium channels.

1.5 Disorders of Potassium channels

1.5.1 Multiple Sclerosis

Multiple Sclerosis is a malady that is prominent in the western world. Compston *et al*., defined Multiple Sclerosis as;[38]

'A disorder of the central nervous system, manifesting as acute focal inflammatory demyelination and axonal loss with limited remyelination, culminating in the chronic multifocal sclerotic plaques from which the disease gets its name.' p 1221

Typically, Multiple Sclerosis (MS) becomes clinically noticeably around the start of early adulthood and tends to affect females more than males. The disease has a prevalence of about 120 per 100,000.[38] Classification of MS is split into three stages, the first being 'Clinically Isolated Syndrome' or CIS. During this stage, the patient has experienced a neurologic episode that continued for a period of 24 hours and is caused by inflammation and/or demyelination at one or more sites of the CNS. Some patients do not experience any more symptoms other than this isolated episode, but unfortunately the majority of patients enter a relapsing-remitting MS (known as RRMS) stage of the disease (*Fig 1.14*).[39] During RRMS, the patient goes through periods of remission from their symptoms, along with periods where their symptoms reoccur and new symptoms are observed. After a number of years of RRMS, the disease progresses to a stage called Secondary Progressive MS (SPMS) in 30-50 % of patients.[39]

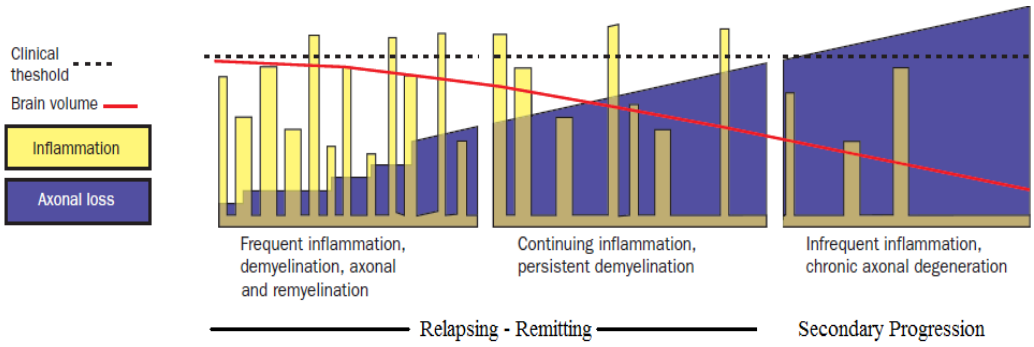

Fig 1.14: Graph showing progression of RRMS to SPMS:[38] *p 1227*

10-15% of people with MS present with Primary Progressive MS (PPMS). PPMS patients do not have remission periods where their symptoms calm. The disease

rapidly progresses, with the only remission periods being when the symptoms level out for a period of hours or days. The exact cause of MS is still unknown and studies on the topic show a number of different ideas as to what precisely causes the disease. Early investigators found that MS occasionally appeared commonly grouped in families, which suggested a possible genetic susceptibility. However, others argued that this could mean they had all been exposed to the same environmental factor, some 'MS virus' in the air that caused the onset of the disease.[40] This idea of a singular MS virus has mostly been left aside, but most researchers agree that a combination of environmental and genetic factors give rise to the propagation of MS.[41]

1.5.2 Treatment of Multiple Sclerosis

According to Compston[38] p 1226, the treatment of MS aims to;

- *Reduce relapse rates*
- *Prevent fixed disability directly attributable to relapse*
- *Provide symptomatic management of fixed neurological deficits*
- *Prevent disability acquired through progression*
- *Treat established progression.*

Current methods of first-line treatment are aimed at preventing clinical relapses of symptoms. Interferon-β acts by altering the balance of two types of cytokines, increasing the concentration of the immunoregulatory cytokines, while simultaneously inhibiting pro-inflammatory types. It also acts to '*downregulate T-cell resistance to apoptosis*'[42] p 11. Research is still being done into the exact mode of action of Interferon-β as some of its effects have only been demonstrated *in vitro*.[39] Another compound used in the first-line treatment of MS is Glatiramer acetate (GA), more commonly known as Copaxone. It consists of a random polymer combination of four amino acids, L-lysine, L-alanine, L-glutamic acid and L-tyrosine, and combines in a certain ratio to give the active drug (*Fig 1.15*).[43] GA acts as a T-cell receptor antagonist, and as a potent inducer of regulatory T-cells.[43]

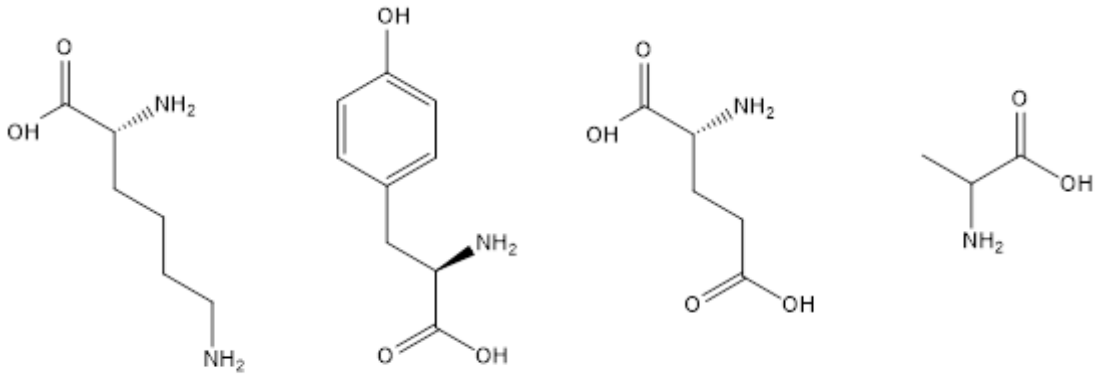

Fig 1.15: Structure of the four amino acids present in Glatiramer acetate:

Many of the drugs currently used to treat MS affect, to some degree, T-cells (T-lymphocytes). T-lymphocytes play an important role in cell-mediated immunity. Cell-mediated immunity is part of the immune response that does not involve antibodies, but instead consists of the activation of cytotoxic antigen-specific T-lymphocytes. In multiple sclerosis, the activation of $CD4^+$ T cells leads to their subsequent attack on the myelin oligodendrocyte glycoprotein (MOG) antigen, causing the degradation of the myelin sheath.[44] Blockage of these T cells can therefore help slow down the course of MS and help ameliorate the neurological symptoms associated with demyelination. Patch clamp studies on T-lymphocytes showed the presence of a K_v channel similar to those found in human nerves and muscle.[45]

1.5.3 K_v channel blockers

According to Judge S.I, compounds that are able to block or modulate K_v channels, are classified into three general categories:[46]

1. Organic compounds
2. Venom-derived peptide toxins
3. Charged elements

Aminopyridines and 4-aminopyridine in particular, block a large number of different K_v channels.

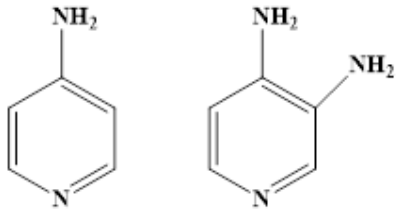

Fig 1.16: Structure of 4-Aminopyridine and 3, 4-Diaminopyridine:

4-aminopyridine has greater efficacy against delayed rectifying channels and its potency against the K_v channel family is in the range of micromolar (μM) to millimolar (mM) concentrations.[46] This number varies between individual subtypes of K_v channel.

1.5.4 Mode of action of 4-Aminopyridine

4-AP works by blocking the K_v channel from the inside of the cell (the intracellular side). It blocks while in its cationic form. In *Fig 1.17*, a structural representation of a typical K^+ channel is shown along with examples of where the different classes of K_v blockers attach.

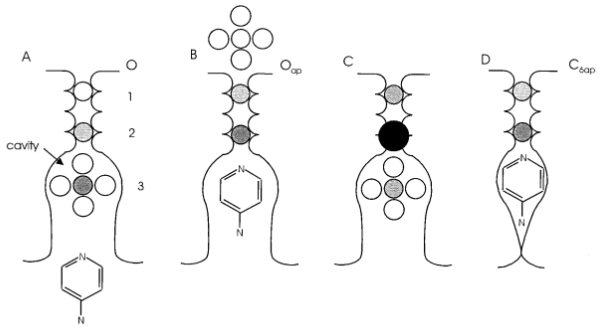

Fig 1.17: Diagram showing approach and blockage of 4-AP:[47] p 866

Armstrong[47] proposed a model for 4-AP blockage of K_v channels. They proposed that the 4-AP molecule entered the channel from the cytoplasm and subsequently moved all ions in the channel one space back in their channel progression. They found that Cs^+ ions significantly slowed the action of 4-AP binding in the channel cavity, because of its size (see part C of *Fig. 1.17*). This mechanism is shown in step form in *Fig 1.17*. The mechanism by which 4-AP blocks K_v channels relies on a number of factors including the frequency of stimulation and kinetic state of the channel.[48] The location of attachment for 4-AP is dependent on whether the specific K_v channel is activated, deactivated or inactivated. 3,4-Diaminopyridine is also used as a K_v channel blocker and has been found to have similar potency to its un-

substituted precursor 4-AP. Both drugs also have similar pharmacologic properties. Both 4-AP and 3,4-diaminopyridine have serum half-lives of about one to three hours.[46] 4-aminopyridine has good lipophilicity and so can pass through the blood brain barrier (BBB), hence it can be used to block K^+ channels in both the central and peripheral nervous system. 3,4-Diaminopyridine, on the other hand, is only soluble in aqueous solution and so cannot cross the BBB. It cannot be used to block channels in the CNS, only in the PNS.[46] There have been documented problems with adverse side effects with prolonged use of both the aforementioned drugs. In a study by Polman *et al.*, 23 patients were treated for 6 to 32 months with 4-AP.[49] Twenty out of twenty-three patients reported therapeutic benefits. Side effects for the majority were mild, but two patients suffered from grand mal seizures and one had liver function problems until treatment was halted.

1.5.5 Venom-derived peptide toxins

The venom of snakes, scorpions and sea anemones have been found to contain very potent and highly selective peptide toxins that affect and block many different types of ion channel, including K^+ channels. The most potent K_v blocker found so far is ShK from the Caribbean Sea anemone *Stichodactyla helianthus*. According to Chandy *et al.*, it has a "*K_d value of 11 pM and exhibits >1000-fold selectivity over IKCa1 channels"*[50] pg 282. ShK is extremely potent and selective to the K_v1.3 channel. ChTX is another toxin isolated from scorpion venom and also has a very high potency. It is not as selective, however as it affects K_v1.3 and IKCa1 to about the same degree (see *Fig 1.18*). Maurotoxin (MTX) is an example of a IKCa1 selective peptide toxin. It was first isolated from the venom of *Scorpio maurus.*[51] Its efficacy is much greater for IKCa1 than for K_v1.3, by a factor of about 150.

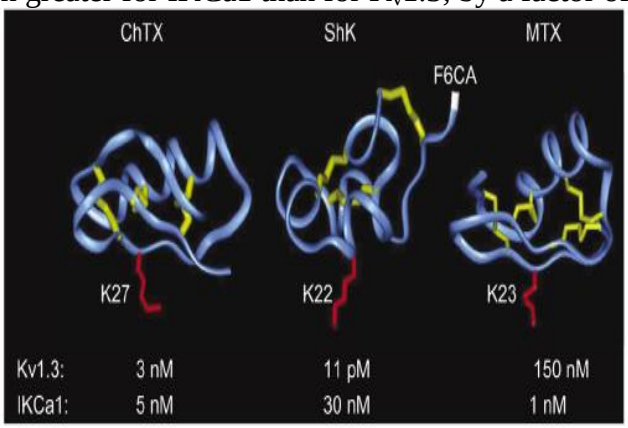

Fig 1.18: Structures of ChTX, ShK and MTX:[50] p 283

1.5.6 Recent Developments

There has been much work done in the past ten years in the treatment of Multiple Sclerosis. Many new drugs are currently in stage II and III trials. Natalizumab, for example is a highly specific human monoclonal antibody that works by attaching to an adhesion molecule on the surface of T-leucocytes. It prevents the leucocytes from moving from the blood into the brain. This was proved using EAE modelling, which stands for experimental autoimmune encephalomyelitis, a neurodegenerative disease that can be induced in rats, which has similar characteristics to multiple sclerosis in humans.[52] Over 2000 MS patients were enrolled in its phase III trials and when its clinical efficacy was proven the FDA fast-tracked its release and according to Menge *et al*. as of May 2008, over 32 000 patients have received the drug.[39] There have been a small number of severe side effects during the course of the clinical trials. Two patients have died due to PML during trials and a further three cases since drug release. PML is a lethal CNS infection for which there is no treatment.[53] Due to this, careful enrolment procedures are now used and prospective patients are carefully vetted before receiving natalizumab.

A number of small molecules with varying target sites have also been synthesized in recent years (*Fig 1.19*). Clofazamine, an immunomodulatory agent used in treating leprosy, was found to suppress Calcium movements in T-cells by blocking $K_v1.3$ channels. Its IC_{50} value was quoted as 300 nM.[54] The psoralen group of compounds were discovered when researchers looked into reports that tea made from Garden Rue, (*Ruta graveolens*) relieved the symptoms of MS. Psora-4, a derivative made from the initial parent psoralen compound, was shown to block the $K_v1.3$ channel with an IC_{50} of 3 nM and was selective over the rest of the K_v1 channels with the exception of $K_v1.5$.[55]

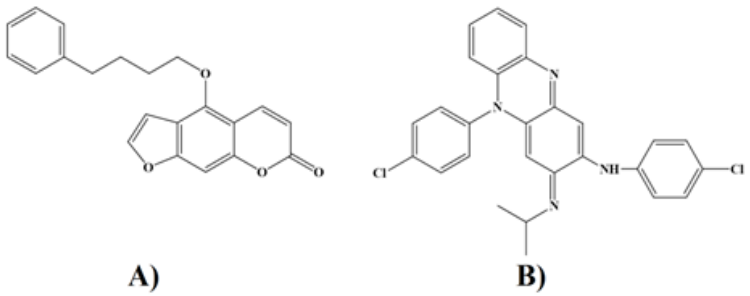

Fig 1.19: Structure of A) Psora-4 & B) Clofazamine:

1.6 Anti-Arrhythmic Drugs

Cardiac Arrhythmias make up a large part of current cardiovascular disease research. Atrial fibrillation affects over a million people worldwide and in the US alone over 400,000 patients are killed by sudden cardiac death, which onsets as ventricular fibrillation.[56] A lot of research has gone into drug therapeutics for arrhythmia over the past few decades but problems have been encountered with toxicity and serious side effects. In the Cardiac Arrhythmia Suppression Trial (CAST) in the early nineties, clinical trials were run in three class I_C agents, flecainide, encainide and moricizine. The trials showed that there were marked differences between the placebo group and the patients receiving the drug, with the placebo group showing greater survival rates.[56]

As a consequence of the negative results of the CAST trials, interest in developing class I anti-arrhythmics has significantly declined. More focus has been placed on class III anti-arrhythmic drugs, which affect different target sites than the class I drugs did. The classification system for anti-arrhythmics, as set down by Singh & Vaughan Williams in the 1970s, is based on the mechanism of the drugs affect.[57]

Class I drugs were the main focus of the pharmaceutical community up until the CAST trials and act by blocking sodium channels.

Class II drugs are known as β-blockers. They act on β_1-adrenergic receptors, preventing attachment of hormones released as a response to stress.

Class III drugs work by blocking potassium channels. Examples include Amiodarone and Sotalol.

Class IV drugs act on Calcium channels, and help reduce the contractility of the heart.[56]

1.6.1 Class II anti- arrhythmic drugs: β-blockers

The first β-blocker widely used, propranolol, was first introduced as an anti-anginal drug. It subsequently became the archetypal β-blocker molecule on which all future drugs were modelled on. The β-adrenergic blockers currently being used are separated into a number of categories based on their anti-adrenergic qualities and

other associated properties.[58] In the β-Blocker Heart Attack (BHAT) study, it was shown that patients suffering from heart failure who were treated with propranolol over a number of months had a greater survival rate than those on the placebo.[59] Propranolol is classified as a first-generation nonselective β-blocker because it blocks both the β_1 and β_2 receptor with equal selectivity (*Fig 1.20*).

Two examples of second-generation β-blockers are metoprolol and bisoprolol. They are both more cardioselective than propranolol and selectively block the β_1 receptor. According to Armstrong and Moe,

'*The Metoprolol in Dilated Cardiomyopathy (MDC) Trial evaluated 383 functional class II and III heart failure patients*'[60] pg 2944.

It found that the use of metoprolol significantly reduced the number of patients that required a heart transplant, compared to the placebo group. Sotalol is a first-generation β-blocker that does not follow the classification in so far as it also acts as a class III anti-arrhythmic. Sotalol has a β-blocking potency on a milligram scale, approximately one third of the potency of propranolol. It was initially released as a hypertension drug.

Following its release, a number of arrhythmia studies were conducted using Sotalol, which led to the FDA approving it for the treatment of ventricular arrhythmias in 1992.[61] Its β-blocking and K channel activities show separate dose *vs*. response relationships. The usual dosage is 80 mg of orally administered drug twice daily.[61]

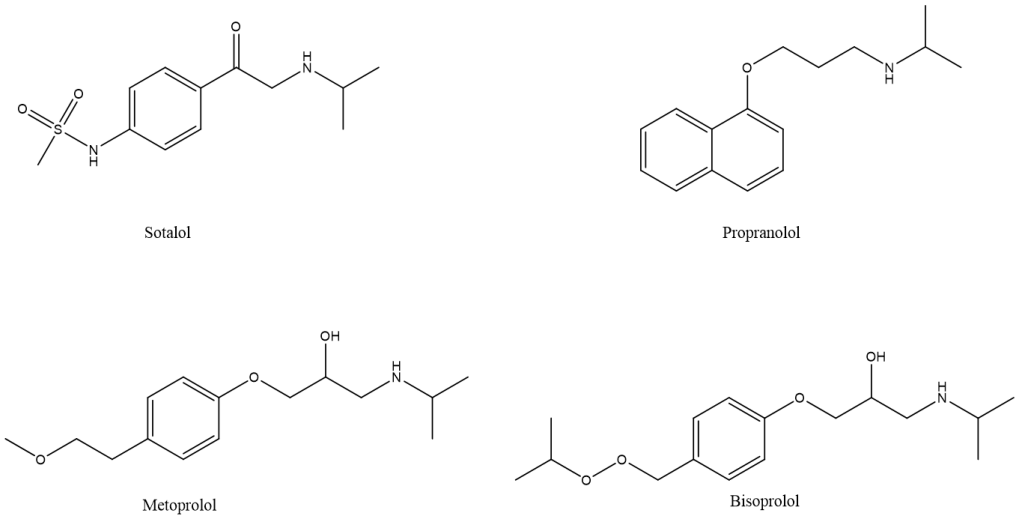

Fig 1.20: Structures of β-blocking Drugs:

1.6.2 Class III anti-arrhythmic drugs: K^+ blockers

Class III anti-arrhythmics function by blocking K^+ channels specific to heart muscle. The gene that encodes these potassium channels in humans is the ether-à-go-go related gene (HERG). The HERG gene, according to Vandenberg *et al*., is '*important in maintaining normal action potential repolarisation in cardiac myocytes*'[62] p 241.

Sotalol, a drug discussed previously, has both class II and class III properties. However, its risk of side effects, even though it is slight, led researchers to start looking at 'pure' class III drugs. One of the so called pure drugs made was Ibutilide. The FDA approved its use for monitored intravenous injection, as there is a risk of proarrhythmia during the application of the drug. Proarrhythmia is a type of rare arrhythmia, which leads to ventricular fibrillation and death if the problem is not remedied.[63] It was found subsequently that these types of pure class III drugs did not give any more activity that the mixed class drugs and also did not reduce the danger of proarrhythmia occurring.

Amiodarone, in contrast, is a drug not associated with increased mortality and indeed has been effective in several studies. Amiodarone is a class III anti-arrhythmia drug that shows additional class I, II and IV properties.[64] It has not been associated with side effects involving proarrhythmia, although it has side effect problems of its own, mostly due to toxicity. A number of patients have had mild side effects, while the occurrence of liver and thyroid problems has been infrequent to rare.[65] Amiodarone derivatives have been made that attempt to fix the toxicity problem by making the compounds half-life in the body shorter, giving a better risk to benefit ratio. One such derivative is Celivarone. It differs from amiodarone in that it has no iodine in its structure and has an extra side chain on the benzofurane ring system (*Fig 1.21*).[66]

Dronedarone is also an amiodarone derivative lacking the iodine in its structure. A number of studies, including the ATHENA study, showed that patients treated with dronedarone over a number of months had a significantly smaller chance of being hospitalised for arrhythmia related problems than the placebo group.[67] Budiodarone was synthesised with a mind to keeping amiodarone's unique multiclass activity intact while attempting to remove the side effects caused by the drugs accumulation in the body. The PASCAL study tested 72 patients with differing doses of

budiodarone over a period of a few months. Budiodarone was shown to reduce the occurrences of atrial fibrillation by 75% compared to the placebo group.[68]

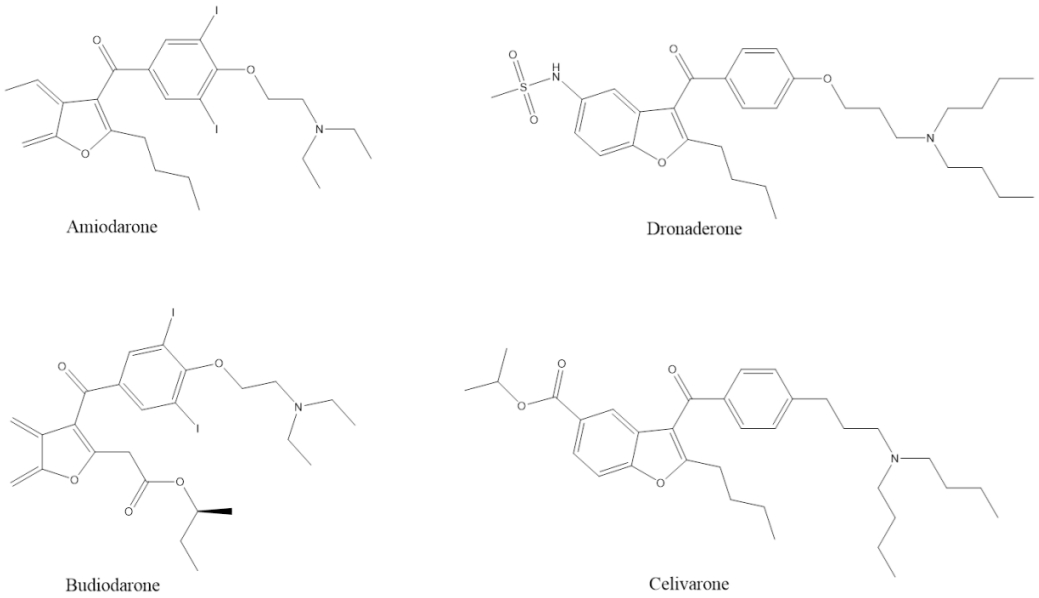

Fig 1.21: Structure of Amiodarone and some of its derivatives:[69]p 589

1.6.3 Recent Developments

Currently, pharmaceuticals are the first option considered for the treatment of arrhythmias, so numerous studies are being carried out to find the next novel drug with activity better than the current amiodarone derivatives, and less toxicity issues. A drug called Vernakalant is currently in its late Phase III clinical trials for its oral and intravenous formulations (*Fig 1.22*). It is primarily a class III anti-arrhythmic, but also has action versus sodium channels in the heart. This action caused the problem with the amiodarone range of compounds, but in vernakalant's case the action is rate and voltage dependent, meaning it is much less of a worry.[69] During trials, patients on vernakalant had no occurrences of proarrhythmia and the side effects observed were dysgeusia (distortion of the sense of taste), sneezing and nausea.[66]

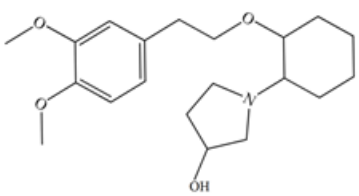

Fig 1.22: Structure of vernakalant:

1.7 Diabetes

Diabetes Mellitus (more commonly known as Diabetes) is a group of metabolic disorders where a patient suffers from high blood sugar levels, either because their body cannot produce enough insulin, or because their body does not recognise the insulin that is produced.[70] 'Type I' diabetes results from the bodies' inability to produce enough insulin. It normally begins its onset in childhood or adolescence. Insulin in the body is produced by the pancreas (*Fig 1.23*), and in type I diabetes, the insulin-secreting islet β cells stop insulin production due to an autoimmune response. At some point in the patient's childhood, their body's immune system attacked the β cells in their pancreas, causing a drastic reduction in the amount of the hormone produced from that point forward. The reason for this immune response is, as yet, still unknown, but the end result is the onset of type I diabetes.[71] 'Type II' diabetes is usually adult onset, and is the result of the combined effect of insulin resistance and a deficiency in insulin production. The treatment for both types of diabetes focuses on maintaining a stable level of insulin, as well as improving the current insulin production in type II patients.

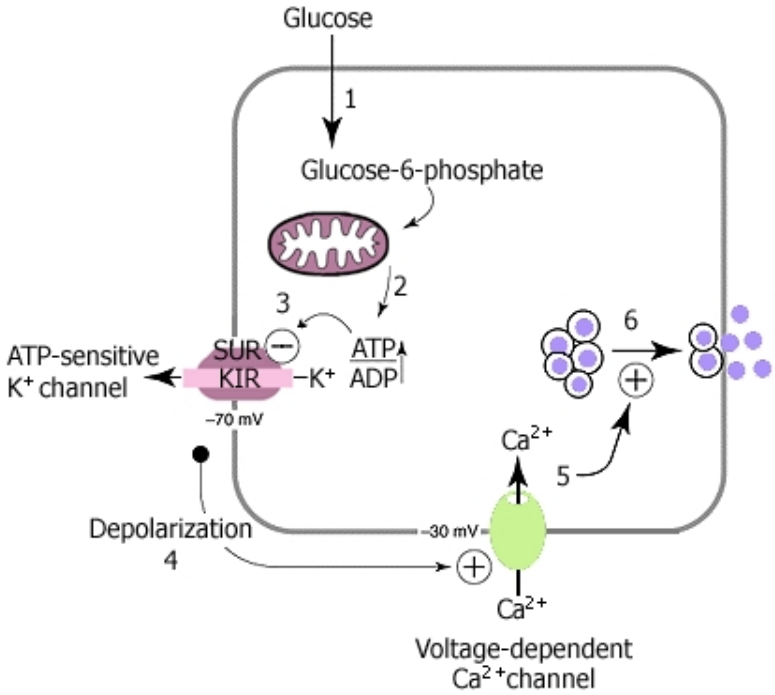

Fig 1.23: Mechanism of Insulin secretion from β cells:[71] p 5

1.7.1 Mechanism of insulin secretion/release

The hormone insulin is secreted from the 'islets of Langerhans', clusters of pancreatic β cells. The amount of insulin released is dependent on ATP sensitive K^+ channels.[21] The diagram below shows the process of insulin secretion. Glucose is brought into the β cell and metabolised. During this process ATP is released. The increase in the ATP:ADP ratio causes the ATP sensitive K^+ channel to close, causing a build-up of positive K^+ ions. The positive charge in the cell allows its voltage-gated calcium channels to open, and the calcium entering the cell stimulates the secretion of insulin.[71]

1.7.2 Sulphonylureas and their modes of action

Sulphonylureas have been used to enhance the production of insulin in β cells for the past 50 years. They work by affecting the potassium permeability of the cell membrane. Specifically, the sulphonylurea drugs interact with the ATP sensitive K^+ channels present in the β cells. These channels are responsible for maintaining the membrane potential of the cell and, when blocked, lead to a build-up of ions inside the cell. This depolarization of the cell induces insulin secretion.[72] Studies of cloned K_{ATP} channels have shown that sulphonylureas interact at two sites, a low affinity site on Kir6.2 and a high-affinity site on SUR1.[72] When bound to SUR1, they induce channel closure. The channel does not completely close however, meaning that high-affinity inhibition is not complete, even at high concentration.[73]

The first generation of sulphonylureas were marketed in the 1950's. Tolbutamide and chlorpropamide (*Fig 1.24*) were some of the most well known drugs for the treatment of type II diabetes at the time, and were some of the few oral agents available in the US until 1994.[74] It has now been largely replaced with newer derivatives. The main reason they are no longer in use is the severity of their side effects compared to the newer generation of drugs. Their side effects included hypoglycaemia and some incidences of gastrointestinal problems.

Hypoglycaemia occurs when there is a drop in blood sugar level and the brain cannot get an adequate supply of glucose, and can lead to seizures, loss of consciousness and in severe cases, brain damage and death.[73] Unfortunately sulphonylureas tend to cause this problem to some extent in patients, as their primary function is to increase

insulin levels. In doing this, the amount of glucose in the blood is affected. The half-lives of the first generation agents caused them to remain in the body too long, causing a reduction of glucose present in the blood and the subsequent side effects described above.[75]

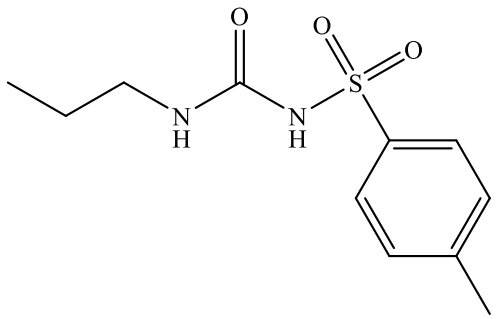

Tolbutamide

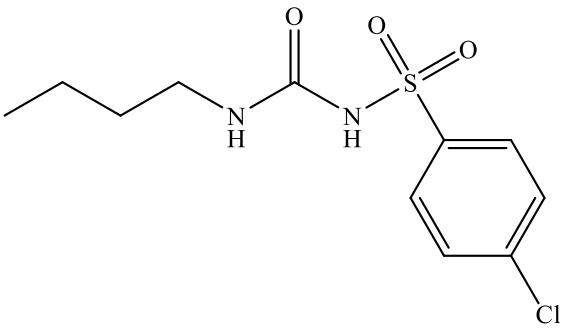

Chloropropamide

Fig 1.24: Structure of two 'first generation' sulphonylureas:

1.7.3 'Second' generation sulphonylureas

First generation sulphonylureas have now been largely replaced in the treatment of type II diabetes by newer agents like gliclazide, glipizide and glibenclamide (Glyburide). The structures of these molecules are shown in *Fig 1.25*.

Like all sulphonylureas, they act on the sulphonylurea receptor on the K_{ATP} channels located on the pancreatic β cells. Gliclazide increases insulin excretion in both fasting states and after meals and so can be taken at any time. Its half-life in the blood is around 12 hours. Hypoglycaemia can occur when taking gliclazide, and if combined with drugs like aspirin or oral anti-coagulants, these effects can be exacerbated.[73] This can lead to problems with patients on multiple types of medication.

Glipizide has a half-life of about 4 hours, which cuts down the amount of time it is present in the body. It acts on the same sulphonylurea receptor as the rest of the agents mentioned. Glibenclamide, or glyburide as it is also known, had issues with its side effects. While its potency and mode of action is similar to its second generation brethren, the risk of severe hypoglycaemia is increased compared to the rest.

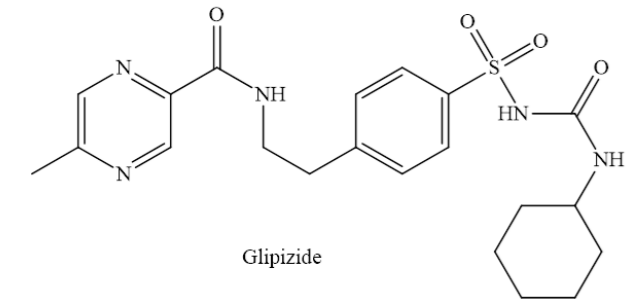

Glipizide

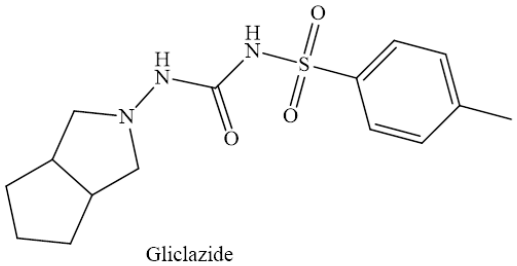

Gliclazide

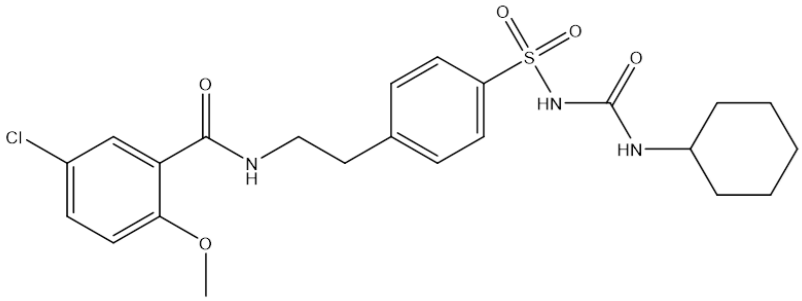

Glibenclamide

Fig 1.25: Structures of second generation sulphonylureas:

In a study by Szoke, the difference in amounts of glucose in the blood after the administering of glyburide and another sulphonylurea agent (glimepiride) were recorded.[76] It was shown that no significant differences in potency between the two drugs. However, differences were noted in the recovery period of blood glucose both drugs, with glyburide taking significantly longer.

The results of the study showed that glyburide activity did not stop immediately after the patient stopped taking it, whereas with glimepiride, activity stopped when the drug stopped being administered.[76] As glyburide has also been shown to accumulate in the pancreatic β cells, these two facts combined may account for the large difference in the occurrence of severe side effects when taking glyburide as opposed to another similar sulphonylurea.[77]

1.7.4 Recent Developments

In the past 10 years, steps have been made in finding agents that have the same mode of action and relative potency as the sulphonylureas, without the risk of dangerous side effects. This new class of drugs are called the Meglitinides (*Fig 1.26*). The first of these non-sulphonylurea agents was Repaglinide, which was released on the market in 1998.[78] It works by inhibiting the same K_{ATP} channel as the sulphonylureas, but attaches at a different spot on the channel.

When compared to glyburide, the rate of insulin increase in the blood was faster for repaglinide. This rapid increase does not last for very long however, which greatly reduces the chances of hypoglycaemia occurring. Another factor that adds to repaglinides safety profile is its very short half-life of 1 hour.[73] In addition to this, over 90% of the drug is recovered in the faeces, which means that it does not have to be broken down in the liver, making it suitable for elderly patients and patients suffering from liver disorders.[78]

Nateglinide is another meglitinide-like agent which was released in 2001. It binds to the sulphonylurea receptor on pancreatic β cells with good specificity and works rapidly to increase the insulin secretion after application. Like repaglinide, it has a short half-life of about 1 to 3 hours. This drug exhibits significant benefits to repaglinide.

It acts on the K_{ATP} channels and closes them three times as quickly as repaglinide, allowing even faster insulin secretion. It also detaches from the K_{ATP} channel five times as fast as repaglinide, which gives a rapid and short response on insulin secretion.[79]

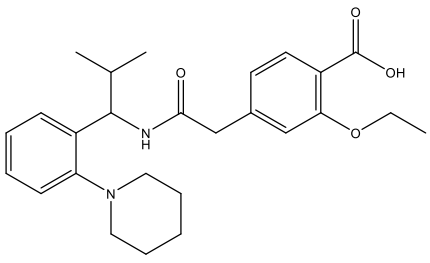

Repaglinide

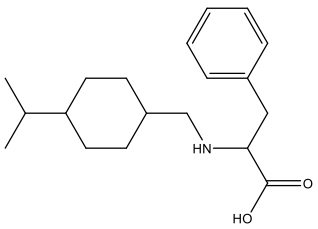

Nateglinide

Fig 1.26: Repaglinide and Nateglinide:

1.8 Foldamers

Research into foldamer chemistry has accelerated ever since its inception in the 90's. The word "foldamer" is defined as;

"*Any oligomer that folds into a conformationally ordered state in solution, the structures of which are stabilized by a collection of non-covalent interactions between nonadjacent monomer units*"[80] pg 3895

If we consider the huge numbers of proteins present in the body, all with clearly defined roles and parameters, consist of a combination of the 20 naturally occurring amino acids, we can see that research into adding non-natural monomers to this list could lead to innumerable new insights and protein-like compounds. To synthesise useful foldamers, we first must look at what each prospective foldamer candidate must achieve. According to Gellman, there are three major hurdles.[81] Foldamers must have;

1. Determining novel backbones capable of folding into an ordered state
2. Efficient synthetic methods
3. Interesting chemical functions, *i.e.* functional groups
4. There are two general types of foldamer backbone, one consisting of aliphatic monomer subunits, the other incorporating aromatic compounds in its monomer chain. A few examples of typical foldamer backbones can be seen below in *Fig. 1.27.*

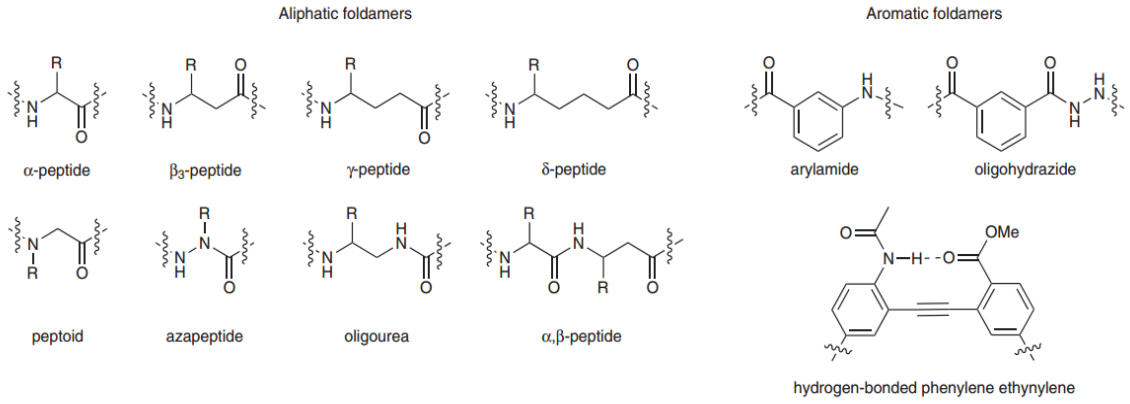

Fig 1.27: Typical Foldamer backbones:[82] *pg 253*

1.8.1 Secondary structure in proteins *vs.* Foldamers

In order to successfully mimic proteins in a biological system, foldamers must assemble in the same ways as proteins do. Just as a protein's primary structure is made up of a combination of amino acids, foldamers are composed of repeating units of a non-biological monomer. The secondary structure of a protein refers to the three dimensional local configuration of the protein. The most well known protein secondary structures were put forth by Pauling, and are the Alpha (α) Helix and the Beta (β) sheet (*Fig 1.28*).[83] These structures are held in place by a hydrogen bonding interaction between backbone oxygen and amide hydrogen.

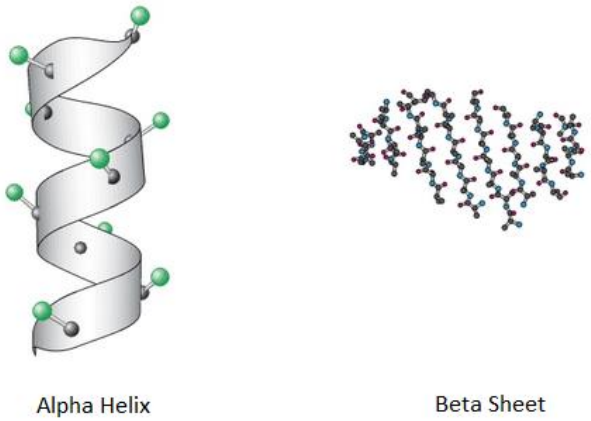

Fig 1.28: Diagram of an α Helix and a β sheet: Biochemistry 5th edition[84] adapted

The tertiary structure of proteins tells us about how the protein's secondary structure arranges itself geometrically *i.e.* how α helices stack with each other to form a discrete shape, a protein domain. In order for these biopolymers to perform their function biologically, a specific tertiary structure is usually required to allow the arrangement of functional groups that make up the active site.[81] These sites are made up of groupings of different areas of the polypeptide chain. The stability of the overall tertiary structure is important to analyse also, as the folded structure will be stronger than the sum of its parts.[85] This information on protein structure gives the researcher guidelines to follow when attempting to design a new foldamer backbone. Firstly, monomer selected must allow for the formation of α helices and β sheets, as these structures allow for stable tertiary structures to occur.[86] According to Gellman, for a foldamer to exhibit a stable, single tertiary structure;[81]

"The molecule must be a heteropolymer i.e. it must consist of two or more types of monomer"

Research into foldamer secondary structure in the past decade has yielded a number of different viable conformations and significant strides have been taken towards the emulation of a number of different proteins (*Fig 1.29*).

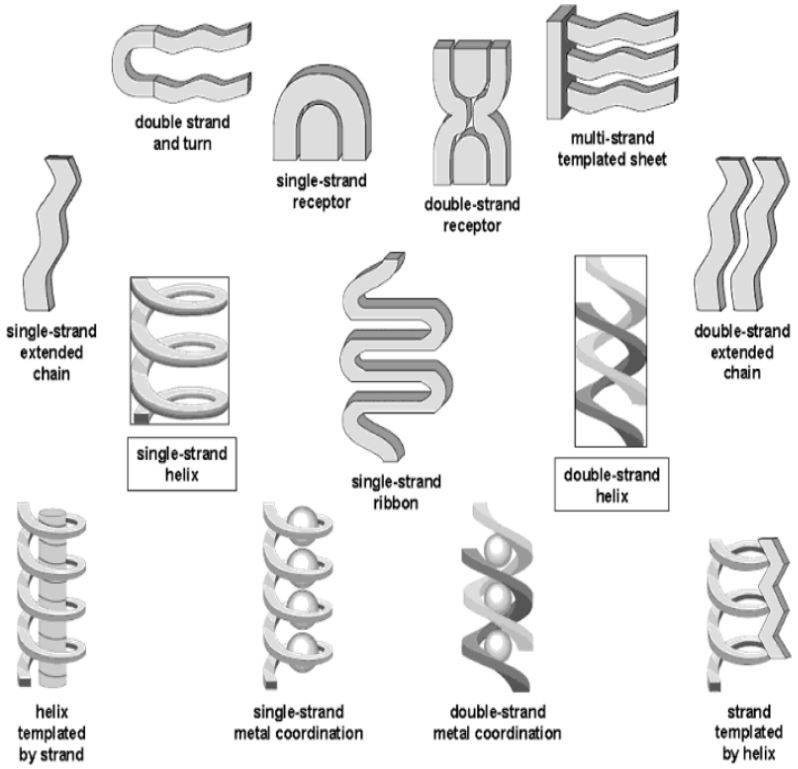

Fig 1.29: Foldamer secondary structures to date:[80]

1.8.2 β-peptide mimetics

Cell penetrating peptides (CPPs) are used as a vehicle to allow for the transportation of therapeutic agents across the membrane, while keeping their biological activity.[87] Protein sequences rich in arginine are particularly effective, with short oligo-arginine peptides among the most efficient CPPs.[88] Foldamers, because of their stable secondary structure and resistance to degradation, are prime candidates for use in intracellular delivery. Foldamers based on a number of different backbones have shown promise in the area of CPP's, including a β peptide based compound.[89] These foldamers must contain some cationic groups in order to increase cell permeability. Potocky *et al.* showed that a β peptide possessing both hydrophilic and lipophilic attributes (amphipathic) was able to penetrate the cell to a concentration of 8 μM.[90] A number of other CPP's have been synthesised, including an aromatic amide

oligomer, which was again functionalised with cationic groups.[91] Both molecules can be seen in *Fig 1.30* below.

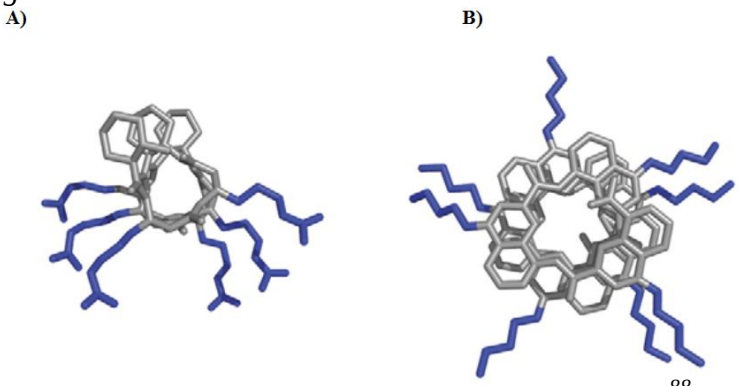

Fig 1.30: A) Cationic β-peptide; (B) aromatic amide polymer:[88]pg 686(adapted)

1.8.3 Protein-Protein interactions

β-peptides, as stated above, have many of the necessary characteristics for foldamer efficacy. They fold into stable secondary structures and thus cannot be broken down by proteases. This allows a foldamer consisting of β-peptides significantly more time to bind to an active site in the body.[92] Work by Seebach showed that β-peptides can form helical secondary structures when in organic solvents.[93] These helices are named after the number of atoms in the rings made by a specific hydrogen bond, and examples of these structures can be seen in *Fig 1.31*.

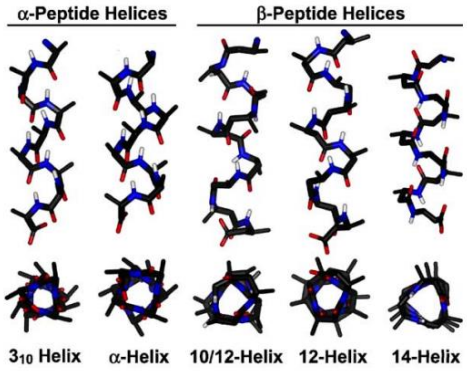

Fig 1.31: Secondary structures formed by α and β peptides:[92] pg 12

In order for these helices to be useful as potential therapeutic agents, they must be able to maintain their secondary structure in aqueous solution. Arvidsson[94] found that with the addition of charged side chains to the lead molecule, the formation of salt bridges in solution was possible. The charged side chains were positioned in such a way as to allow salt bridges to form at two points on the peptide (*Fig 1.32*).

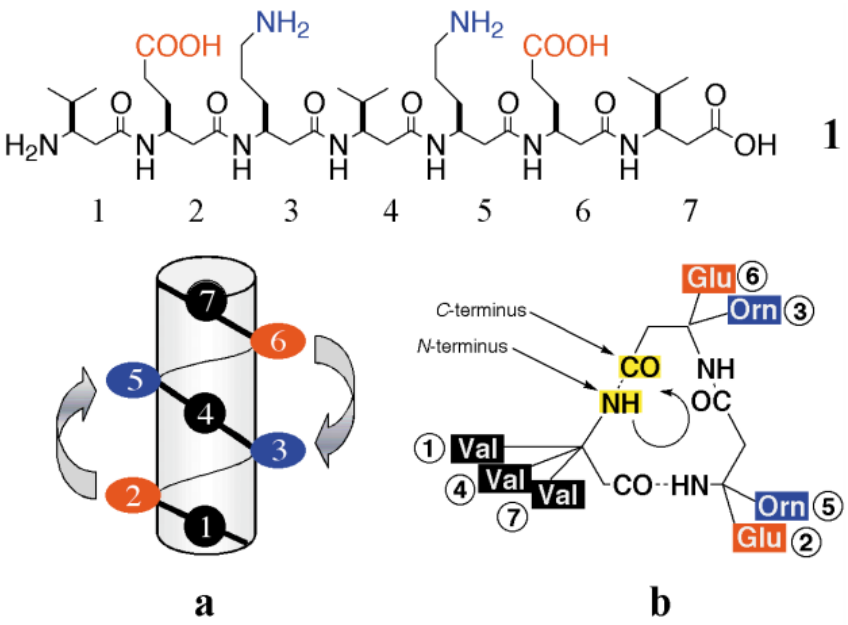

Fig 1.32: Formula of β peptide showing a) helical conformation and b) position of blue positively charged residues and red negatively charged residues:[94] *pg 649*

1.8.4 DNA/RNA analogues

With the discovery by Watson and Crick of DNA base pair structure, work began to find and target specific genes responsible for a variety of disorders. If an appropriate gene sequence can be identified as the cause of a certain disease, it can be targeted by antisense therapy. Rather than inundate the body with harsh, cytotoxic chemotherapeutic agents, chemically modified nucleic acids (CNA's) can be used to attach and interfere to the specific sequence causing the malady. Prospective CNAs must meet a number of criteria before they can be put forward as viable alternatives to chemotherapy.

1. They must be cheap and easy to produce on a large scale.
2. Their structure must be stable in the body.
3. They must be able to enter and be retained by the target cells long enough to have a therapeutic effect.
4. They must be able to successfully interact with their targets while not interacting with any other cell process.[95]

A wide range of CNAs have been synthesised over the last decade, with one of the most thoroughly researched being Phosphorothioate oligonucleotides. CNAs can reach nearly all types of tissues and organs within minutes of intravenous dosage, with the exception of the brain and testes.

For Phosphorothioate oligonucleotides, the major sites of accumulation are the liver and the kidneys, with the spleen and lymph nodes also showing lesser signs of accumulation.[96] This widespread, systematic dispersal of CNA allows for excellent overall delivery into the target cells. Phosphorothioate oligonucleotides are broken down in the body by nucleases, and MS analysis has shown that 30 to 40% of the CNA has lost at least a nucleotide from one end within 5 minutes of application.[96] The half-life of these types of CNAs range from 12-24 hours in tissue.[97] Neurath used p65 antisense phosphorothioate oligonucleotides in the treatment of mice with chronic intestinal inflammation, the symptoms of which mimic Crohn's disease in humans. [98] They found that local application of the CNA was more effective than daily administration of glutocorticoids.

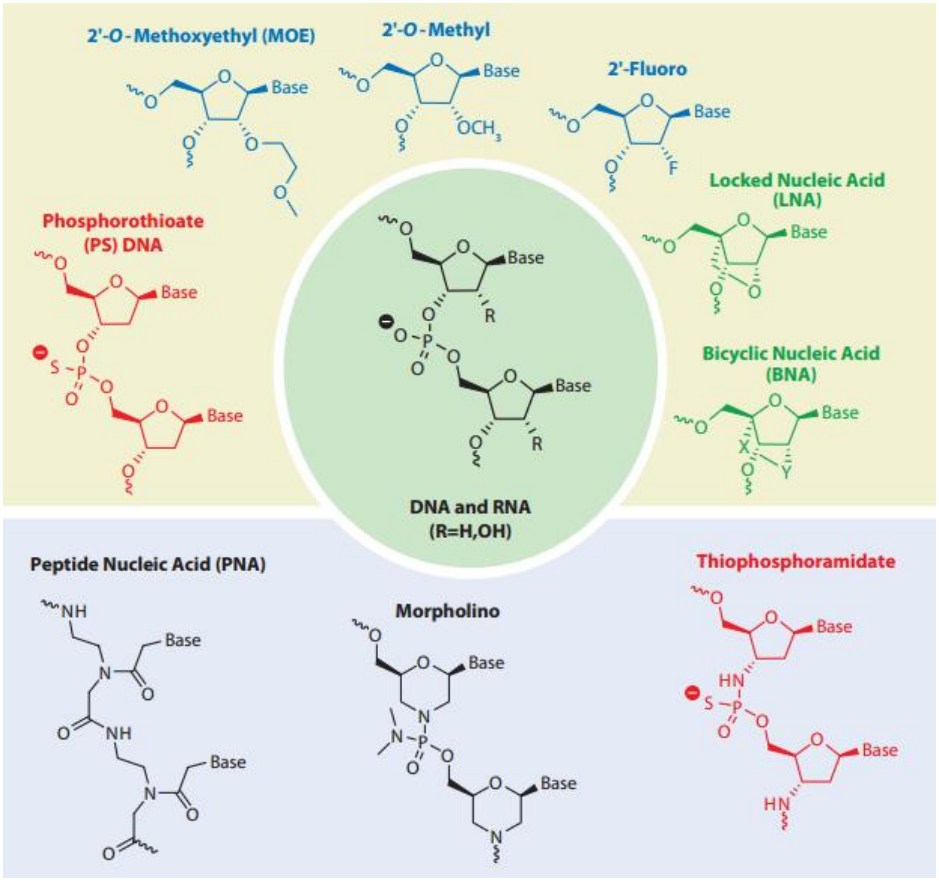

Fig 1.33: Chemical modifications used in antisense therapy:[99] *pg 272*

Alicaforsen (ISIS 2302) is a CNA used to treat ulcerative colitis and has found to have therapeutic effects when administered either intravenously or via daily topical administration.[100] There are numerous different modifications used in CNA research, a few of which can be seen in *Fig 1.33*. Morpholino based CNAs are used to modify gene expression, 'knocking down' certain genes to prevent protein formation.[101] This process is used as a tool to identify the function of unknown proteins in organisms.

1.9 References

1. Pascal R. Catalysis through induced intramolecularity: What can be learned by mimicking enzymes with carbonyl compounds that covalently bind substrates? European Journal of Organic Chemistry 2003 MAY 2003(10):1813-24.

2. Zasloff M. Antimicrobial peptides of multicellular organisms. Nature 2002 JAN 24 2002;415(6870):389-95.

3. Pattabiraman VR, Bode JW. Rethinking amide bond synthesis. Nature 2011 DEC 22;480(7378):471-9.

4. Ghose AK, Viswanadhan VN, Wendoloski JJ. A knowledge-based approach in designing combinatorial or medicinal chemistry libraries for drug discovery. 1. A qualitative and quantitative characterization of known drug databases. J Comb Chem 1999 JAN 1999;1(1):55-68.

5. Berg JM, Tymoczko JL, Stryer L. Section 29.1, protein synthesis requires the translation of nucleotide sequences into amino acid sequences. In: Biochemistry. 5th edition ed. New York: W H Freeman; 2002.

6. Montalbetti CAGN, Falque V. Amide bond formation and peptide coupling. Tetrahedron 2005 NOV 14 2005;61(46):10827-52.

7. Sheehan JC, Hess GP. A new method of forming peptide bonds. J Am Chem Soc 1955 1955;77(4):1067-8.

8. Valeur E, Bradley M. Amide bond formation: Beyond the myth of coupling reagents. Chem Soc Rev 2009 2009;38(2):606-31.

9. König W, Geiger R. Eine neue methode zur synthese von peptiden: Aktivierung der carboxylgruppe mit dicyclohexylcarbodiimid unter zusatz von 1-hydroxy-benzotriazolen. Chem Ber 1970(103):788-98.

10. Olah G, Kuhn S. Organic fluorine compounds: preparation of acyl fluorides with anhydrous hydrogen fluoride - general use of method of colson and fredenhagen. J Org Chem 1961;26(1):237.

11. Al-Zoubi RM, Marion O, Hall DG. Direct and waste-free amidations and cycloadditions by organocatalytic activation of carboxylic acids at room temperature. Angewandte Chemie-International Edition 2008;47(15):2876-9.

12. Lodish H, Berk A, Kaiser AC, Krieger M, Scott PM, Bretscher A, Ploegh H, Matsudaira P. Molecular cell biology. 6th Edition ed. New York: W. H. Freeman and Company; 2007.

13. Alberts B, Johnson A, Lewis J, Raff M, Roberts K, Walter P. Molecular biology of the cell. 4th Edition ed. New York: Garland Science; 2002.

14. Hille B. Ionic channels in excitable membranes. Biophysical Journal 1978;22(2):283-94.

15. MacKinnon R. Potassium channels and the atomic basis of selective ion conduction (Nobel lecture). Angewandte Chemie-International Edition 2004;43(33):4265-77.

16. Hodgkin AL, Huxley AF. A quantitative description of membrane current and its application to conduction and excitation in nerve. Journal of Physiology-London 1952;117(4):500-44.

17. Hodgkin AL, Keynes RD. The potassium permeability of a giant nerve fibre. Journal of Physiology-London 1955;128(1):61-88.

18. Armstrong CM. Evidence for ionic pores in excitable membranes. Biophysical Journal 1975;15(1):932-3.

19. Neher E, Sakmann B. Single-channel currents recorded from membrane of denervated frog muscle fibres. Nature 1976;260(5554):799-802.

20. MacKinnon R. Potassium channels. FEBS Lett 2003 NOV 27;555(1):62-5.

21. MacDonald PE, Wheeler MB. Voltage-dependent K^+ channels in pancreatic beta cells: Role, regulation and potential as therapeutic targets. Diabetologia 2003 AUG;46(8):1046-62.

22. Choe S. Potassium channel structures. Nature Reviews Neuroscience 2002;3(2):115-21.

23. Tombola F, Pathak MM, Isacoff EY. How does voltage open an ion channel? Annual Review of Cell and Developmental Biology 2006;22(1):23-52.

24. Doyle DA, Morais Cabral J, Pfuetzner RA, Kuo A, Gulbis JM, Cohen SL, Chait BT, MacKinnon R. The structure of the potassium channel: Molecular basis of K^+ conduction and selectivity. Science 1998 Apr 3;280(5360):69-77.

25. Armstrong CM, Hille B. Voltage-gated ion channels and electrical excitability. Neuron 1998 MAR;20(3):371-80.

26. Armstrong CM, Benzanilla F. Inactivation of the sodium channel II. gating current experiments. Journal of General Physiology 1977;70(5):549-66.

27. Sah P, Faber ESL. Channels underlying neuronal calcium-activated potassium currents. Progress in Neurobiology 2002;66(5):345-53.

28. Meech RW, Strumwas F. Intracellular calcium injection activates potassium conductance in aplysia nerve cells. Federation Proceedings 1970;29(2):A834.

29. Adelman JP, Shen KZ, Kavanaugh MP, Warren RA, Wu YN, Lagrutta A, Bond CT, North RA. Calcium-activated potassium channels expressed from cloned complementary DNAs. Neuron 1992;9(2):209-16.

30. Meera P, Wallner M, Song M, Toro L. Large conductance voltage- and calcium-dependent K^+ channel, a distinct member of voltage-dependent ion channels with seven N-terminal transmembrane segments (S0-S6), an extracellular N terminus, and an intracellular (S9-S10) C terminus. Proceedings of the National Academy of Sciences of the United States of America 1997;94(25):14066-71.

31. Brenner R, Jegla TJ, Wickenden A, Liu Y, Aldrich RW. Cloning and functional characterization of novel large conductance calcium-activated potassium channel b subunits, hKCNMB3 and hKCNMB4. Journal of Biological Chemistry 2000;275(9):6453-61.

32. Vergara C, Latorre R, Marrion NV, Adelman JP. Calcium activated potassium channels. Current Opinion in Neurobiology 1998;8(3):321-9.

33. Nichols CG, Lopatin AN. Inward rectifier potassium channels. Annu Rev Physiol 1997;59:171-91.

34. Bichet D, Haass FA, Jan LY. Merging functional studies with structures of inward rectifier K^+ channels. Nature Reviews Neuroscience 2003;4(12):957-67.

35. Fujiwara Y, Kubo Y. Ser165 in the second transmembrane region of the Kir2.1 channel determines its susceptibility to blockade by intracellular Mg^{2+}. Journal of General Physiology 2002;120(5):677-92.

36. Kuo AL, Gulbis JM, Antcliff JF, Rahman T, Lowe ED, Zimmer J, Cuthbertson J, Ashcroft FM, Ezaki T, Doyle DA. Crystal structure of the potassium channel KirBac1.1 in the closed state. Science 2003;300(5627):1922-6.

37. Kubo Y, Murata Y. Control of rectification and permeation by two distinct sites after the second transmembrane region in Kir2.1 K^+ channel. Journal of Physiology-London 2001;531(3):645-60.

38. Compston A, Coles A. Multiple sclerosis. Lancet 2002 APR 6;359(9313):1221-31.

39. Menge T, Weber MS, Hemmer B, Kieseier BC, von Buedingen H, Warnke C, Zamvil SS, Boster A, Khan O, Hartung H, Stuve O. Disease-modifying agents for multiple sclerosis recent advances and future prospects. Drugs 2008;68(17):2445-68.

40. Kurtzke JF. Epidemiologic evidence for multiple-sclerosis as an infection. Clin Microbiol Rev 1993 OCT;6(4):382-427.

41. Noseworthy JH, Lucchinetti C, Rodriguez M, Weinshenker BG. Medical progress: Multiple sclerosis. N Engl J Med 2000 SEP 28;343(13):938-52.

42. Billiau A, Kieseier BC, Hartung HP. Biologic role of interferon beta in multiple sclerosis. J Neurol 2004 JUN;251:10-4.

43. Arnon R, Aharoni R. Mechanism of action of glatiramer acetate in multiple sclerosis and its potential for the development of new applications. Proc Natl Acad Sci U.S.A 2004 OCT 5;101:14593-8.

44. Lang SK, Burow A, Kurrer M, Lang AP, Recher M. The role of the innate immune response in autoimmune disease. Journal of Autoimmunity 2007;29(4):206-12.

45. Oleson RD, DeFelice JL, Donahoe MR. A comparison of K^+ channel characteristics in human T cells:Perforated-patch versus whole-cell recording techniques. The Journal of Membrane Biology 1993;132(3):229-41.

46. Judge SI, Bever CT. Potassium channel blockers in multiple sclerosis: Neuronal K_V channels and effects of symptomatic treatment. Pharmacol Ther 2006 JUL;111(1):224-59.

47. Armstrong CM, Loboda A. A model for 4-aminopyridine action on K channels: Similarities to tetraethylammonium ion action. Biophysical Journal 2001;81(2):859-904.

48. Choquet D, Korn H. Mechanism of 4-aminopyridine action on voltage-gated potassium channels in lymphocytes. Journal of General Physiology 1992;99(2):217-40.

49. Polman CH, Bertelsmann FW, DeWaal R, Vandiemen HAM, Uitdehaag BMJ, Vanloenen AC, Koetsier JC. 4-aminopyridine is superior to 3,4-diaminopyridine in the treatment of patients with multiple sclerosis. Archives of Neurology 1994;51(11):1136-9.

50. Chandy KG, Wulff H, Beeton C, Pennington M, Gutman GA, Cahalan MD. K+ channels as targets for specific immunomodulation. Trends In Pharmacological Sciences 2004;25(5):280-9.

51. Kharrat R, Mabrouk K, Crest M, Darbon H, Oughideni R, MartinEauclaire MF, Jacquet G, ElAyeb M, VanRietschoten J, Rochat H, Sabatier JM. Chemical synthesis and characterization of maurotoxin, a short scorpion toxin with four disulfide bridges that acts on K+ channels European Journal of Biochemistry 1996;243(3):491-8.

52. Yednock TA, Cannon C, Fritz LC, Sanchezmadrid F, Steinman L, Karin N. Prevention of experimental autoimmune encephalomyelitis by antibodies angainst alpha-4-beta-1 integrin. Nature 1992;356(6364):63-6.

53. Berger JR, Koralnik IJ. Progressive multifocal leukoencephalopathy and natalizumab - unforeseen consequences. New England Journal of Medicine 2005;353(4):414-6.

54. Ren YZR, Pan F, Parvez S, Fleig A, Chong CR, Xu J, Dang YJ, Zhang J, Jiang HS, Penner R, Liu JO. Clofazimine inhibits human Kv1.3 potassium channel by perturbing calcium oscillation in T lymphocytes. PLOS ONE 2008;3(12):1-11.

55. Vennekamp J, Wulff H, Beeton C, Calabresi PA, Grissmer S, Hansel W, Chandy KG. Kv1.3-blocking 5-phenylalkoxypsoralens: A new class of immunomodulators. Molecular Pharmacology 2004;65(6):1364-74.

56. Matyus P, Varro A, Papp JG, Wamhoff H, Varga I, Virag L. Antiarrhythmic agents: Current status and perspectives. Medicinal Research Reviews 1997;17(5):427-51.

57. Pugsley MK. Antiarrhythmic drug development: Historical review and future perspective. Drug Development Research 2002;55(1):3-16.

58. Singh BN, Kowey PR. Evidence and potential: Beta-blockers as antiarrhythmic agents in the patient with cardiovascular disease. JOURNAL OF Cardiovascular Pharmacology and Therapeutics 2005;10(1):S1-2.

59. Friedman LM. A randomized trial of propranolol in patients with acute myocardial infarction I. mortality results. Journal of the American Medical Association 1982;247(12):1707-14.

60. Armstrong PW, Moe GW. Medical advances in the treatment of congestive heart failure. Circulation 1993;88(6):2941-52.

61. Anderson JL, Prystowsky EN. Sotalol: An important new antiarrhythmic. American Heart Journal 1999;137(3):388-409.

62. Vandenberg JI, Walker BD, Campbell TJ. HERG K^+ channels: Friend and foe. Trends in Pharmacological Sciences 2001;22(5):240-6.

63. Brendorp B, Pedersen OD, Torp-Pedersen C, Sahebzadah N, Kober L. A benefit-risk assessment of class III antiarrhythmic agents. Drug Safety 2002;25(12):847-65.

64. Van Gelder IC, Brugemann J, Crijns, H. J. G. M. Current treatment recommendations in antiarrhythmic therapy. Drugs 1998;55(3):331-46.

65. Podrid PJ. Amiodarone: Reevaluation of an old drug. Annals of Internal Medicine 1995;122(9):689-700.

66. Savelieva I, Camm J. Anti-arrhythmic drug therapy for atrial fibrillation: Current anti-arrhythmic drugs, investigational agents, and innovative approaches. EUROPACE 2008;10(6):647-65.

67. Hoy SM, Keam SJ. Dronedarone. Drugs 2009;69(12):1647-63.

68. Carlsson l, Duker G, Jacobson I. New pharmacological targets and treatments for atrial fibrillation. Trends in Pharmacological Sciences 2010;31(8):364-71.

69. Mason PK, DiMarco JP. New pharmacological agents for arrhythmias. Circulation-Arrhythmia and Electrophysiology 2009;2(5):588-97.

70. Zimmet P, Alberti K.G.M.M., Shaw J. Global and societal implications of the diabetes epidemic. Nature 2001;414(6865):782-7.

71. Dean L, McEntyre J. The genetic landscape of diabetes. 1st ed. New York: Bethesda; 2004.

72. Ashcroft FM, Gribble FM. ATP-sensitive K^+ channels and insulin secretion: Their role in health and disease. Diabetologia 1999 AUG;42(8):903-19.

73. Rendell M. The role of sulphonylureas in the management of type 2 diabetes mellitus. Drugs 2004;64(12):1339-58.

74. Sheehan MT. Current therapeutic options in type 2 diabetes mellitus: A practical approach. Clinical Medicine & Research 2003;1(3):189-200.

75. Harrower ADB. Comparative tolerability of sulphonylureas in diabetes mellitus. Drug Safety 2000;22(4):313-30.

76. Szoke E, Gosmanov NR, Sinkin JC, Nihalani A, Fender AB, Cryer PE, Meyer C, Gerich JE. Effects of glimepiride and glyburide on glucose counterregulation and recovery from hypoglycemia. Metabolism-Clinical and Experimental 2006;55(1):78-83.

77. Hellman B, Sehlin J, Taljedal IB. Glibenclamide is exceptional among hypoglycaemic sulphonylureas in accumulating progressively in beta-cell-rich pancreatic islets. Acta Endocrinologica 1984;105(3):385-90.

78. Mizuno CS, Chittiboyina AG, Kurtz TW, Pershadsingh HA, Avery MA. Type 2 diabetes and oral antihyperglycemic drugs. Current Medicinal Chemistry 2008;15(1):61-74.

79. Kahn SE, Montgomery B, Howell W, Ligueros-Saylan M, Hsu CH, Devineni D, McLeod JF, Horowitz A, Foley JE. Importance of early phase insulin secretion to intravenous glucose tolerance in subjects with type 2 diabetes mellitus. Journal of Clinical Endocrinology & Metabolism 2001;86(12):5824-9.

80. Hill D, Mio M, Prince R, Hughes T, Moore J. A field guide to foldamers. Chem Rev 2001 DEC;101(12):3893-4011.

81. Gellman S. Foldamers: A manifesto. Acc Chem Res 1998 APR;31(4):173-80.

82. Goodman CM, Choi S, Shandler S, DeGrado WF. Foldamers as versatile frameworks for the design and evolution of function. Nat Chem Biol 2007 May;3(5):252-62.

83. Pauling L, Corey R. Atomic coordinates and structure factors for 2 helical configurations of polypeptide chains. Proc Natl Acad Sci U.S.A 1951;37(5):235-40.

84. Nelson DL, Lehninger AL, Cox MM. Lehninger principles of biochemistry. Macmillan; 2008.

85. Stanger H, Syud F, Espinosa J, Giriatt I, Muir T, Gellman S. Length-dependent stability and strand length limits in antiparallel beta-sheet secondary structure. Proc Natl Acad Sci U.S.A 2001 OCT 9;98(21):12015-20.

86. Chan H, Dill K. Polymer principles in protein-structure and stability. Annu Rev Biophys Biophys Chem 1991;20:447-90.

87. Richard J, Melikov K, Vives E, Ramos C, Verbeure B, Gait M, Chernomordik L, Lebleu B. Cell-penetrating peptides - A reevaluation of the mechanism of cellular uptake. J Biol Chem 2003 JAN 3;278(1):585-90.

88. Bautista AD, Craig CJ, Harker EA, Schepartz A. Sophistication of foldamer form and function in vitro and in vivo. Curr Opin Chem Biol 2007 DEC;11(6):685-92.

89. Umezawa N, Gelman M, Haigis M, Raines R, Gellman S. Translocation of a beta-peptide across cell membranes. J Am Chem Soc 2002 JAN 23;124(3):368-9.

90. Potocky T, Menon A, Gellman S. Effects of conformational stability and geometry of guanidinium display on cell entry by ss-peptides. J Am Chem Soc 2005 MAR 23;127(11):3686-7.

91. Gillies ER, Deiss F, Staedel C, Schmitter J, Huc I. Development and biological assessment of fully water-soluble helical aromatic amide foldamers. Angewandte Chemie-International Edition 2007;46(22):4081-4.

92. Kritzer J, Stephens O, Guarracino D, Reznik S, Schepartz A. Beta-peptides as inhibitors of protein-protein interactions. Bioorg Med Chem 2005 JAN 3;13(1):11-6.

93. Seebach D, Overhand M, Kuhnle FNM, Martinoni B, Oberer L, Hommel U, Widmer H. Beta-peptides: Synthesis by arndt-eistert homologation with concomitant peptide coupling. structure determination by NMR and CD spectroscopy and by X-ray crystallography. helical secondary structure of a beta-hexapeptide in solution and its stability towards pepsin. Helv Chim Acta 1996;79(4):913-41.

94. Arvidsson P, Rueping M, Seebach D. Design, machine synthesis, and NMR-solution structure of a beta-heptapeptide forming a salt-bridge stabilised 3(14)-helix in methanol and in water. Chem Commun 2001(7):649-50.

95. Stein CA, Cheng YC. Antisense oligonucleotides as therapeutic agents - is the bullet really magical. Science 1993 AUG 20 1993;261(5124):1004-12.

96. Levin AA. A review of issues in the pharmacokinetics and toxicology of phosphorothioate antisense oligonucleotides. Biochimica Et Biophysica Acta-Gene Structure and Expression 1999 DEC 10 1999;1489(1):69-84.

97. Crooke ST. Progress in antisense technology. Annu Rev Med 2004 2004;55:61-95.

98. Neurath M, Pettersson S, ZumBuschenfelde K, Strober W. Local administration of antisense phosphorothioate oligonucleotides to the p65 subunit of NF-kappa B abrogates established experimental colitis in mice. Nat Med 1996 SEP;2(9):998-1004.

99. Bennett CF, Swayze EE. RNA targeting therapeutics: Molecular mechanisms of antisense oligonucleotides as a therapeutic platform. Annu Rev Pharmacol Toxicol 2010 2010;50:259-93.

100. Miner PB. Bioavailability and therapeutic activity of alicaforsen (ISIS 2302) administered as a rectal retention enema to subjects with active ulcerative colitis. Aliment Pharmacol Ther 2006 MAY 15 2006;23(10):1427-34.

101. Heasman J. Morpholino oligos: Making sense of antisense? Dev Biol 2002 MAR 15 2002;243(2):209-14.

CHAPTER 2

Synthesis and Characterisation of a Range of Substituted Benzamide Isomer Grids

2.1 Introduction

2.1.1 Structural systematics

Over the past three decades, huge leaps have been made in the area of combinatorial chemistry, which allows for the high throughput synthesis, characterisation and screening of small organic molecules.[1] This approach to finding a viable 'lead' molecule creates libraries of similar organic molecules.[2] Once a suitable molecule with the correct properties is found, it is analysed and biologically screened for activity on its target. A *Structure-Activity Relationship* (SAR) study can also be run.

A SAR study is a computational method used to ascertain whether a similar molecule with slightly different functional groups have the same effect in the cell.[3] This technique makes the assumption that similar molecules will react similarly under the same conditions.[4] In some cases, a good 'lead' is found but has functional groups that react unfavourably in the body. To keep the same bioactivity, a 'Bioisostere' must be used in place of the functional group in question. The definition of a bioisostere is:

"*Compounds or groups that possess near-equal molecular shapes and volumes, approximately the same distribution of electrons, and which exhibit similar physical properties.*" [5]

One issue with this particular branch of chemistry is that it focuses strongly on single molecule analysis. Once a molecule is found to fit the necessary solubility, bioactivity and lipophilicity needed to transport itself across the various cell membranes, full analysis is performed.[6] This includes but is not limited to NMR, Mass Spectrometry and X-ray crystallography. Any structural features that look unusual could be written off as outliers or experimental errors.
Structural systematics allows for a different approach towards small molecule analysis. By looking at a number of similar compounds, any unusual features can be rationalized and explained in physiochemical terms.[7]

Structural systematics relies on multidisciplinary techniques to allow the researcher to analyse and rationalise a wide variety of structural and physiochemical data using a combination of X-ray crystallography and molecular modelling.

2.1.2 Benzamides

The structural study undertaken for Chapter 2 involves the synthesis of *N*-(pyridyl)benzamides, a system with two aromatic rings connected by an amide. The substituents used were bromine atoms incorporated as *(*Bromo-*N*-(pyridyl)benzamide) **Brxx**, and iodine atoms (Iodo-*N*-(pyridyl)benzamide), **Ixx**. The 3×3 isomer grids were built by varying the position of the halogen atoms and as well as the position of the pyridine nitrogen atom (*Fig 2.1*).

Benzamides have previously been shown to have therapeutic value as K_v channel blockers and activators, and are used in the treatment of multiple sclerosis and Lambert–Eaton myasthenic syndrome.[8-9] Pyridinecarboxamides were also included in the structural study, as they are near identical to the pyridine derivatives analysed (as congeners), differing only in the direction of the amide bridge between aromatic rings. Some simple carboxamides, for example nicotinamide, has recently been shown to prevent cognitive deficits in mice models with Alzheimer's disease.[10] Both these isomer grids will be useful for structural and medicinal studies in future research work and are depicted in *Fig 2.1*.

The nomenclature for the chapter 2 compounds is summarized in Tables 2.1 and 2.2;

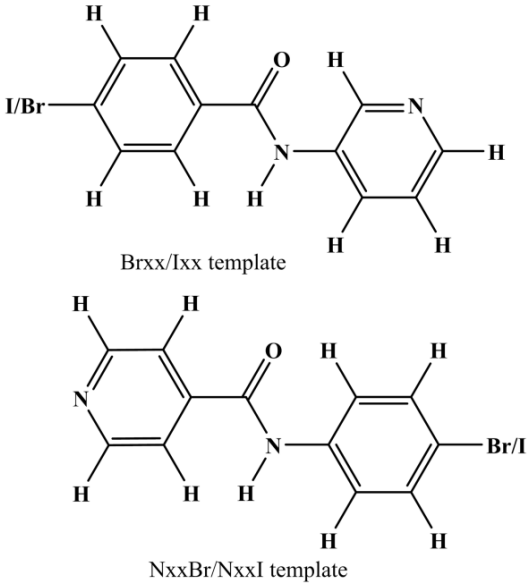

Fig 2.1: Chapter 2 ***Brxx/Ixx/NxxBr*** *template:*

*Table 2.1 Structures and nomenclature of **Brxx** and **Ixx** isomer grids.*

	Brxx			**Ixx**		
	***p*-bromo benzoyl**	***m*-bromo benzoyl**	***o*-bromo benzoyl**	***p*-iodo benzoyl**	***m*-iodo benzoyl**	***o*-iodo benzoyl**
***para* (4-aminopyridinyl)**	**Brpp**	**Brmp**	**Brop**	**Ipp**	**Imp**	**Iop**
***meta* (3-aminopyridinyl)**	**Brpm**	**Brmm**	**Brom**	**Ipm**	**Imm**	**Iom**
***ortho* (2-aminopyridinyl)**	**Brpo**	**Brmo**	**Broo**	**Ipo**	**Imo**	**Ioo**

*Table 2.2: Nomenclature of **NxxBr** and **NxxI** grid.*

	NxxBr			**NxxI**		
	***para* (4-Bromophenyl)**	***meta* (3-Bromophenyl)**	***ortho* (2-Bromophenyl)**	***para* (4-Bromophenyl)**	***meta* (3-Bromophenyl)**	***ortho* (2-Bromophenyl)**
4-pyridine carboxamide	**NppBr**	**NpmBr**	**NpoBr**	**NppI**	**NpmI**	**NpoI**
3-pyridine carboxamide	**NmpBr**	**NmmBr**	**NmoBr**	**NmpI**	**NmmI**	**NmoI**
2-pyridine carboxamide	**NopBr**	**NomBr**	**NooBr**	**NopI**	**NomI**	**NooI**

The mechanism of the reaction is depicted as follows;

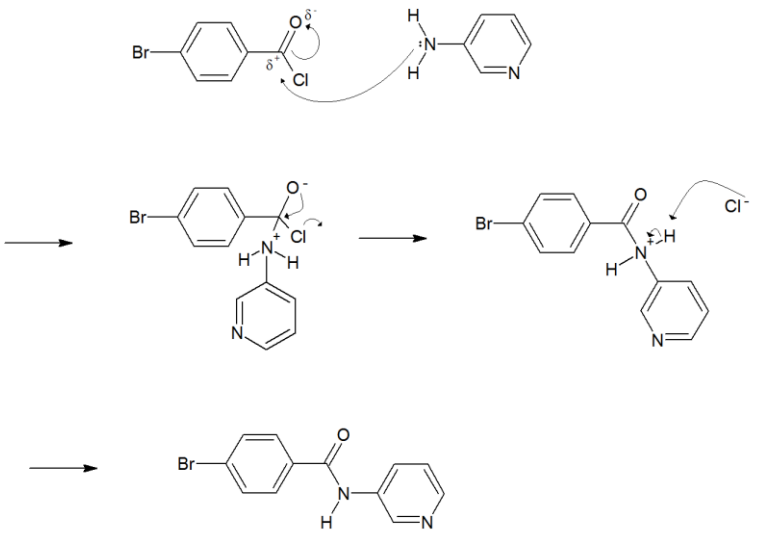

Fig 2.2: Schotten-Baumann reaction mechanism:

The acyl chloride group acts as an electrophile in the reaction, with the amine acting as the nucleophile. The quaternary carbon is electron deficient as it is bonded to two electron-withdrawing species, which both pull electron density away from the carbon. This δ^+ charge attracts the lone pair of the primary amine attached to the pyridine ring system and a C-N bond forms with loss of the Cl^-. This loss of chlorine also helps the reaction proceed as it is a good leaving group and makes the reaction thermodynamically favourable (*Fig 2.2*).

The acyl chloride group, however, causes some problems with the relative ease of which it will lose the chlorine atom. Acyl chlorides undergo hydrolysis to the corresponding carboxylic acid in the presence of water. For this reaction, bromo-benzoic acid would be the unwanted product formed. To prevent this unwanted formation of a carboxylic acid, the reaction is performed in the absence of water, under nitrogen gas and with anhydrous solvents used where possible (*Fig 2.3*).

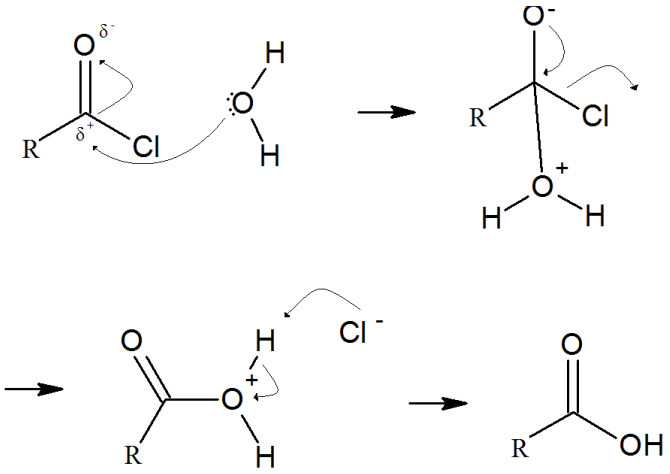

Fig 2.3: Competitive reaction of acyl chlorides with water:

The C-N bond formation results in a positive charge on the nitrogen, which in turn causes the loss of an H^+ ion to the solution. The H^+ ion is then picked up by the chlorine, forming HCl. This formation of hydrochloric acid is an issue, as the presence of acid will inhibit the aminopyridines ability to donate its lone pair, by protonating the amine group as seen in *Fig 2.4*.

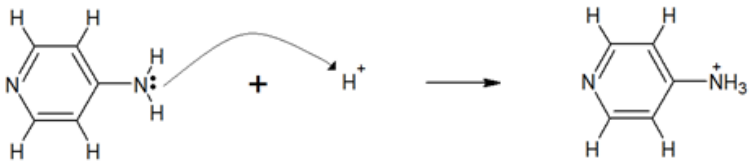

Fig 2.4: Unwanted protonation of the amine group:

This side reaction is prevented by the addition of a base, in this case triethylamine (TEA). The TEA neutralises the acid, producing a triethylamine salt, which can be removed from the product by washing as depicted in *Fig 2.5*.

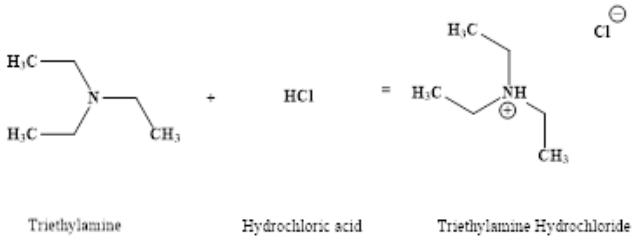

Fig 2.5: Neutralisation of HCl using TEA:

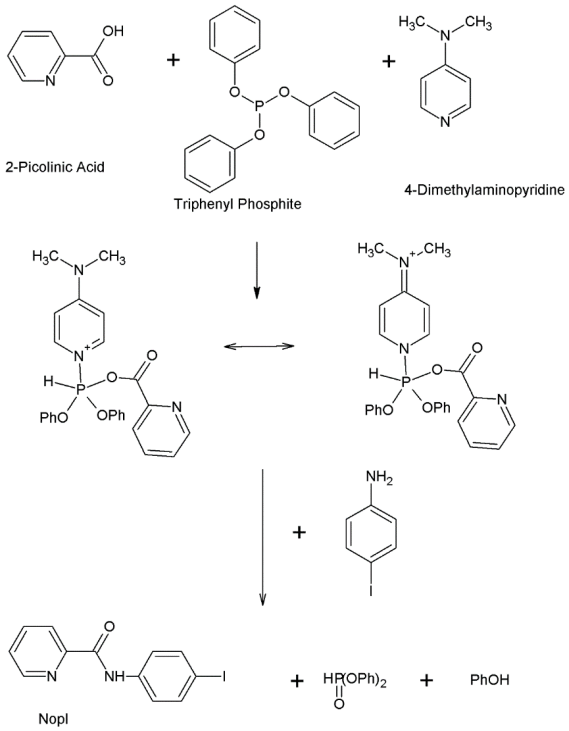

*Fig 2.6: Reaction scheme for **NxxBr** and **NxxI** ortho series:*

For the **NxxBr**, **NxxI** *ortho* series of compounds and the majority of the **Ixx** reactions, a different approach to amide bond synthesis was undertaken. The mechanism used in these reactions was also an acyl chloride nucleophilic substitution but was carried out by reacting a carboxylic acid with an amine in the presence of triphenyl phosphite and pyridine. This reaction required separating the desired isomer by ionizing the amide substituent on the product and allowing it to dissolve into an aqueous layer; it was then separated from the organic layer, and neutralized to allow for the precipitation of the target compound. The triphenyl phosphite forms an intermediary species with the 2-picolinic acid, which has two resonance forms that transfer the charge across the two nitrogens.

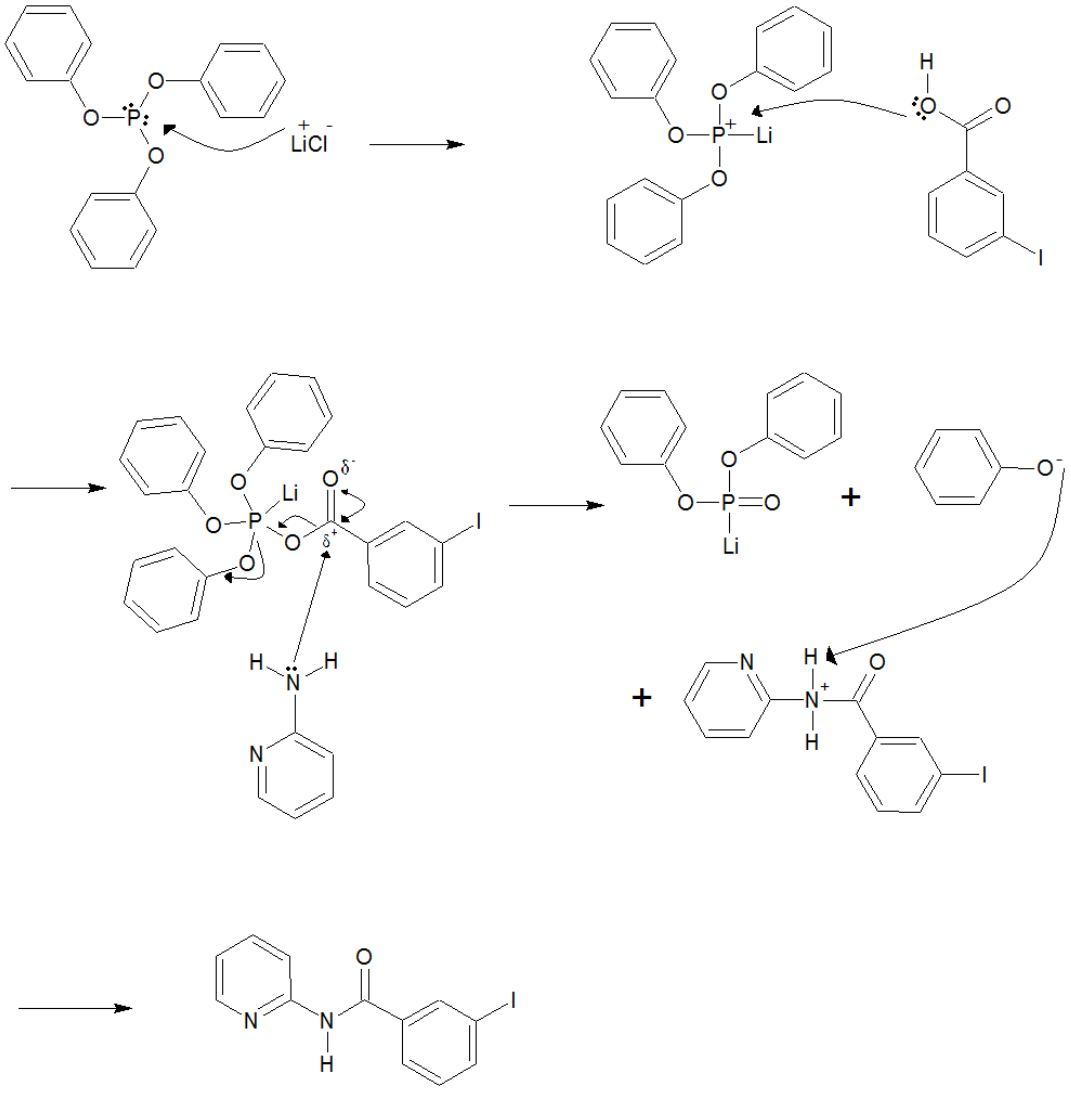

*Fig 2.7: Reaction mechanism for **NxxBr/NxxI/Ixx** ortho- series:*

2.2 Synthetic Procedure

2.2.1 Brxx series

Into a round bottomed flask, approximately 30ml of dichloromethane (CH_2Cl_2) was added. 0.941 g (0.005 mol) of the appropriate aminopyridine was then added to the flask, with stirring. In order to keep the reaction in a relatively water-free environment, the reaction was performed under nitrogen. A nitrogen bubbler was attached to the top of the flask and nitrogen was passed through the reaction vessel for a few minutes to ensure all the air in the flask was removed before the addition of the bromobenzoyl chloride. 2.78ml of triethylamine (TEA) was added to the flask, again with stirring. The appropriate bromobenzoyl chloride compound was then added. The reaction commenced on addition of the bromobenzoyl chloride. The reaction was then allowed to run for 12 hours, with stirring and a slow, steady flow of nitrogen. In some cases, a precipitate was formed during the reaction. After the reaction was completed, the reaction mixture was filtered to separate this precipitate using vacuum filtration. This precipitate was then washed with cold CH_2Cl_2 (DCM) and stored separately until it could be ascertained whether it was product or an impurity. The filtrate was then washed further to separate impurities from the product. The reaction mixture was transferred to a 250 ml separating funnel and washed using 4×100 ml 1% w/v $KHCO_3$ aqueous solution, which was made by the addition of 1 g of $KHCO_3$ to 100ml water. A 100 ml aliquot of the $KHCO_3$ solution was added to the reaction mixture. Separation was then carried out.

*Table 2.3: Reagents used for **Brxx** series:*

Reagent	Molar Mass (g/mol)	Density (g/cm^3)	Volume (ml)	Mass (g)	Concentration (mol)
2-Aminopyridine	94.1	n/a	n/a	0.941	0.01
3-Aminopyridine	94.1	n/a	n/a	0.941	0.01
4-Aminopyridine	94.1	n/a	n/a	0.941	0.01
2-Bromobenzoyl Chloride	219.46	1.679	1.30	n/a	0.01
3-Bromobenzoyl Chloride	219.46	1.662	1.32	n/a	0.01
4-Bromobenzoyl Chloride	219.46	n/a	n/a	2.19	0.01
Triethylamine	101.19	0.726	2.78	n/a	0.02

2.2.2 NxxBr series

For the **NpxBr** and **NmxBr** reactions, the setup was similar to the one used in the **Brxx** reactions. Into a round bottomed flask, approximately 30 ml of dichloromethane was added. 0.01 mol of the appropriate bromoaniline was then added to the flask, with stirring. After the addition of 3 ml of TEA, 0.01 mol of the corresponding acyl chloride was added and the reaction was left overnight under nitrogen. In the **NoxBr** trio of reactions, a different synthetic procedure was used, due to the lack of reactivity of the *ortho*- bromoaniline under the previous acyl chloride reaction conditions. A round bottomed flask was clamped in a sand bath on a stirring plate and heater and a magnetic stirrer placed in it. Then 2.46 g picolinic acid was transferred into the flask along a solution of 0.85 g lithium chloride and 5.2 ml triphenylphosphite in 40-50 ml pyridine. Then 0.02 M of the relevant bromoaniline was added to the flask and a reflux condenser was fitted to the top. The reaction mixture was then heated under reflux at 110°C for at least 4-5 hours.

The product was then rotary evaporated and re-dissolved in 100-150 ml dichloromethane and transferred to a separating funnel. The product was washed with a 150ml 1:1 aqueous hydrochloric acid (HCl) solution. The aqueous phase was retained and the organic phase was washed another 2-3 times with aqueous HCl. The aqueous phases were then combined and neutralized using sodium carbonate to cause the product to precipitate out of the solution. The product was then removed by gravity filtration.

*Table 2.4: Reagents used for **NxxBr** series:*

Reagent	Molar mass (g/mol)	Density (g/cm^3)	Volume (ml)	Mass (g)	Concentration (mol)
2-bromoaniline	172.02	n/a	n/a	1.72	0.01
3-bromoaniline	172.02	1.58	1.089	n/a	0.01
4-bromoaniline	172.02	n/a	n/a	1.72	0.01
Isonicotinoyl chloride	178.02	n/a	n/a	1.78	0.01
Nicotinoyl chloride	178.02	n/a	n/a	1.78	0.01
Picolinic acid	123.11	n/a	n/a	2.46	0.02
Triethylamine	101.19	0.726	2.788	n/a	0.02
Triphenylphosphite	310.28	1.184	5.24	n/a	0.02
Lithium chloride	42.4	n/a	n/a	0.85g	0.02

2.2.3 Ixx series

A two-neck round-bottomed flask with Liebig condenser and stirring bar was set up for a reflux reaction. 2-picolinic acid (5.17 mmol) was weighed out accurately using an analytical balance and added into the RBF. Then 15 ml of pyridine and 20 ml of toluene were added into the RBF and allowed to stir until the 2-picolinic acid had fully dissolved. 0.2195 g of lithium chloride (5.18 mmol), 5-10 mg of DMAP, 1.31 ml of triphenylphosphite and 2.1 ml of TEA were added (over two minutes) into the solution. The solution was allowed to stir before adding 5.0 mmol of the relevant iodoaniline (5.03 mmol). The reaction mixture was heated under reflux at 110°C for 4-5 hours. After this time had elapsed, the solution was cooled and capped.

The reaction mixture was then washed similarly to the **NxxBr** *ortho* series above.

*Table 2.5: Reagents used for **Ixx** series.*

Reagent	Molar mass (g/mol)	Density (g/cm^3)	Volume (ml)	Mass (g)	Concentration (mol)
2-aminopyridine	94.11	n/a	n/a	0.47	0.005
3-aminopyridine	94.11	n/a	n/a	0.47	0.005
4-aminopyridine	94.11	n/a	n/a	0.47	0.005
4-iodobenzoyl chloride	266.46	n/a	n/a	1.33	0.005
2-iodobenzoyl chloride	266.46	n/a	n/a	1.33	0.005
3-iodobenzoic acid	248.02	n/a	n/a	1.24	0.005
Triethylamine	101.19	0.73	3	n/a	0.02
Triphenylphosphite	310.28	1.19	1.31	n/a	0.005
Lithium Chloride	42.39	n/a	n/a	0.21	0.005

2.2.4 NxxI series

The first six compounds of the **NxxI** series were synthesised using the method outlined in the **Brxx** synthetic procedure above, see section 2.2.1. The *ortho*-series, however, had very low reactivity, and no usable products were isolated from the standard LiCl and triphenylphosphite reaction. An EDC coupling reaction was used to form the amide bridge.[11]

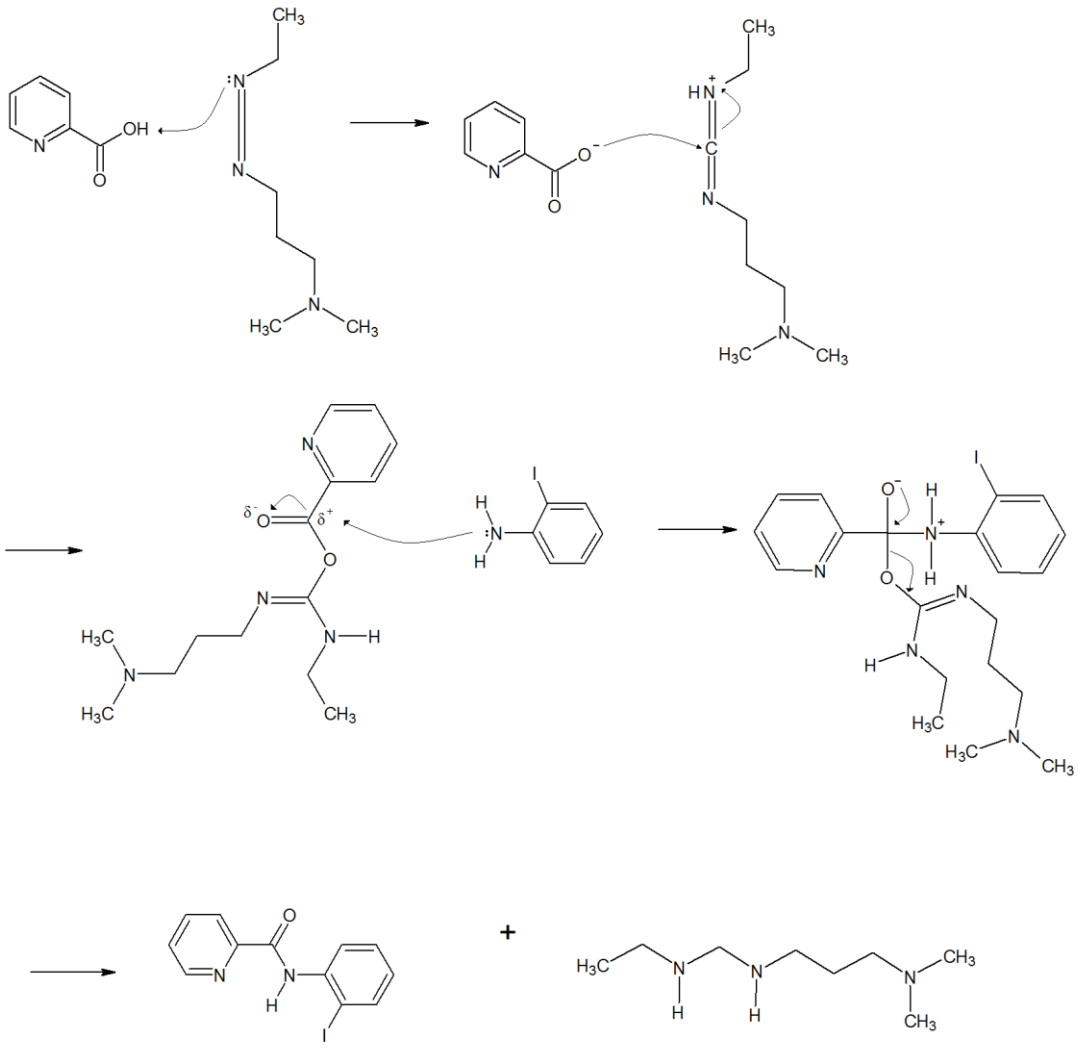

Fig 2.8: EDC coupling reaction mechanism:

2.3 Synthetic Results

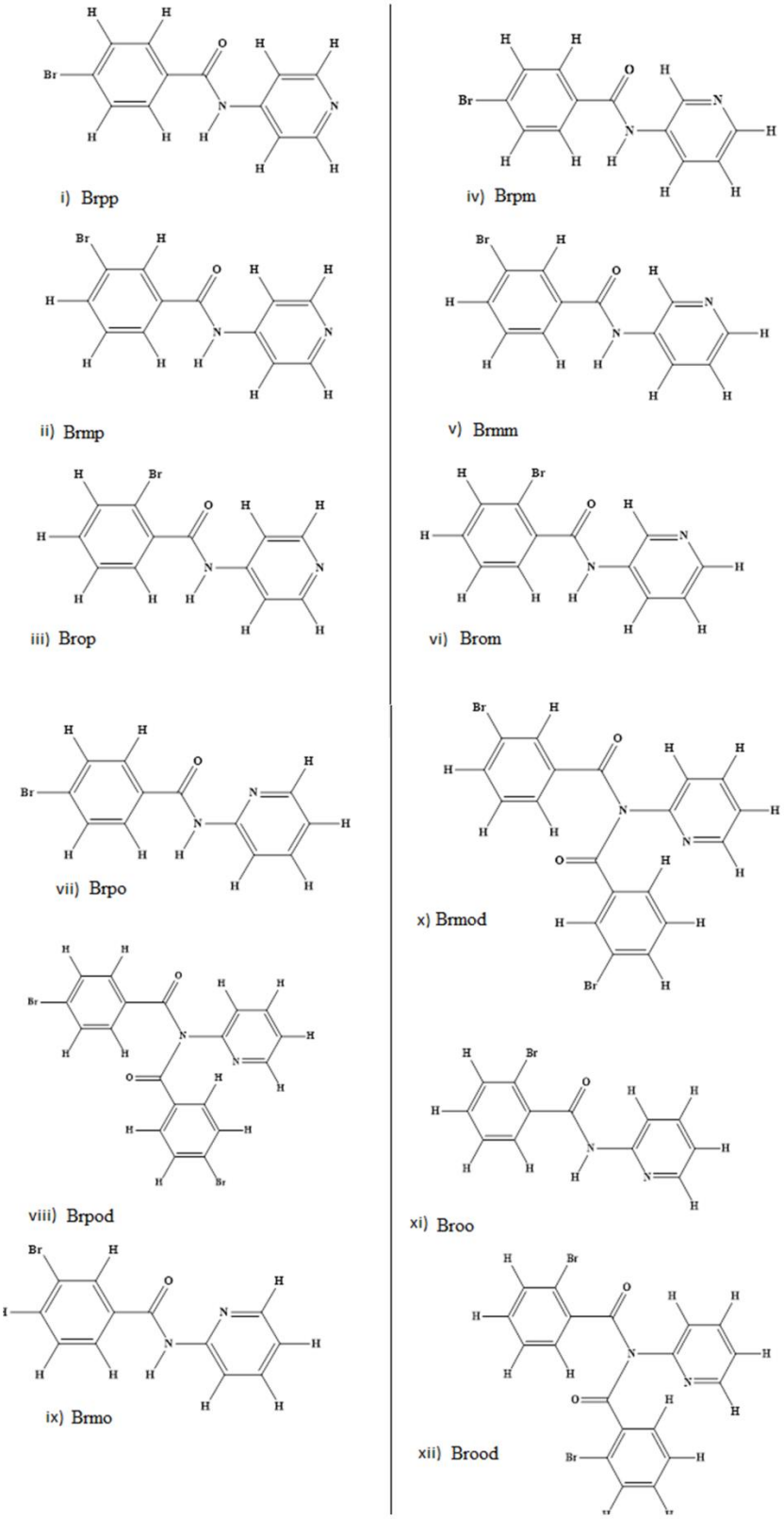

*Fig 2.9: Structures of 12 compounds synthesised in **Brxx** series:*

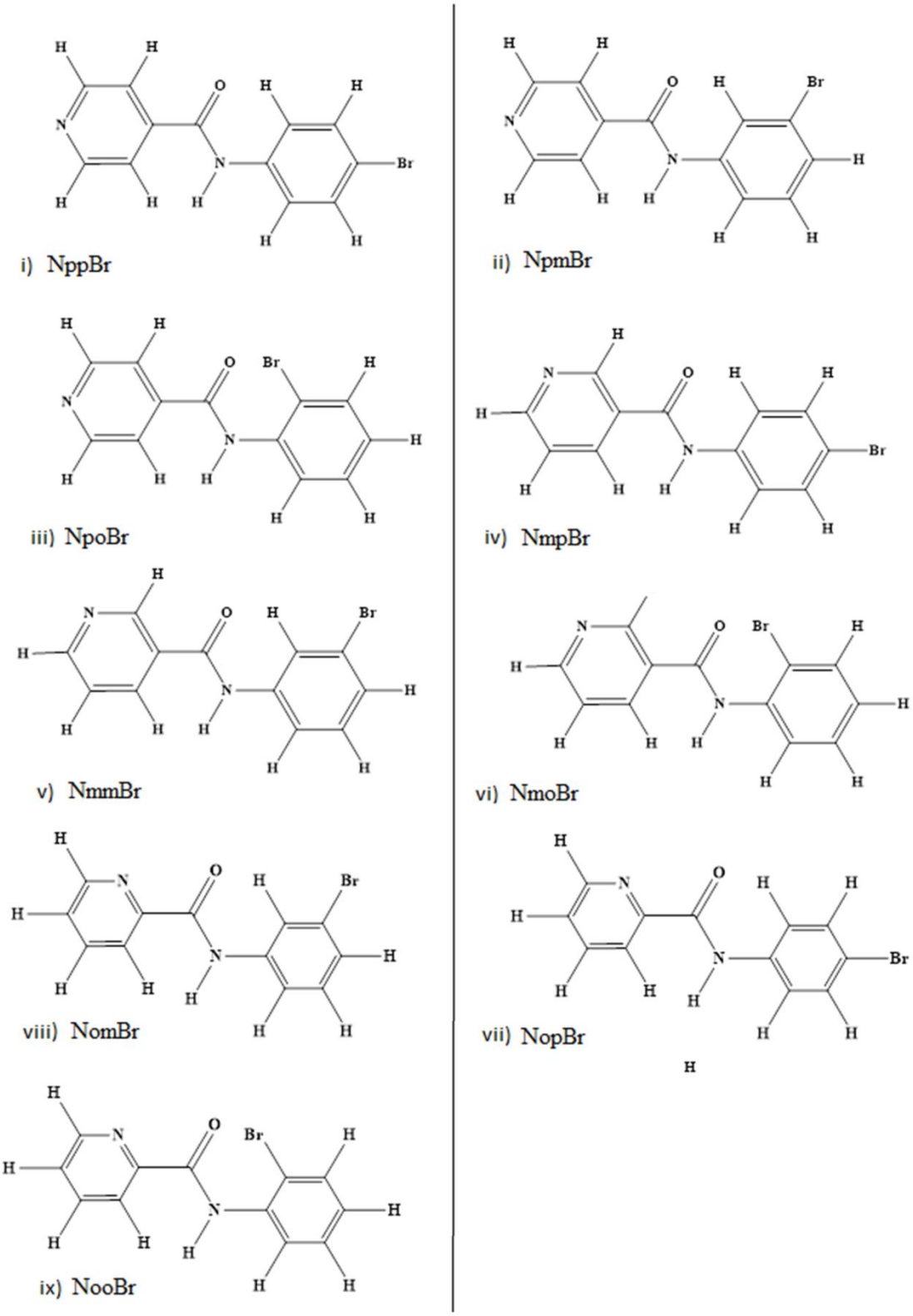

*Fig 2.10: Structures of 9 compounds synthesised in **NxxBr** series:*

*Table 2.6: Results of **Brxx** reactions:*

	Melting Point (°C)	**Yield (g)**	**N-H Peak DMSO d^6 (ppm)**	**N-H Peak $CDCl_3$ (ppm)**	**Significant IR Peaks (cm^{-1})**
Brpp	187-189	1.4 51%	10.68	7.94	3250, 1677, 1502
Brpm	157-160	1.124 41%	10.52	8.6	3333, 1653, 1520
Brpo	130-134	1.63 59%	n/a	8.56	2952, 1673, 1584
Brmp	161-162	1.64 59%	10.71	7.89	2929, 1674, 1504
Brmm	121-123	1.427 52%	10.57	8.0	3111, 1683, 1542
Brmo	115-120	1.345 49%	10.96	n/a	3248, 1680, 1580
Brop	175-178	1.412 51%	10.92	8.87	2971, 1684, 1521
Brom	117-120	1.27 46%	10.75	8.13	2816, 1686, 1584
Broo	n/a	1.08 38% mix	n/a	n/a	n/a
Brpod	160-162	n/a	n/a	n/a	2703, 1690, 1583
Brmod	145-147	n/a	n/a	n/a	2921, 1683, 1580
Brood	n/a	n/a	n/a	n/a	n/a

Significant peaks in IR indicate the presence of an N-H stretching vibration around 3200-2700 cm^{-1}, as well as C=O carbonyl stretching at 1690-1653 cm^{-1} and C=C stretching at 1500-1580 cm^{-1}. N/A is used in the tables in this chapter to denote where the reactions did not yield enough product for a full spectroscopic workup. In some cases only DMSO d^6 NMRs were run to leave enough compound to attempt crystal growth.

*Table 2.7: Results of **NxxBr** reactions:*

	Melting Point (°C)	**Yield (g)**	**N-H Peak DMSO d^6 (ppm)**	**N-H Peak $CDCl_3$ (ppm)**	**Significant IR Peaks (cm^{-1})**
NppBr	161-162	1.265 22%	10.64	8.04	3309, 3048, 1658
NpmBr	224-225	0.752 13%	10.59	8.44	3233, 3035, 1685, 1588
NpoBr	165-166	0.1930 5%	10.32	9.98	3056, 1681, 1585, 1519
NmpBr	184-185	0.4025 7%	10.65	7.5	3245, 3075, 1670
NmmBr	126-127	1.098 19%	10.60	8.39	3320, 1654, 1586, 1537
NmoBr	105-106	1.55 14%	10.85	8.6	3059, 1691, 1578, 1480
NopBr	133-134	0.8106 14%	10.60	8.39	3320, 3041, 1654, 1586
NomBr	89-91	2.71 mix	10.34	8.42	3265, 1655, 1587, 1515
NooBr	121-122	0.201 2%	n/a	n/a	3282, 3100, 1607, 1587

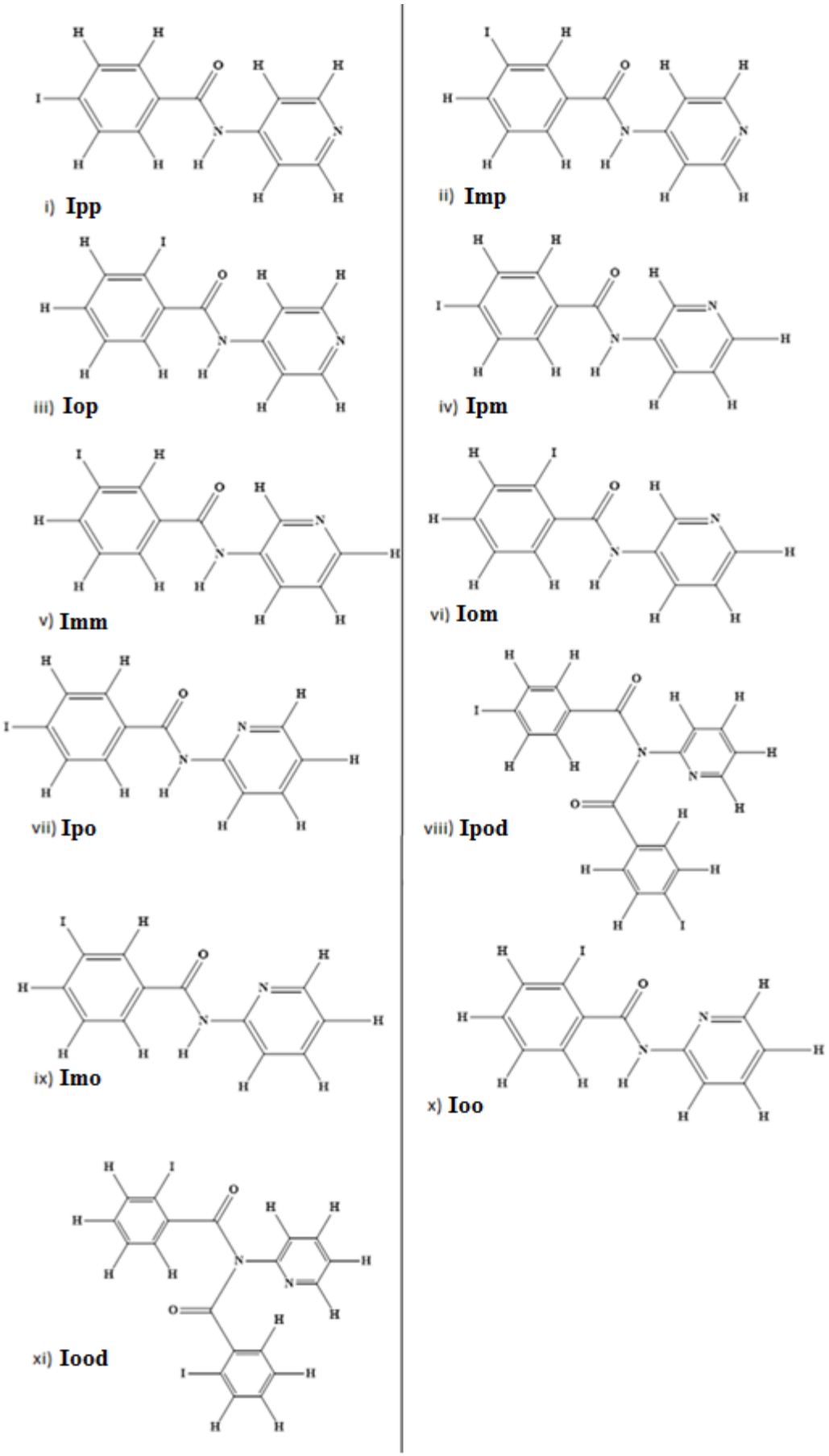

*Fig 2.11: Structures of the 11 compounds synthesised in **Ixx** series.*

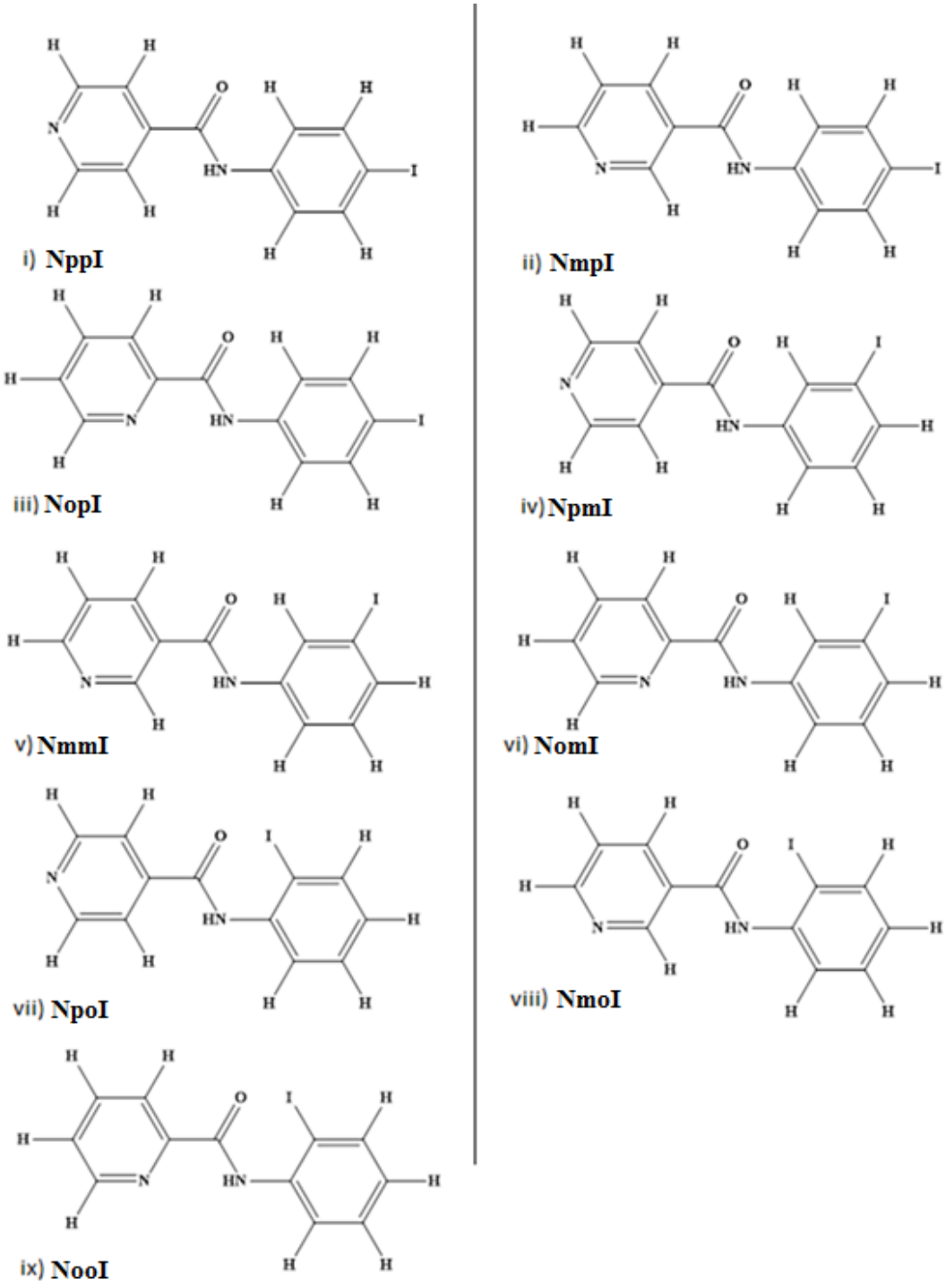

*Fig 2.12: Structures of the 9 compounds synthesised in **NxxI** series:*

*Table 2.8: Results of **Ixx** reactions:*

	Melting Point (°C)	Yield (g)	N-H Peak DMSO d^6 (ppm)	N-H Peak $CDCl_3$ (ppm)	Significant IR Peaks (cm^{-1})
Ipp	n/a	0.041 9%	n/a	n/a	n/a
Ipm	185-186	0.083 18%	10.52	7.95	3038, 1645, 1529, 1477
Ipo	134-139	0.105 22%	10.87	8.61	3064, 1650, 1580
Imp	168-170	0.092 20%	10.67	7.21	3150. 1686, 1589, 1485
Imm	165-167	0.61 n/a (mix)	10.54	8.04	3119, 1650, 1594, 1479
Imo	n/a	n/a	n/a	n/a	n/a
Iop	180-182	0.224 47%	10.85	7.67	3323, 1678, 1515
Iom	143-145	0.103 22%	8.72	7.87	3087, 1665, 1583, 1476
Ioo	n/a	0.047 10%	n/a	n/a	n/a
Ipod	150-152	0.074 16%	n/a	n/a	2955, 1695, 1581, 1533
Imod	n/a	n/a	n/a	n/a	n/a
Iood	129-134	0.17 36%	n/a	n/a	2955, 1697, 1584

Table 2.9: Results of NxxI reactions:

	Melting Point (°C)	Yield (g)	N-H Peak DMSO D^6 (ppm)	N-H Peak $CDCl_3$ (ppm)	Significant IR Peaks (cm^{-1})
NppI	241.0-241.6	0.14 4%	10.6	n/a	n/a
NpmI	217.5-217.9	0.149 5%	10.57	n/a	n/a
NpoI	122.0-123.2	0.071 2%	10.4	n/a	n/a
NmpI	195.5-196.0	0.46 14%	10.5	n/a	n/a
NmmI	155.6-159.9	0.303 19%	10.52	8.72	3346, 1682, 1603, 1536,
NmoI	139.7-143.6	0.0812 5%	10.33	9.18	3264, 1637, 1576, 1478
NopI	150.2-155.8	0.281 17%	10.15	n/a	3331, 1676, 1515, 1484
NomI	83.4-87.1	0.461 29%	10.77	n/a	3337, 1685, 1576, 1477
NooI	57.4-59.0	0.389 12%	n/a	n/a	n/a

2.4 Discussion

2.4.1 Brxx series

With the exception of the *ortho*-series of compounds, the reaction between the 2 and 3-aminopyridines with the bromobenzoyl chlorides went as expected and good yields were obtained. All spectroscopic data for all series in Chapter 2, including ^{1}H-NMR, ^{13}C-NMR, and IR are presented in Appendix I.

As can be seen in Table 2.6 above, the yields for the first six reactions were all reasonable with the majority having around a 50% yield. In a reaction such as this, the yield would be expected to be higher, however, the number of washings performed on each of the compounds could account for the reduced yields. Each compound was washed four times to remove impurities and some product was lost in each washing. The purification of the product and subsequent characterisation of said pure product was more important than the yield of the reaction, so this was not a major concern. Each reaction yielded 1.3g of product on average, more than enough to both fully characterise and attempt to grow crystals.

With the *ortho*-series of compounds, it was observed on both ^{1}H-NMR and TLC that the reaction had not proceeded as expected. Analysis of the reaction showed the presence of two spots on TLC for the product. As washings had been carried out similar to the *para*- and *meta*-series, there was little to no starting material present on the product. After running a column to separate the two products, the second product in the *ortho*-series was found to be Bis(bromo)-*N*-(pyridinyl)benzamide. It was found to contain a 2:1 ratio of Bromobenzoyl Chloride:Aminopyridine.

The formation of this 2:1 product is due to a number of factors. Firstly, with the nitrogen in the *ortho*-position of the pyridine ring, the electron withdrawing effect on the carbon to which the amide linkage is attached, is at its largest. In the *para*- or *meta*-position, the pyridine nitrogen is not close enough to the carbon to pull electron density from it and, in doing so, weaken the bond between the amide nitrogen and its hydrogen.

Another possible reason for the formation of the imide products is the presence of an intramolecular pyridine N22…H1-N1 interaction. With the pyridine nitrogen in the

ortho-position, it is within 2.3 Å of the amide hydrogen. This is only slightly larger than the distance of intermolecular H-bonding in the crystal, which is about 2.2 Å. The presence of a hydrogen bonding interaction between the *ortho*-nitrogen and the amide hydrogen would weaken the N-H bond of the amide. This interaction, combined with the electron withdrawing effects of the nitrogen, seems to have weakened the N-H bond of the amide sufficiently to allow the hydrogen to be lost. This allows for a second molecule of bromobenzoyl chloride to bond to the nitrogen, forming the imide product.

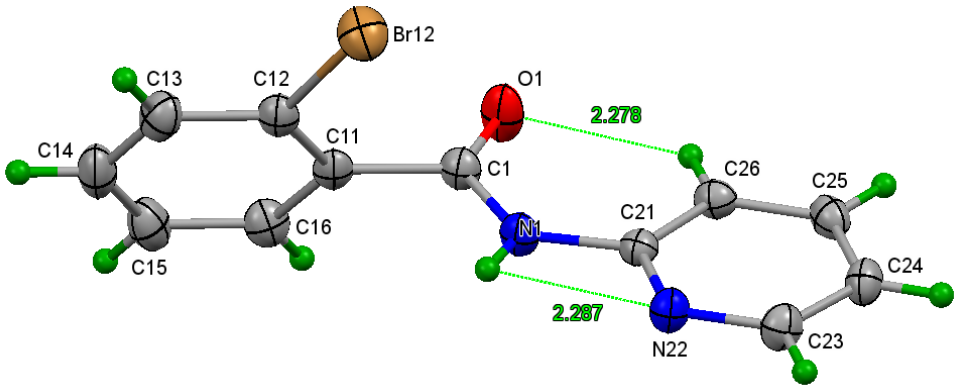

Fig 2.13: Distance between N-H…N and C-H…O=C in ***Broo*** *(distances in Å):*

^{1}H-NMRs were run in both $CDCl_3$ and DMSO. The data obtained allowed the purity of the synthesised compound to be determined. It also allowed the chemical shift of the amide hydrogen in all the 1:1 reactions to be examined. The amide hydrogen was a good candidate for analysing trends in the series as it shows up as a broad singlet in both $CDCl_3$ and DMSO. In some compounds, the $CDCl_3$ ^{1}H-NMR spectra were less resolved than their DMSO counterparts, so for the trend analysis, the DMSO chemical shifts will be used except in the case of the *ortho* series. It was observed that for both the *para*-series and the *meta*-series, there was an increase in the chemical shift of amide proton as the bromine was positioned from the *para*-position. This trend can be seen in Table 2.6.

For the *para*-series of compounds, as the position of the bromine was moved from the *para*-position to the *meta*- and then *ortho*-position, there was a clear increase in chemical shift of the amide proton. This could be due to a dipole interaction between the electron withdrawing bromine, which would have a δ^- charge, and the amide hydrogen, which has a δ^+ charge.

As the bromine moves closer to the hydrogen, from *para*- to *meta*- to *ortho*-position, this interaction becomes stronger. This caused the proton to become more deshielded as the bromine gets closer to the amide.

For the *meta*-series, the same trend is in evidence. The *para*-position has the smallest shift of the amide proton, and as the bromine is moved from the *para*-position, to the *meta*- position, to the *ortho*-position, the chemical shift gets larger. This is again due to the increased interaction between the bromine and the hydrogen as it moves closer to the amide linkage.

For the *ortho*-series, due to the presence of the imide 2:1 compounds, clean ^{1}H-NMRs could not be obtained until the two products were successfully separated by column chromatography. In order to attempt crystal growth at a later stage with these pure separated compounds, **Brpo** was run in $CDCl_3$ while **Brmo** was run in DMSO. This was done as only a small amount of **Brpo** was separated from the 200mg of crude product added to the column, which indicates the reaction for **Brpo** is favoured towards the 2:1 product under the reaction conditions.

The consequence of this is that the ^{1}H-NMR of **Brpo** had to be run in $CDCl_3$, so that the compound was easily recoverable from the solvent and available for crystallisation. This would not have been possible using DMSO, due to its high boiling point, and degradation of the product could occur if exposed to the high temperatures required. Thus, no trends can be drawn from the data obtained.

From the ^{1}H-NMR data of these *ortho*-compounds it can be seen clearly the difference between the 1:1 products and the 2:1 products. The 1:1 compounds all show a clear broad singlet that denotes the presence of an amide proton. This feature is absent from the ^{1}H-NMRs of the 2:1 derivatives. This demonstrates that the 2:1 product is indeed an imide compound, as the absence of the amide hydrogen shows that another moiety is bonded to the amide. It is believed that in this case, another molecule of bromobenzoyl, minus the chlorine, replaces the amino hydrogen.

The integrations of the two different products also established that an imide has been formed in these *ortho*-reactions. The integration for the *para*-, *meta*- and the 1:1 *ortho*- compounds was 9, which corresponds with the 1:1 compound, with four hydrogens on both the pyridine ring and the aromatic ring the bromine is attached to.

The ninth proton is the amide proton in these particular cases. For the 2:1 products, the integration is for 12 hydrogen atoms. This difference of 3 protons, along with the loss of the amide proton singlet, proves that the amide hydrogen has been removed and replaced with a bromobenzoyl moiety, which contains four hydrogen atoms.

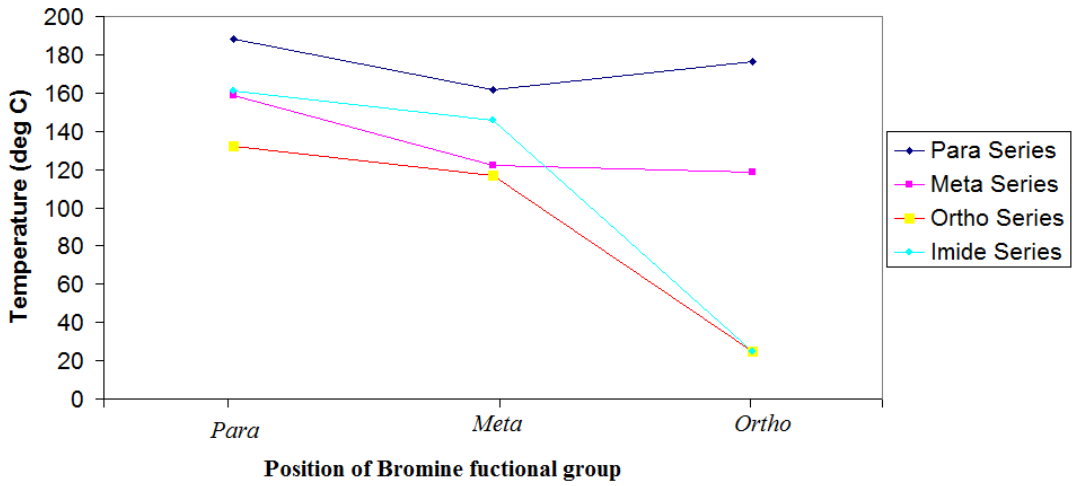

*Fig 2.14: Graph of the melting points of the **Brxx** series:*

Fig 2.14 shows the trends in melting points for the *para*-, *meta*-, *ortho*- and imide series. In the *para*- series of compounds, **Brpp** has the highest melting point (mp) of the three compounds. This is expected according to Carnelley's rule, which states that '*High molecular symmetry is associated with high melting point'*.[12]

Brpp is the most symmetrical of all of the compounds synthesised, with both of its substituents being in the *para*-position. Highly symmetrical molecules also tend to have very efficient packing in the solid state, which can lead to high melting points compared to compounds that pack inefficiently. **Brmp** follows this Carnelley's trend also, with a melting point of 161.5°C, and lower than that of the more symmetrical **Brpp**. The *ortho*-substituted bromine in the *para*-series, however, deviates from this trend, with a melting point of 176°C. This increased melting point could be due to the presence of a hydrogen-bromine intramolecular interaction. With the bromine in the *ortho*-position, it is close enough to form an interaction with the amide moiety, which contributes to increased stability in the crystal structure. This increased stability holds the molecules together for longer meaning a higher melting point.

Another factor that could cause this deviation from Carnelley's rule is that **Brmp** does not seem to have any interactions (hydrogen or halogen bonding) between bromine and the adjacent product molecules in the solid state. Both **Brpp** and **Brop** have bromine interactions of some fashion, both short contact and H-bond intermolecular interactions. This could contribute overall to the lower melting point of **Brmp**.

In the *meta*-series of compounds, Carnelley's rule is adhered to, with the most symmetrical molecule **Brpm**, having the highest melting point. **Brmm** has a melting point of 122°C that is considerably lower than **Brpm**. The compound with the lowest melting point in the *meta*-series is **Brom**, with a melting point of 118.5°C.

The *ortho*-series of compounds also followed this trend, with **Brpo** having the highest melting point, followed by **Brmo** and **Broo**. In fact, **Broo** was found to be viscous oil at room temperature that yielded crystals with difficulty. This could be because of the pyridine nitrogen in the *ortho*-position. Intermolecular interactions would be reduced because of steric pressure and access to the lone pair of the pyridine nitrogen would be more restricted in the *ortho*-position, relative to the *meta*- or *para*-positions.

The melting points of the imide products of the *ortho*-reactions were also collected. **Brpod** had the highest melting point, with **Brmod** next, followed by **Brood**, which was an oil at room temperature and whose melting point was approximated at 25°C. It was found that **Brpod** and **Brmod** had melting points significantly higher than their 1:1 reaction counterparts, **Brpo** and **Brmo**, by approximately 30°C. This increase in melting point could be due to the increased molecular weight of the 2:1 compounds and intermolecular interactions. Another factor could be the addition of another aromatic system, namely a bromobenzoyl moiety, which could increase the amount of $\pi\ldots\pi$ stacking that is possible in the crystal. This would lead to an increase in the intermolecular interactions and increase the amount of energy needed to break and disrupt these bonds in the solid-state.

2.4.2 Brxx X-ray Crystal structure analysis

Crystals were successfully grown for all nine of the **Brxx** series, all crystals were grown by slow evaporation at room temperature, typically from $CHCl_3$, acetone or ethyl acetate. Full geometry tables and structural information for each elucidated structure can be found in the Appendix I.

2.4.2.1 Brpp molecular and crystal structure

The **Brpp** isomer crystallizes in the in $P2_1/c$ space group and has two primary interactions that contribute to aggregation. *a*) N1-H1…N24 hydrogen bonding and auxiliary *b*) Br14…C26-C22-C21 ring π interactions. These interactions can be seen below in *Fig 2.15*. The R factor of the structure was low, with a value of 0.044. This figure is a measure of how closely the X-ray diffraction data is to the computer model the software generates, and is an indication of how well resolved and accurate a structure is.[13]

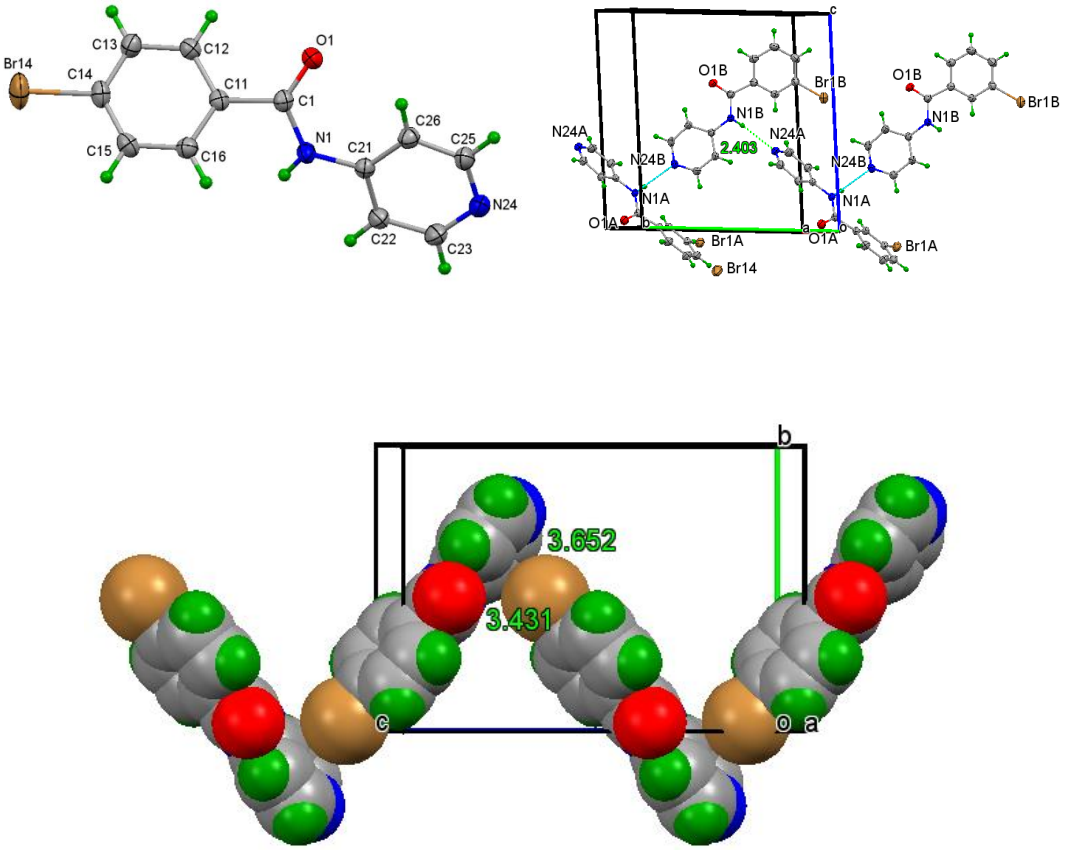

Fig 2.15: ***Brpp*** *with a) N-H…N hydrogen bonding; b) Br…π interactions with bonding Br…C distances (in Å)*

2.4.2.2 Brmp molecular and crystal structure

The **Brmp** isomer crystallizes in the *P-1* space group, and contains two molecules in the unit cell, Z = 2. Some disorder was noted in the structure, and can be seen in the presence of Br in both the *para*- and *meta*- positions, due to some contamination of starting materials for this particular reaction. Br14 was not noted to be involved in any strong interactions in the solid state. N1A-H1A…N24B hydrogen bonding is the main type of aggregation in this structure with a distance of 2.22 Å between the two molecules in the unit cell. The structure was well resolved and optimised, with an R factor of 0.043.

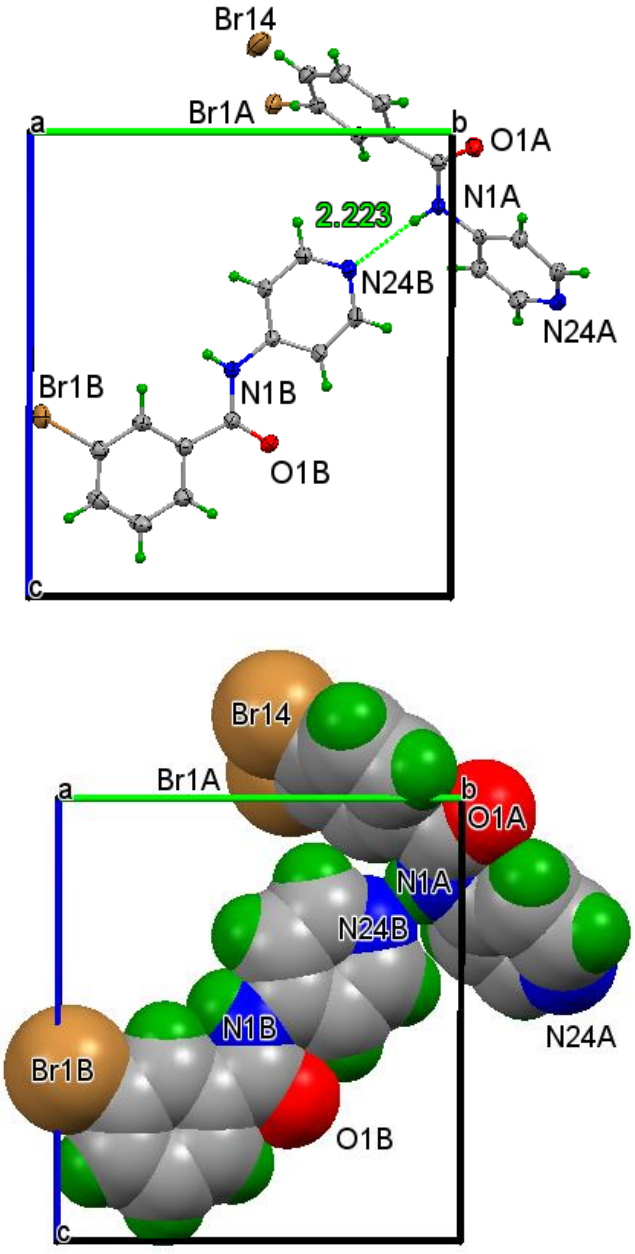

Fig 2.16: N1A-H1A…N24B hydrogen bonding in ***Brmp*** *structure:*

2.4.2.3 Brop molecular and crystal structure

Brop crystallizes in the *Pbca* space group and contains a minor Br site disorder in its structure. The interactions involved in the formation of the crystal structure are primarily N1-H1…N24 hydrogen bonding with some C12-Br12…O1 interactions, as can be seen in *Fig 2.17*. The angle of the C12-Br12…O1 interaction was 167.38°, pointing towards the presence of a Br…O interaction. The structure was well resolved and optimised, with an R factor of 0.035.

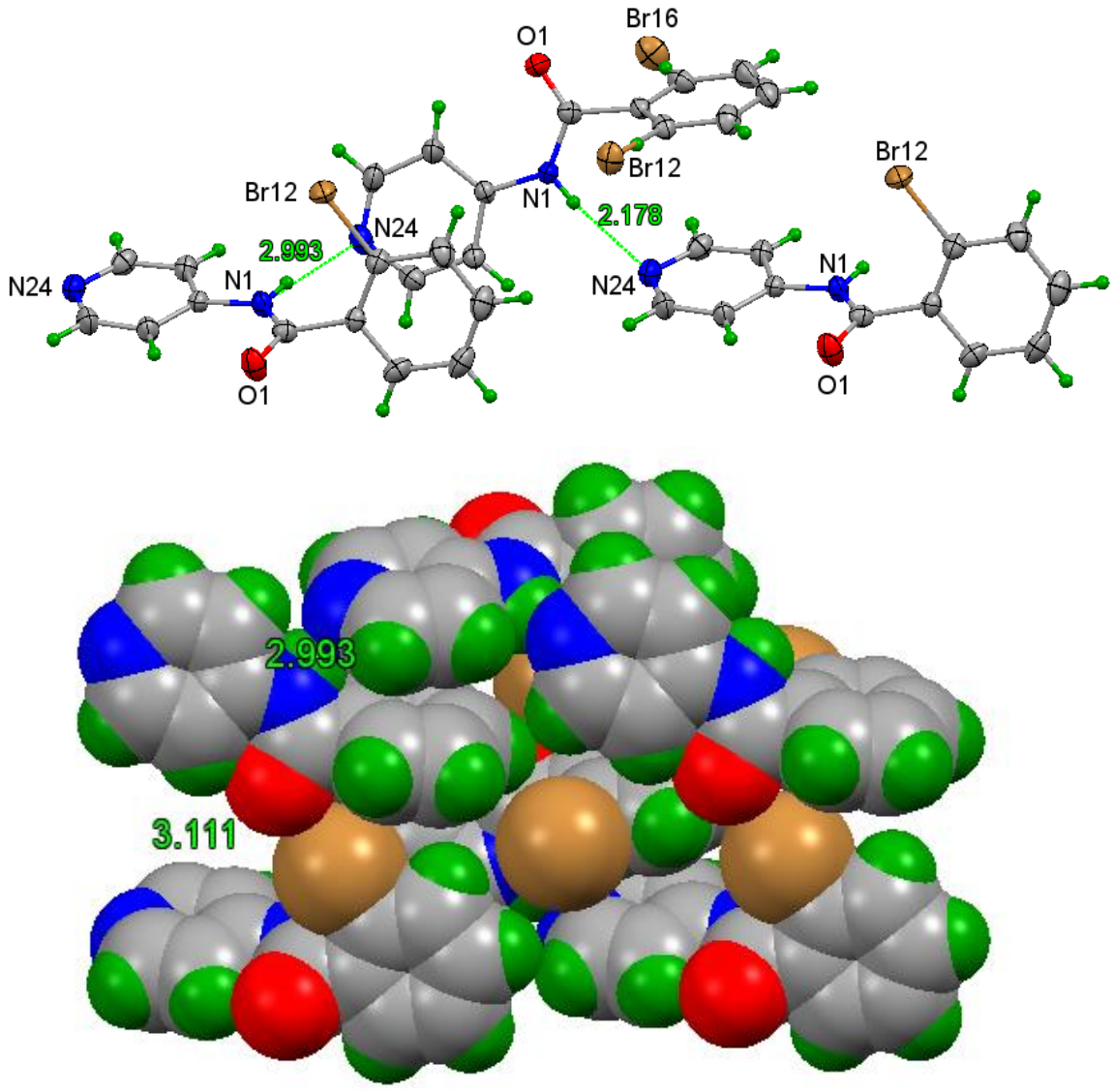

Fig 2.17: ***Brop*** *with N-H…N hydrogen bonding and a CPK view showing the C12-Br12…O1 interactions:*

2.4.2.4 Brpm molecular and crystal structure

Brpm crystallizes in the *C2/c* space group and has one main interaction, N1-H1…O1=C1 hydrogen bonding. The structure has an R factor of 0.032.

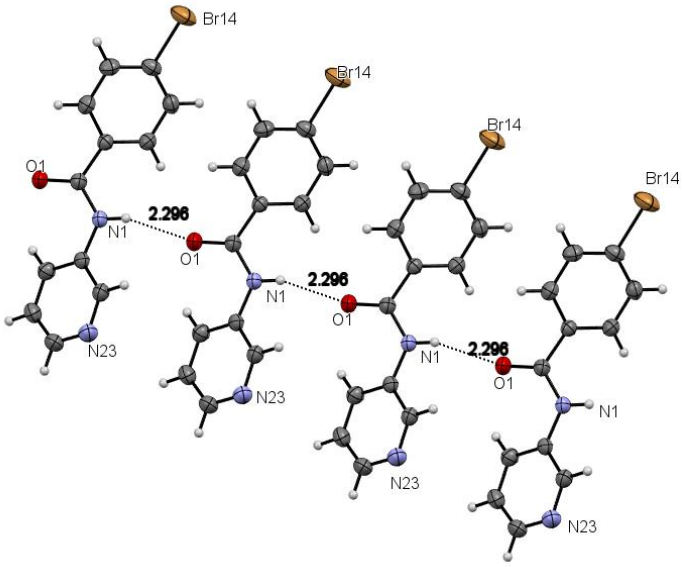

*Fig 2.18: N1-H1…O1=C1 hydrogen bonding in **Brpm**:*

2.4.2.5 Brpo molecular and crystal structure

Brpo crystallizes in the P-1 (No. 2) space group and forms a dimer structure through cyclic hydrogen bonding N1-H1…N22, as can be seen in *Fig 2.19*. This structure is isomorphous with a previously investigated structure Mpo.[14] The R factor of the structure was 0.036.

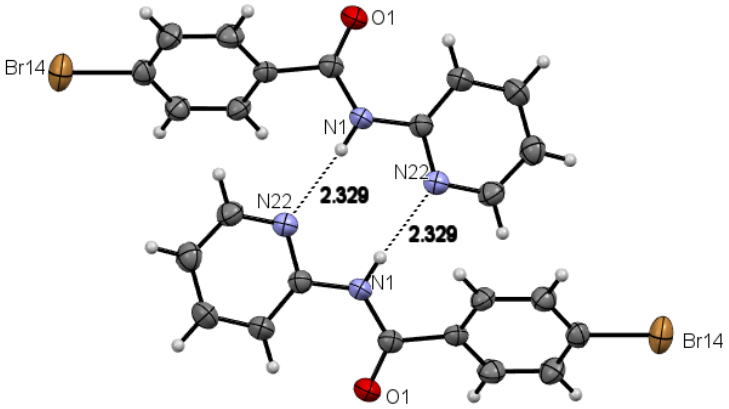

*Fig 2.19: **Brpo** structure showing cyclic N1-H1…N22 hydrogen bonding:*

2.4.2.6 Brmm molecular and crystal structure

Brmm crystallizes in the $P2_1/c$ space group and is a hydrate in the solid state (water from ambient air) and was found to be isomorphous with **Clmm**, work done previously by the Gallagher group.[15]

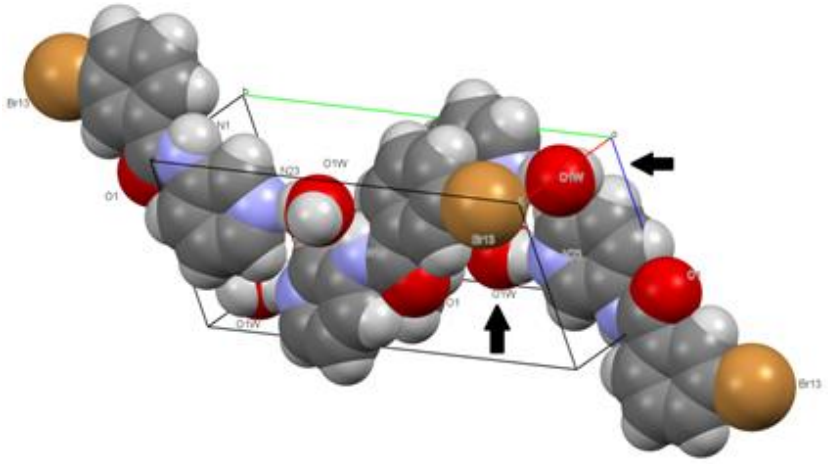

*Fig 2.20: Diagram showing **Brmm** structure showing water molecule:*

2.4.2.7 Brom molecular and crystal structure

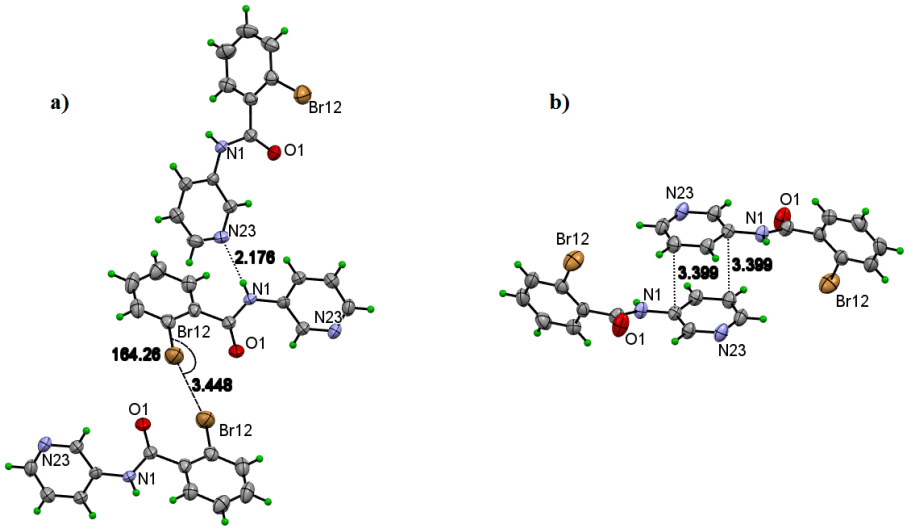

*Fig 2.21: a) N1-H1…N23 hydrogen bonding in **Brom** as well as a Br…Br interaction in **Brom**. Interaction distance of 3.448 Å: b) π…π stacking interaction in **Brom** c)*

Brom crystallizes in the *C2/c* space group and has a number of interesting interactions that cause its aggregation. The primary interaction is N1-H1…N23 hydrogen bonding, seen in *Fig 2.20*. A π…π stacking interaction can be viewed in *Fig 2.21*. A short Br…Br interaction is also present (*Fig 2.21.)*

2.4.2.8 Broo molecular and crystal structure

Broo crystallizes in the *C2/c* space group and forms a dimer through N1-H1…N22 hydrogen bonding. It is isomorphous with **Cloo**, a molecule that differs only with regard to the halogen atom in the *ortho*-position.

A strong π…π stacking interaction was also noted in the solid state. The distance between the molecules was observed to be 3.3 Å, a relatively short interaction, compared to the other examples of π…π stacking in this series.

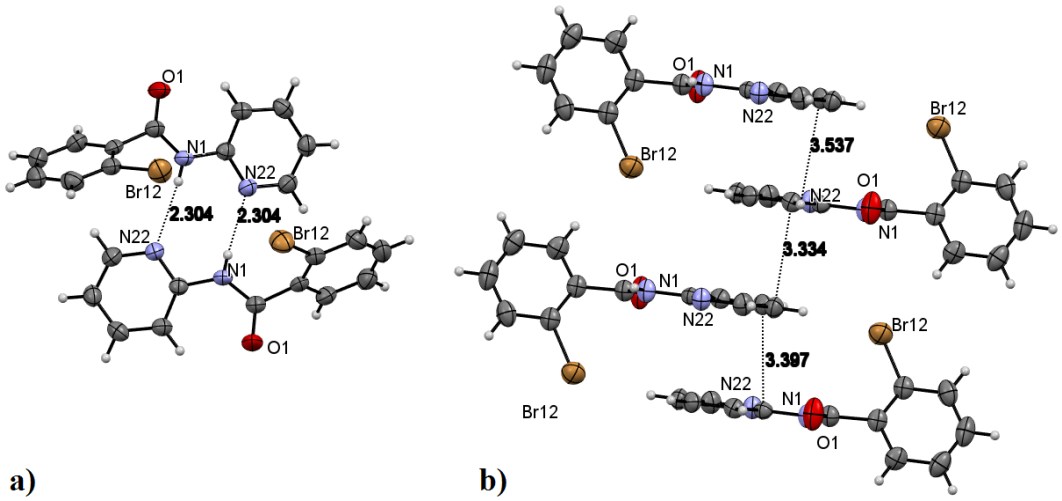

Fig 2.22: a) N1-H1…N22 hydrogen bonding in ***Broo*** *b) π…π stacking interaction in* ***Broo*** *crystal structure:*

2.4.2.9 Brmo molecular and crystal structure

The **Brmo** isomer crystallizes in the $P2_1/c$ space group, and unlike the two other *ortho*-pyridine isomers, does not form a symmetrical dimer. Instead, it was found to form a form of offset unsymmetrical dimer. The major interactions leading to aggregation are N1A-H1A…O1B, and can be seen below in *Fig 2.23*.

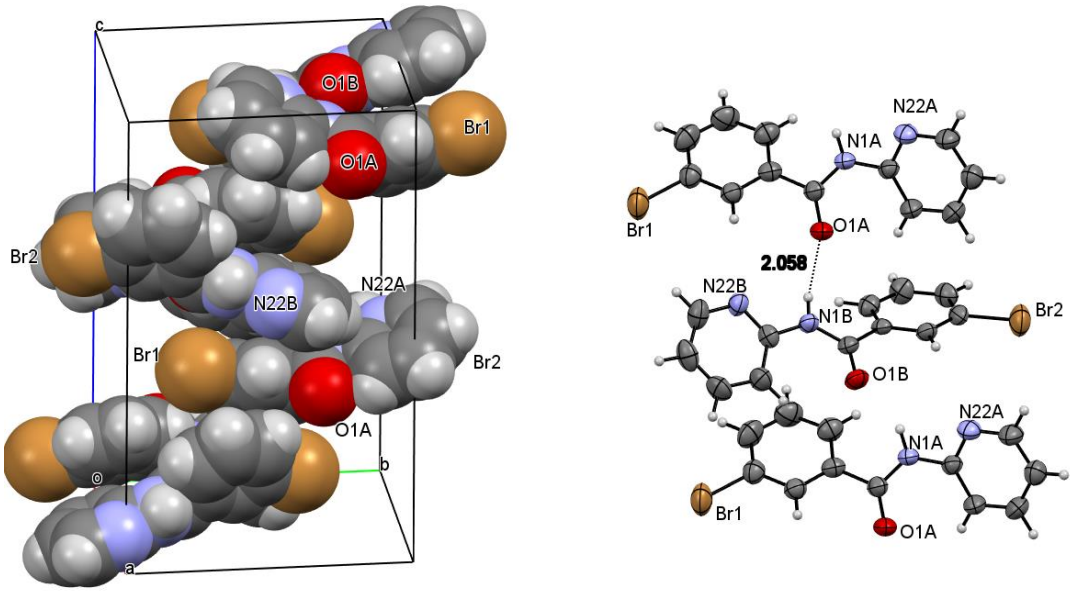

a) **b)**

*Fig 2.23: a) Spacefill diagram of offset dimer in **Brmo** b) The N1A-H1A…O1B interaction in **Brmo**:*

2.4.3 NxxBr isomer grid series

For the reactions involving the reversal of the amide bridge, the **NxxBr** series, yields were in the region of 10-20%, lower than was expected. However, enough product was successfully synthesized to fully characterize all products by NMR, IR and X-ray crystallography. The washings done to remove the TEA salts from the reaction mixture could have factored into this lowering of yields, as during each wash, a small amount of product could have been lost to the water used in the washings. The *ortho*-reactions in the pyridine carboxamide series yielded only the 1:1 moiety, as the position of the amide bridge was flipped, therefore unable to allow the pyridine nitrogen to be in close enough proximity to pull electron density from the amide hydrogen.

The series was analyzed by ^{1}H-NMR, and again a number of trends were observed. The *para*-series showed an increase in the chemical shift of the amide proton as the bromine was moved closer in proximity to the amide bridge. This shift could again be explained by the presence of a dipole interaction between the electron withdrawing bromine and the amide hydrogen. Similar trends were observed in both

the *meta*- and *ortho*-series, with chemical shift increasing as the bromine substituent was moved towards the *ortho*- position. The NMR shifts for this series in DMSO-d^6 and $CDCl_3$ can be seen in Table 2.7.

It was again expected for the melting points to progress similarly to the **Brxx** series, with the most symmetrical of the compounds having the highest melting point. This held true for the majority of the series, with compounds with high symmetry such as **NppBr**, **NmpBr** and **NpmBr** differing from the more unsymmetrical compounds in m.p by up to 100°C. However, it was noted that the compound with the highest mp was not **NppBr** as expected by Carnelley's rule, but **NpmBr**. The reason for this was indicated by the crystal structure of the molecule. The packing arrangement and the intermolecular distances are shown below in the crystallographic discussion.

Comparisons can be made between the different isomers by comparing the IR absorption for the same functional groups present in the **NxxBr** series. The spectra for each product have been examined and the functional groups identified in Table 2.7. The position of some of the characteristic bands is the same for all spectra, for instance the carbonyl C=O band appears as a strong intensity band at 1650-1700cm^{-1} in each spectrum.

The IR spectrum also displays the strength or degree of intermolecular hydrogen bonding within the compounds. The intensity of the peaks for functional groups which are involved in intermolecular bonding in one compound are much weaker than those for the same functional groups which are not involved in any hydrogen bonding in another compound. For instance, the spectrum for **NomBr** shows strong intensity absorptions for the carbonyl and medium intensity absorption for the N-H, which is relatively intense for an N-H stretch. One reason for this is that the molecule does not have any intermolecular bonding occurring within its structure. This is observed from the X-ray crystal structure of **NomBr** which will be discussed in more depth in section 2.5.4.

In contrast to this, the spectrum for **NmmBr** has very weak intensity absorptions for the N-H and only medium intensity absorption for the carbonyl. The reason for this is also revealed by the x-ray crystal structure, as it is the first compound in this series of isomers to be examined that displays two different types of hydrogen bonding. The

crystal displays intermolecular hydrogen bonding between the N-H of the amide and the carbonyl; also it displays hydrogen bonding between the amide and the nitrogen in the pyridine ring. This high degree of hydrogen bonding then manifests as weakened intensity absorptions in the IR spectrum. This is depicted in *Fig 2.32* and *2.32* in the crystallographic discussion below.

2.4.4 NxxBr X-ray Crystal structure analysis

Similar to the **Brxx** series, crystals were successfully grown by slow evaporation at room temperature, again from $CHCl_3$, acetone or ethyl acetate. Full geometry tables and structural information for each elucidated structure can be found in Appendix I. Two of the molecules synthesized, **NopBr** and **NmoBr** have been previously reported as WUVYIU[16] and TICDOZ[17] respectively.

2.4.4.1 NppBr molecular and crystal structure

NppBr crystallizes in the $P2_1$ space group and has a large R factor of 0.105 due to twinning effects. N1-H1…O1 interactions were observed and can be seen in *Fig 2.24*.

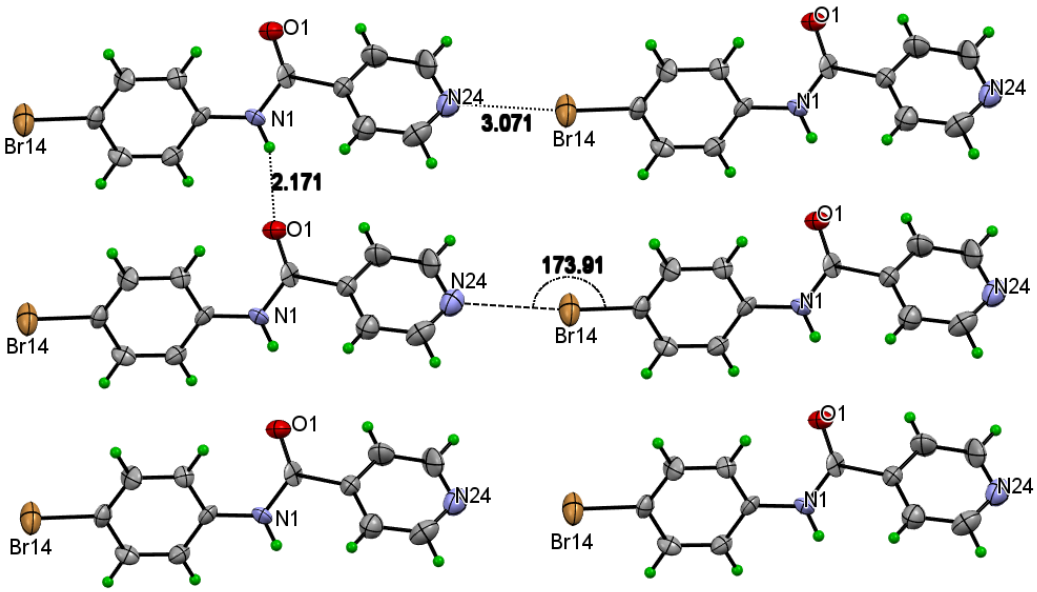

*Fig 2.24: N1-H1…O1 interactions in **NppBr**:*

2.4.4.2 NmpBr molecular and crystal structure

The **NmpBr** isomer crystallizes in the *C2/c* space group. The main interaction in this molecule is an N1-H1…O1 hydrogen bond. The R factor was found to be 0.042. Similar molecules have been synthesized previously by Dr. Mocilac.[18] **NmpF** forms a tetramer in the solid state and was in the *P1* space group, while **NmpCl** was found to be in the $P2_1/c$ space group.

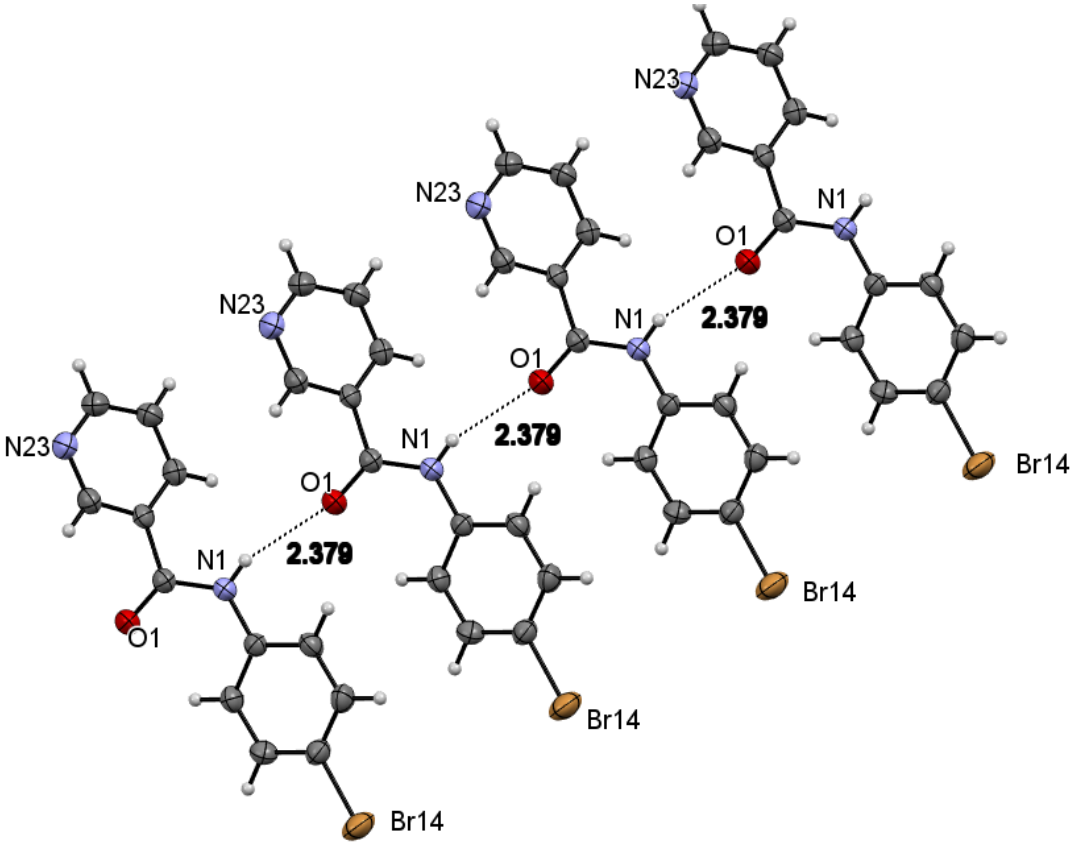

Fig 2.25: N1-H1…O1 hydrogen bond in ***NmpBr****:*

2.4.4.3 NopBr molecular and crystal structure

NopBr crystallizes in the P-1 space group and has been previously reported as WUVYIU by JY Qi *et al.*[16] The major interactions causing aggregation in the sample synthesised for this thesis were C1-O1…H16-C16 hydrogen bonding. The previously published structure was obtained by slow evaporation from a saturated ethanol/water solution at room temperature.[16]

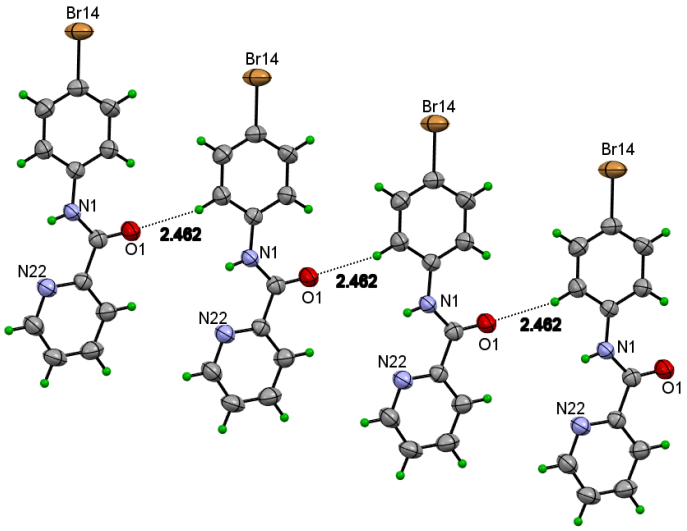

Fig 2.26: a) C1-O1…H16-C16 hydrogen bonding in ***NopBr:***

2.4.4.4 NpmBr molecular and crystal structure

NpmBr crystallizes in the spacegroup $P2_1/n$. The major interactions in this structure are N1-H1…N24 hydrogen bond chains that give rise to a hydrogen bonded catemer structure. The **NpmBr** crystal has very short intermolecular distances between the **NpmBr** moieties as a result of these H-bonding interactions. This catemeric packing arrangement allows for a very ordered packing of the molecules. This property leads to a molecule that is very stable and requires a much higher temperature to break it down and cause it to melt.

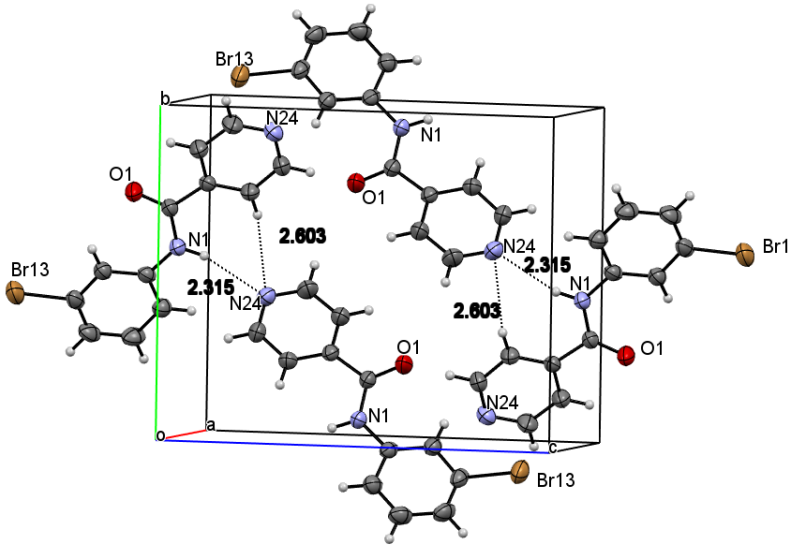

Fig 2.27: Diagram showing interactions in ***NpmBr****, with hydrogen bonds giving rise to the catemer structure highlighted:*

2.4.4.5 NmmBr molecular and crystal structure

The **NmmBr** isomer crystallizes in the P-1 space group and contains 2 molecules in the asymmetric unit Z'=2. The crystal structure contains two different types of hydrogen bonding interactions, both N1A-H1A…N23B and N1B-H1B…O1A. The molecule forms a very unusual tetramer in the solid state (as seen in *Fig 2.29*)

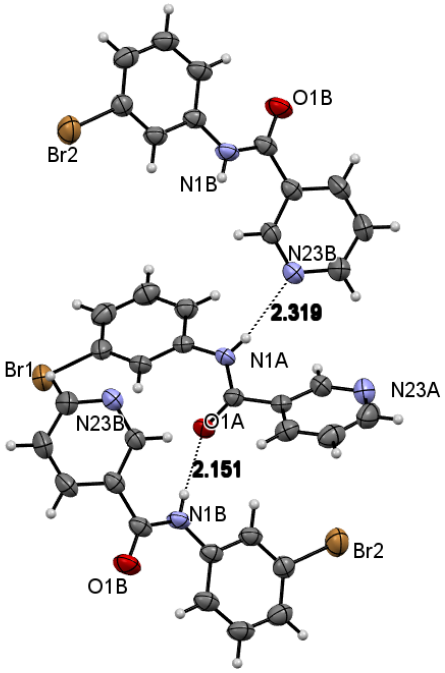

*Fig 2.28: N1A-H1A…N23B and N1B-H1B…O1A H-bonding interactions present in **NmmBr**:*

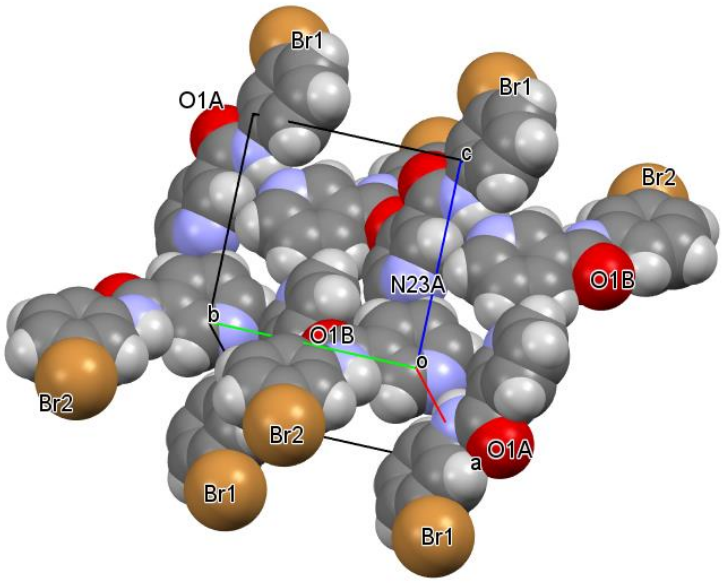

*Fig 2.29: Tetramer formation in **NmmBr** caused by a combination of N1A-H1A…N23B and N1B-H1B…O1A hydrogen bonding interactions:*

2.4.4.6 NomBr molecular and crystal structure

NomBr crystallizes in the *C2/c* spacegroup and forms a dimer in the solid state. The interactions used to give rise to this dimer are C13-Br13…N22 halogen bonds.

Halogen bonds in the solid state can be comparable in strength to weaker variants of H-bonds[19] such as C-H…O bonding, but in this case we note that the melting point is not overly affected by these halogen bonds, as **NomBr** was found to have the lowest melting point of the nine isomers synthesized.

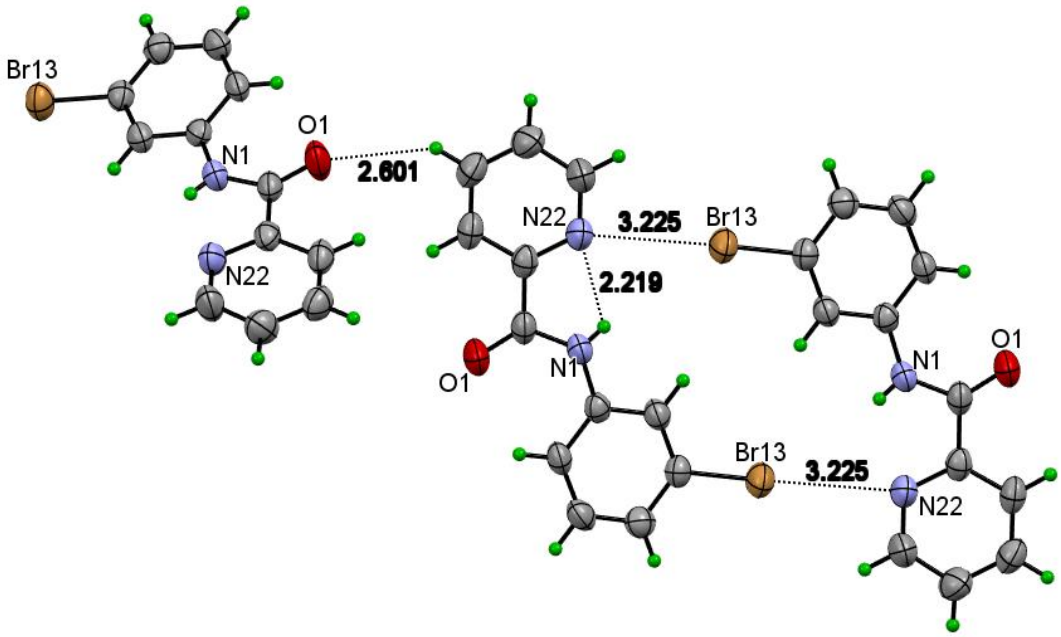

*Fig 2.30: C13-Br13…N22 halogen bonds in dimer **NomBr** structure:*

2.4.4.7 NpoBr molecular and crystal structure

The **NpoBr** isomer crystallizes in the *Cc* space group. The compound has N1-H1…O1=C1 hydrogen bonding as its main interaction in the solid state and is isomorphous with both **NpoM** and **NpoCl** structures previously published by the Gallagher group. It is not isomorphous with the corresponding **NpoF**, however.

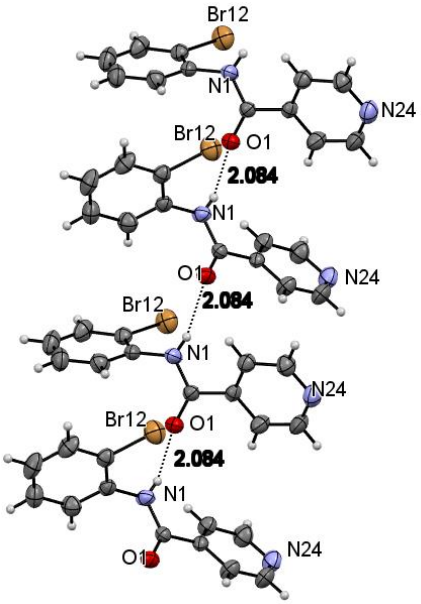

Fig 2.31: N1-H1…O1 hydrogen bonding in ***NpoBr****:*

2.4.4.8 NmoBr molecular and crystal structure

NmoBr has been previously published and is available on the CSD as TICDOZ.[17] The compound synthesised in this series was found to have a space group *Pbca*. The main interactions in the solid state were noted to be N1-H1…O1 hydrogen bonding. The published structure for TICDOZ can be seen below in *Fig 2.32.*[20]

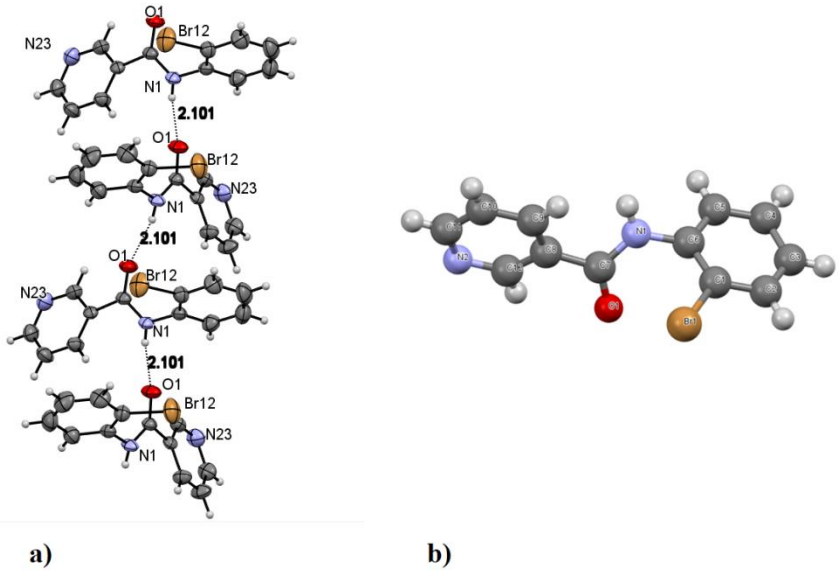

Fig 2.32: a) ***NmoBr*** *with N1-H1…O1 hydrogen bonding interactions. b) Structure of TICDOZ. Grown from hot ethyl acetate and petroleum ether and allowed to cool at room temp until crystallisation occurred.*[20]

2.4.4.9 NooBr molecular and crystal structure

NooBr crystallizes in the *Pbca* space group and has one main interaction that leads to its aggregation, C23-H23…O1 hydrogen bonding. It was found to be isomorphous with previously published structures **NooCl** but not the methyl derivative **NooM.**

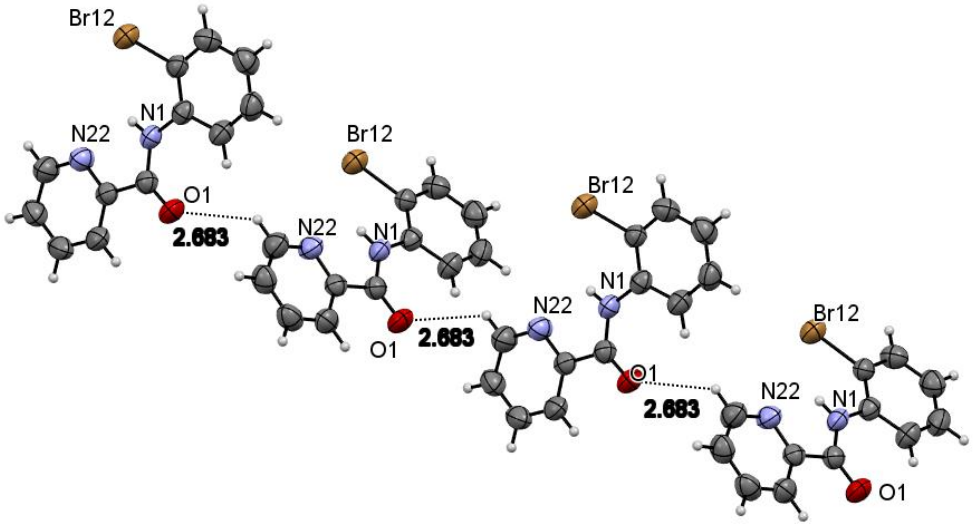

Fig 2.33: C23-H23…O1 hydrogen bonding in ***NooBr***:

2.4.5 Ixx isomer grid series

Difficulties with reactivity were encountered during the synthesis of the **Ixx** series. 6 of the 9 compounds were successfully completed, with full NMR and IR analysis. **Ipp**, **Imo** and **Ioo** were not made. Yields were between 10 and 45% for the compounds that showed reactivity. At the time these reactions were run, the starting materials available were a number of years old and degradation had undoubtedly occurred to some degree, causing issues with reactivity and subsequent low yields.

As with the **Brxx** series, it was noted that the *ortho*-compounds formed an imide backbone, with two molecules of the iodobenzoyl moiety reacting with 2-aminopyridine. Column chromatography was attempted on these compounds, but was unsuccessful. The mixed **Ioo** and **Iood** were left to slowly evaporate in a range of solvents and single crystals were grown, allowing for an X-ray structure of the **Iood** imide to be obtained. ^{1}H NMR trends were similar to the previous series **Brxx**,

with the amide hydrogen peak moving more downfield as the iodine functional group was moved from *para*- to the *ortho*-position.

The *meta*-series deviates from this trend with the **Imm** structure exhibiting the most downshifted proton of the three. The **Iom** molecule has a much lower value than the rest of the compounds analyzed. This discrepancy is due to the shielding effect of the iodine atom, which is in close proximity to the amide proton in **Iom**. All melting points can be seen in Table 2.8 in the results section above, and all compounds show a trend similar to the **Brxx** series. As molecular symmetry increases, so too does the melting point.

2.4.6 Ixx X-ray crystal structure analysis

Crystals were successfully grown for **Imm**, **Iop**, **Imp** and **Iood**. They were grown by slow evaporation at room temperature, from a range of solvents, similar to the **Brxx** series. Full geometry tables and structural information for each elucidated structure can be found in the Appendix I.

2.4.6.1 Imm molecular and crystal structure

The **Imm** isomer was found to be in the *Pa* spacegroup. In the solid state, the compound forms N1-H1…O1=C1 hydrogen bond chains, as can be seen in *Fig 2.34*. A 2D buckled sheet is fashioned by the interactions between C13-I13…N23 *(Fig 2.35)*.

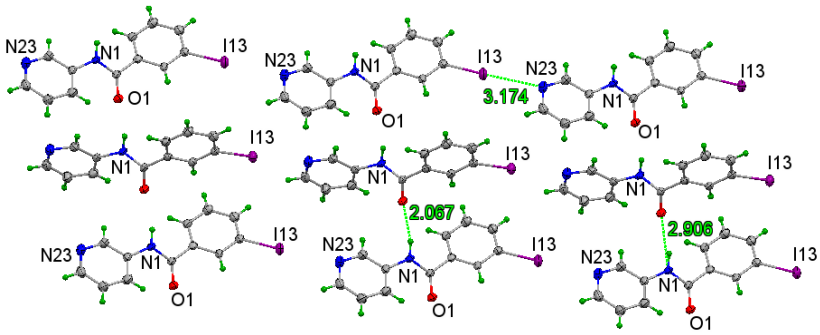

Fig 2.34: N-H…O=C hydrogen bond chains and I…N halogen bonding in ***Imm****:*

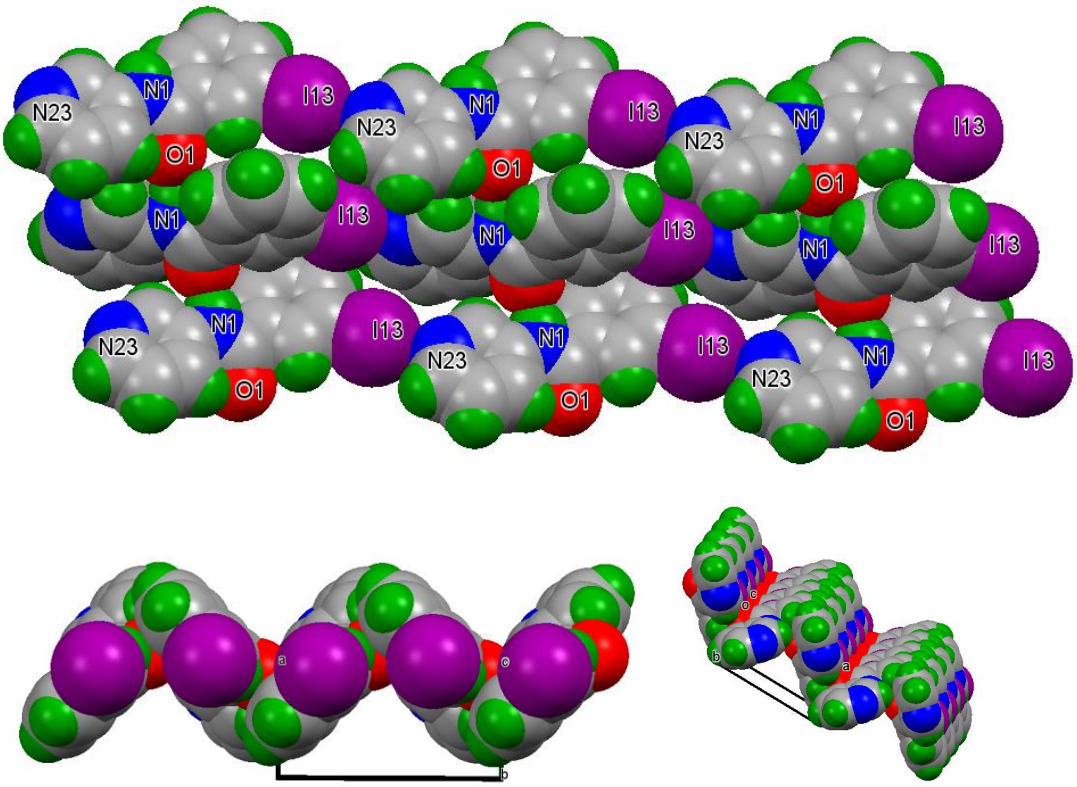

Fig 2.35: 2D buckled sheet formation due to I13…N23 interactions in ***Imm:***

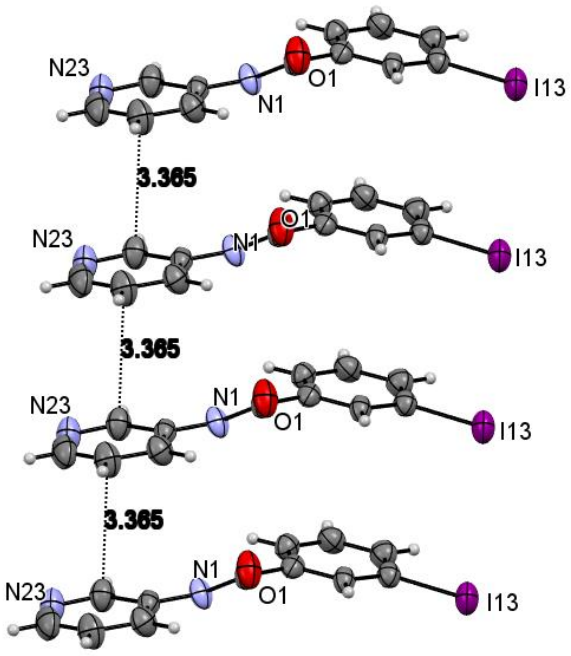

Fig 2.36: π…π stacking interactions in ***Imm*** *join the sheets C…C at a distance of 3.37 Å:*

2.4.6.2 Iop molecular and crystal structure

Iop crystallizes in the *Pbca* space group and shows some disorder with respect to the iodine position. The structures major interactions are N1-H1…N24 hydrogen bonding and C1-O1...I1A. The structure is isomorphous with respect to both **Clop** and **Brop**.

*Fig 2.37: N1-H1…N24 hydrogen bonding and C1-O1...I1A interactions in **Iop**:*

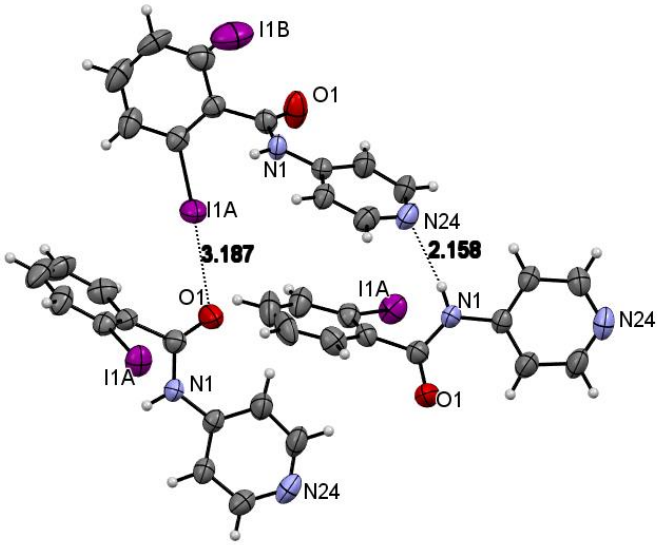

2.4.6.3 Imp molecular and crystal structure

Imp crystallizes in the spacegroup $Pna2_1$ and forms a chain structure due to N1-H1…N24 hydrogen bonding interactions. It also exhibits weak C15-H15…O1 interactions.

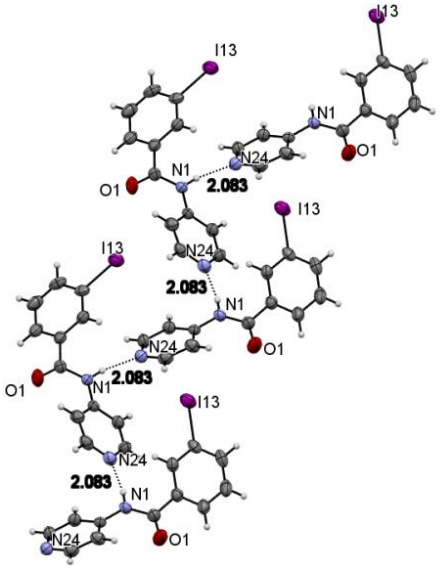

*Fig 2.38: N1-H1…N24 hydrogen bonding chain in **Imp:***

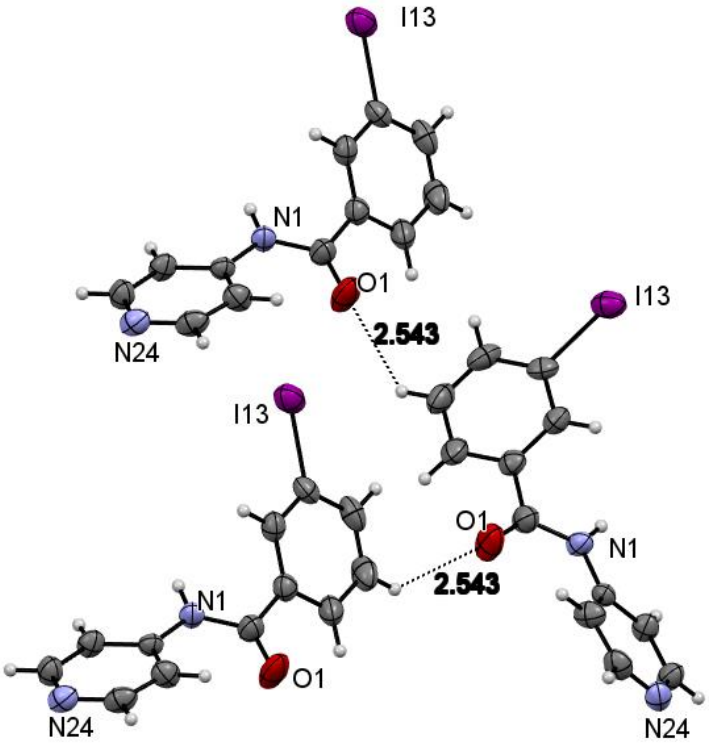

Fig 2.39: C15-H15…O1 interactions in ***Imp*** *structure*:

2.4.6.4 Iood molecular and crystal structure

Iood crystallizes in the space group $P2_1/n$ and has two halogen bonding interactions between C22-I1…N12 with a bond angle of 161.65° and C32-I2…O2, both an intramolecular and intermolecular interaction.

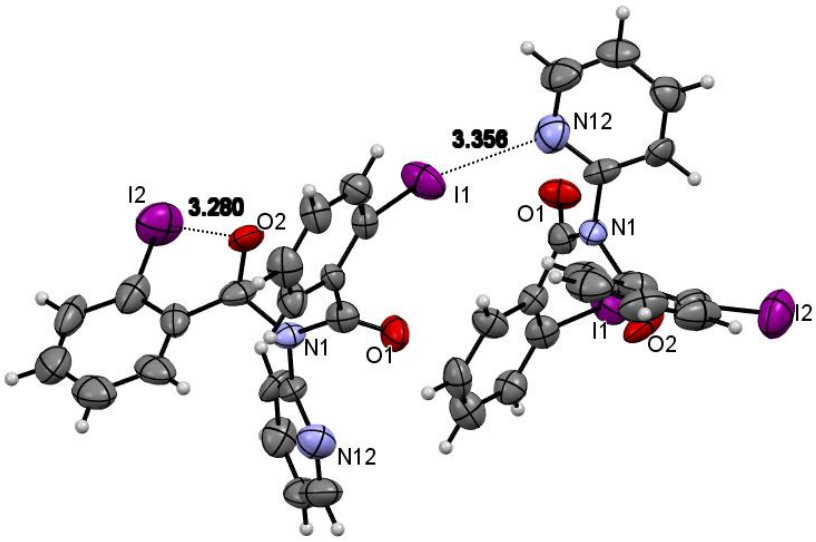

Fig 2.40: I1…N12 and I2…O1 interactions in ***Iood****:*

2.4.7 NxxI series

All nine compounds in the **NxxI** series were successfully synthesized using the methods outlined in the synthetic procedure section. Due to reactivity issues with the iodoaniline starting material, the *para*-series was synthesized using the EDC coupling route.

Yields for the remaining six compounds were in the range of 5-30%. It was noted that an imide bridge forms for the *ortho*-substituted **NooI** product. No amide proton was present in the ^{1}H NMR supporting this fact. ^{1}H NMR trends do not follow those observed in the **NxxBr** series. As the position of the iodine moves closer to the amide proton, a slight decrease in chemical shift is seen. This difference between the series could be due to 'heavy atom' effects.[21] Melting point trends are similar to the **Brxx** and **NxxBr** isomer grids, with melting points of highly symmetrical molecules found to be the highest. All NMR and melting point data are in *Table 2.9*.

2.4.8 NxxI X-ray crystal structure analysis

Three crystal structures were successfully grown by slow evaporation from ethyl acetate, chloroform and mixtures of toluene and methanol. Full geometry tables are presented in the Appendix I.

2.4.8.1 NmmI molecular and crystal structure

The **NmmI** isomer crystallized in the $P2_1/c$ space group, and exhibits some very interesting intermolecular interactions. It is observed to have two molecules in the asymmetric unit (Z'=2). In *Fig 2.41*, three different intermolecular interactions can be noted as N1A-H1A…O1B hydrogen bonding, N1B-H1B…N23A hydrogen bonding and N23B…I1B-C13B halogen bonding. The iodine atom is *cis-related* to the N-H group in one molecule (A) and *trans-related* in molecule (B). There are π…π stacking interactions also present that generate around inversion centres. The combination of interactions can be shown to generate an $(A…B…)_2$ tetramer linked by $(N\text{-}H…O{=}C/N\text{-}H…N)_2$ interactions, further linked by four $I…N_{pyridine}$ halogen bonds per tetramer. This substructure is unusual as tetramers are rare in benzamides

and only seen previously in **NmpF** where only one type of cyclic N-H…N interaction is noted.[22] Dimers are commonly observed in the **Xxo** series (**X** = Me, F; x = *p*-/*m*-/*o*-) and trimers have also been noted in the carbamates **CmmOMe** and **CmoOMe**.[23]

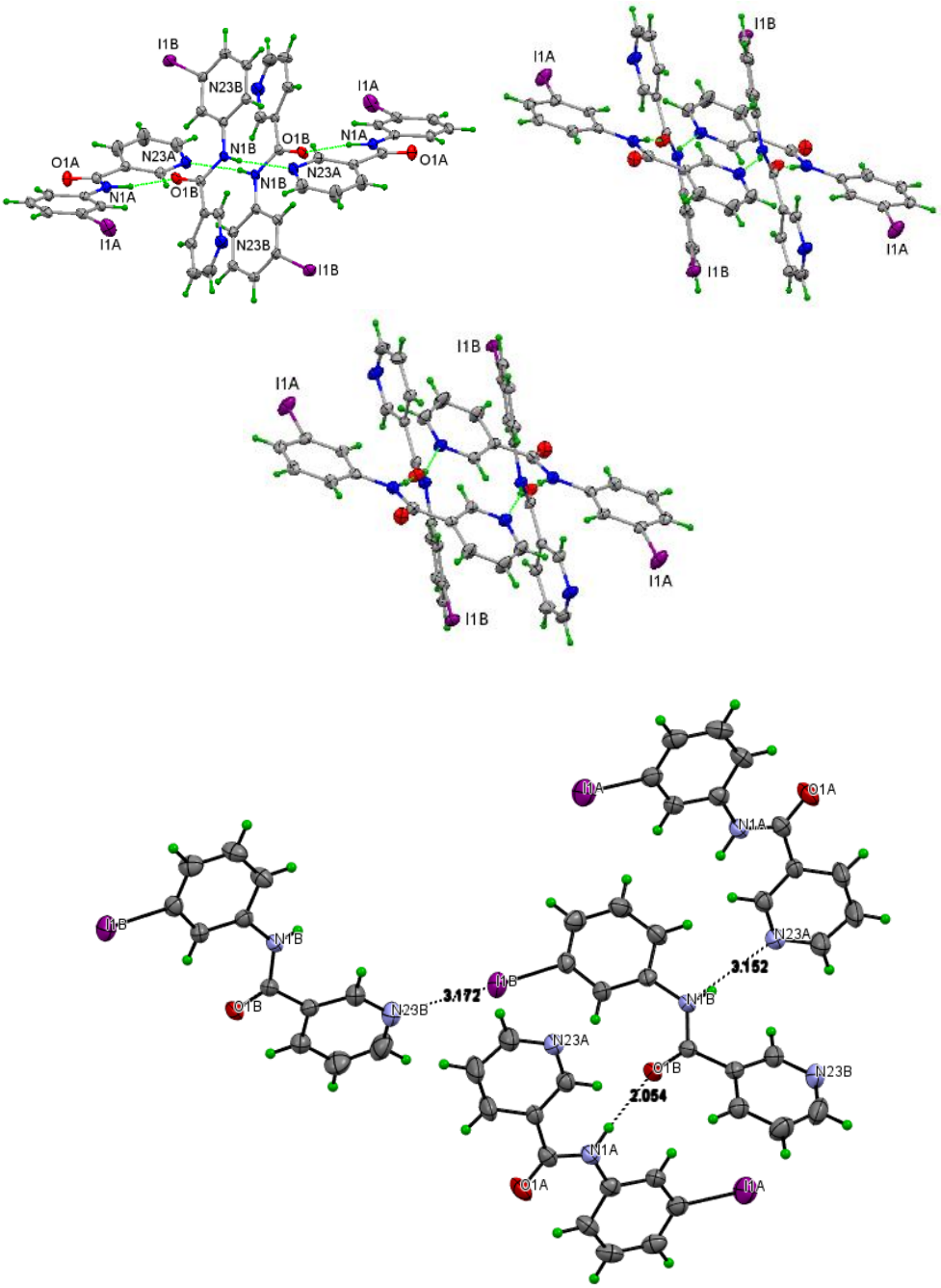

Fig 2.41: Three views of the ***NmmI*** *(N-H…N/N-H…O=C) hydrogen bonded tetramer. Three types of interaction in* ***NmmI****, N1A-H1A…O1B hydrogen bonding with distance=2.05 Å, N1B-H1B…N23A hydrogen bonding with distance=3.15 Å and N23B…I1B-C13B halogen bonding with distance=3.17 Å:*

2.4.8.2 NmoI molecular and crystal structure

NmoI crystallizes in the *Pna2₁* space group and has two interesting intermolecular interactions. Both interactions involve the carbonyl oxygen, with both an N1-H1…O1 hydrogen bonding interaction, and C12-I12…O1=C1 halogen bonding interaction. The principal effect of these two interactions is to give rise to another tetramer unit that aggregates by a combination of N-H…O=C hydrogen and C-I…O=C halogen bonding interactions with the oxygen participating as an acceptor for both N-H and C-I moieties. The iodine atom I12 displaying a σ-hole and interacting with the C=O.[24] The effect is to create a 2D wall (sheet) of molecules that are loosely linked by C-H…C/π contacts into the 3D crystal structure.

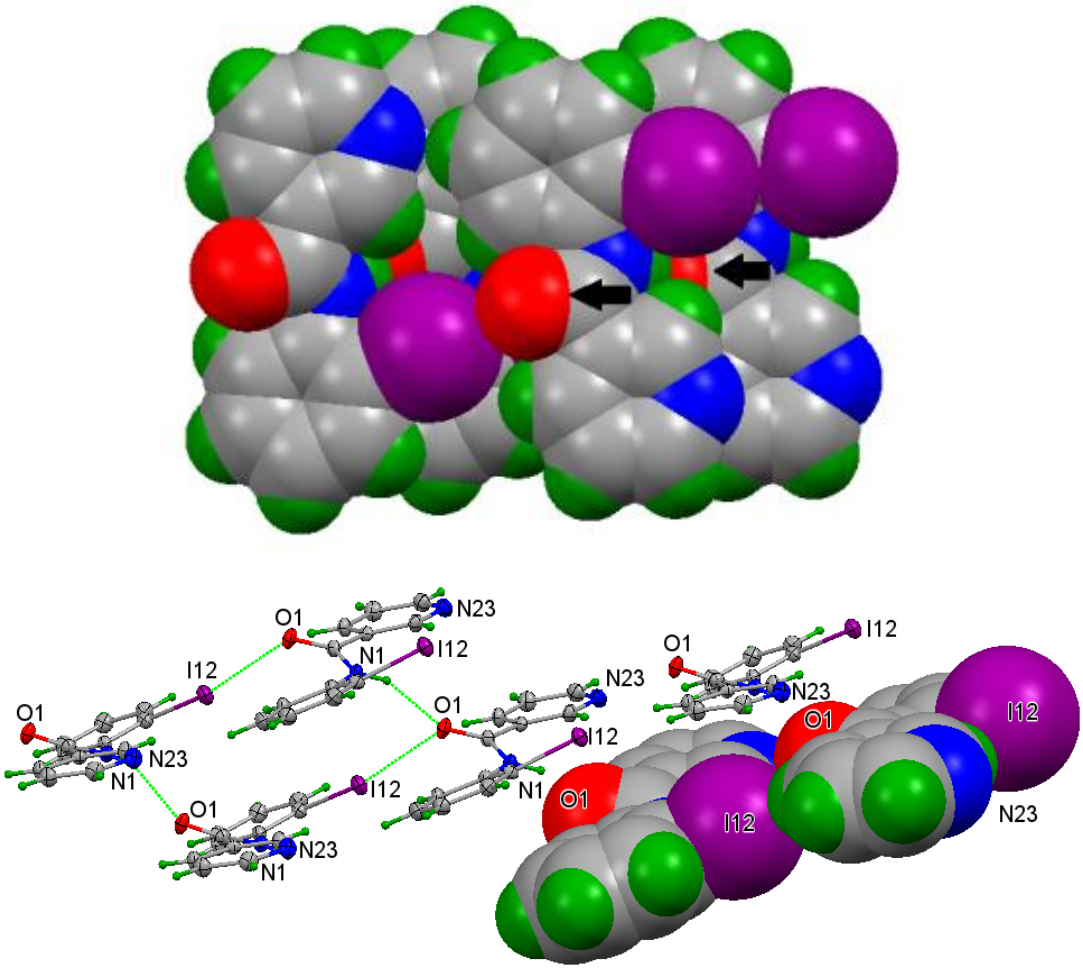

*Fig 2.42: Intermolecular interactions of **NmoI** showing the C-I…O=C and N-H…O=C in a CPK view together with an extended series of **NmoI** molecules:*

2.5 Conclusion

The synthesis and characterization of four 3×3 isomer grids based on a benzamide backbone was carried out. All of the grids exhibited a tendency for the formation of an imide bridge when the pyridine nitrogen was in the *ortho*-position. Further work on these imide derivatives will be discussed in Chapter 5 (section 5.5).

^{1}H NMR analysis showed common trends throughout the grids, with clear downshifting of the amide proton when either functional group was brought in closer proximity. This held true except for the **NxxI** series, which showed a slight upshift when the iodo- functional group was in the *ortho*-position. These deviations were due to spin-induced heavy atom effects.[21]

The melting point analysis of the grids displayed an expected trend of high melting points associated with high molecular symmetry. A number of interesting molecules deviated from this due to hydrogen and halogen bonding interactions in the solid state, causing variances that were not expected.[25] These interactions in the solid state caused a more compact packing arrangement and subsequent higher melting point. The C12-Br12…O1=C1 interaction in **Brop** allowed for a higher than expected melting point of 175-178°C. **NpmBr** showed hydrogen bonding with distances of 2.32 Å, allowing for a high melting point of 224-225°C.

Crystal structure analysis was carried out on all compounds for which crystals of sufficient quality were grown. A number of interesting structures were found. The **Brpo** structure contained cyclic hydrogen bonding leading to the formation of a dimer in the solid state. **Brom** was found to have a Br…Br interaction. The **NxxBr** series had two structures of particular interest. **NpmBr** displayed very short distance intermolecular hydrogen bonding, which allowed the formation of a catemer structure in the solid state. The **NomBr** structure contained halogen bonding between C13-Br13…N22.

The **Ixx** and **NxxI** series had three structures of note, **Imm**, **Iood** and **NmmI**. **Imm** displayed N1-H1…O1=C1 hydrogen bonding chains leading to the formation of a 2D buckled sheet in the solid state. **Iood** contained two halogen bonding interactions, one intramolecular, C22-I2…N22, and one intermolecular, C22-I2…O2=C2. **NmmI** was observed to have three different types of intermolecular interactions, leading to tetramer formation in the solid state.

2.6 References

1. Ghose AK, Herbertz T, Salvino JM, Mallamo JP. Knowledge-based chemoinformatic approaches to drug discovery. Drug Discov Today 2006 DEC;11(23-24):1107-14.

2. Ghose AK, Viswanadhan VN, Wendoloski JJ. A knowledge-based approach in designing combinatorial or medicinal chemistry libraries for drug discovery. 1. A qualitative and quantitative characterization of known drug databases. J Comb Chem 1999 JAN 1999;1(1):55-68.

3. Eckert H, Bojorath J. Molecular similarity analysis in virtual screening: Foundations, limitations and novel approaches. Drug Discov Today 2007 MAR;12(5-6):225-33.

4. Gilbert AM, Antane MM, Argentieri TM, Butera JA, Francisco GD, Freeden C, Gundersen EC, Graceffa RF, Herbst D, Hirth BH, Lennox JR, McFarlane G, Norton NW, Quagliato D, Sheldon JH, Warga D, Wojdan A, Woods M. Design and SAR of novel potassium channel openers targeted for urge urinary incontinence. 2. selective and potent benzylamino cyclobutenediones. J Med Chem 2000 MAR 23;43(6):1203-14.

5. Alfred B. Isosterism and bioisosterism in drug design. In: Jucker Ernst, editor. Progress in drug research. 1st ed. Switzerland: Birkhäuser Basel; 1991. Pg 287.

6. Balakin K, Tkachenko S, Okun I, Skorenko A, Ivanenkov Y, Savchuk N, Ivashchenko A, Nikolsky Y. Bioisosteric morphing in primary hit optimization. Chimica Oggi-Chemistry Today 2004 JAN-FEB;22(1-2):15-8.

7. Orpen A. Structural systematics in molecular inorganic-chemistry. Chem Soc Rev 1993 JUN;22(3):191-7.

8. Armstrong CM, Loboda A. A model for 4-aminopyridine action on K channels: Similarities to tetraethylammonium ion action. Biophysical Journal 2001;81(2):859-904.

9. Wirtz PW, Verschuuren JJ, van Dijk JG, de Kam ML, Schoemaker RC, van Hasselt JGC, Titulaer MJ, Tjaden UR, den Hartigh J, van Gerven JMA. Efficacy of 3,4-diaminopyridine and pyridostigmine in the treatment of lambert-eaton myasthenic syndrome: A randomized, double-blind, placebo-controlled, crossover study. Clin Pharmacol Ther 2009 JUL;86(1):44-8.

10. Green KN, Steffan JS, Martinez-Coria H, Sun X, Schreiber SS, Thompson LM, LaFerla FM. Nicotinamide restores cognition in alzheimer's disease transgenic mice via a mechanism involving sirtuin inhibition and selective reduction of Thr231-phosphotau. J Neurosci 2008 NOV 5;28(45):11500-10.

11. Desai M, Stramiello L. Polymer-bound edc (P-edc) - a convenient reagent for formation of an amide bond. Tetrahedron Lett 1993 NOV 26;34(48):7685-8.

12. Pinal R. Effect of molecular symmetry on melting temperature and solubility. Organic & Biomolecular Chemistry 2004;2(18):2692-9.

13. Woolfson MM. An introduction to X-ray crystallography. Cambridge University Press; 1997.

14. Mocilac P, Tallon M, Lough AJ, Gallagher JF. Synthesis, structural and conformational analysis of a 3 x 3 isomer grid based on nine methyl-N-(pyridyl)benzamides. Crystengcomm 2010;12(10):3080-90.

15. Mocilac P, Gallagher JF. Structural systematics and conformational analyses of a 3 x 3 isomer grid of nine N-(tolyl)pyridinecarboxamides and three chlorinated relatives. Crystengcomm 2011;13(17):5354-66.

16. Qi J, Yang Q, Lam K, Zhou Z, Chan A. N-(4-bromophenyl)pyridine-2-carboxamide. Acta Crystallographica Section E-Structure Reports Online 2003 MAR;59:O374-5.

17. Percival D, Storey JMD, Harrison WTA. N-(2-Bromophenyl)pyridine-3-carboxamide. Acta Crystallographica Section E 2007;63(4):o1851-2.

18. Mocilac P, Donnelly K, Gallagher JF. Structural systematics and conformational analyses of a 3 3 isomer grid of fluoro-N-(pyridyl)benzamides: Physicochemical correlations, polymorphism and isomorphous relationships. Acta Crystallogr Sect B-Struct Sci 2012 APR;68:189-203.

19. Viger-Gravel J, Leclerc S, Korobkov I, Bryce DL. Direct investigation of halogen bonds by solid-state multinuclear magnetic resonance spectroscopy and molecular orbital analysis. J Am Chem Soc 2014 MAY 14;136(19):6929-42.

20. Percival D, Storey JMD, Harrison WTA. N-(2-bromophenyl)pyridine-3-carboxamide. Acta Crystallographica Section E-Structure Reports Online 2007 APR;63:O1851-2.

21. Kaupp M, Malkina O, Malkin V, Pyykko P. How do spin-orbit-induced heavy-atom effects on NMR chemical shifts function? validation of a simple analogy to spin-spin coupling by density functional theory (DFT) calculations on some iodo compounds. Chemistry-a European Journal 1998 JAN;4(1):118-26.

22. Mocilac P, Lough AJ, Gallagher JF. Structures and conformational analysis of a 3× 3 isomer grid of nine N-(fluorophenyl) pyridinecarboxamides. CrystEngComm 2011;13(6):1899-909.

23. Mocilac P, Gallagher JF. The first phenyl-N-pyridinylcarbamate structures: Structural and conformational analysis of nine methoxyphenyl-N-pyridinylcarbamates. Crystal Growth & Design 2013;13(12):5295-304.

24. Clark T, Hennemann M, Murray JS, Politzer P. Halogen bonding: The σ-hole. Journal of Molecular Modeling 2007;13(2):291-6.

25. Boese R, Kirchner MT, Dunitz JD, Filippini G, Gavezzotti A. Solid-state behaviour of the dichlorobenzenes: Actual, semi-virtual and virtual crystallography. Helv Chim Acta 2001 2001;84(6):1561-77.

CHAPTER 3

Further Work on Difluoro-substituted benzamide isomer grids

3.1 Introduction

3.1.1 Fluorine NMR

Fluorine 19 is present at 100% abundance in nature and is a spin 1/2 nucleus.[1] The method for obtaining ^{19}F NMR spectra is similar to the standard approach of proton NMR.[2] Fluorine NMR can give us a deeper understanding of the environment in the vicinity of the F nucleus as it contains 9 electrons, allowing for a wide range of chemical shifts and interactions between neighbouring protons. Its van der Waal's radius (1.47 Å) is close to that of hydrogen (1.20 Å), which enables easy substitution in organic compounds and a relatively sterically unchanged product.[3]

Fluorine spins are capable of energy exchange with both protons and other fluorines. This exchange can occur through bonds, which is spin-spin coupling,[4,5] and over short distances through space, called dipole-dipole coupling.[6] These couplings can give us detailed information about internuclear distances in fluorinated compounds, similar to NOE studies.[7]

Because of its similarity to H protons, fluorine NMR has been used to map out the structural features of a large number of different proteins too complex to be analysed by traditional proton NMR. The sensitivity of the ^{19}F resonance to its surroundings has revealed important kinetic and structural characteristics of conformational changes to proteins. Proteins are labelled by the addition of fluorinated amino acids, most commonly fluorotryptophan and fluorophenylalanine.[8] These mono-substituted amino acids differ only slightly in their sterics in relation to the unsubstituted amino acids, and as such do not cause any differences in the overall protein folding/interactions.

Fluorine rarely occurs naturally in biological systems, so the ^{19}F spectrum cannot be obscured by additional signals. Because the labelled amino acids may be present in a number of different positions in the overall structure of the protein, a detailed view of the folding/unfolding of the protein can be observed.

After work was completed on the **Brxx/NxxBr** series, the next step undertaken was to synthesise a larger series of compounds, this time altering the position of three functional groups on the benzamide backbone. These 18 compound isomer grids allow us to observe and rationalise trends in NMR, IR and M.p data, and link it with crystallographic data to provide a detailed picture of these molecules in the solid state.

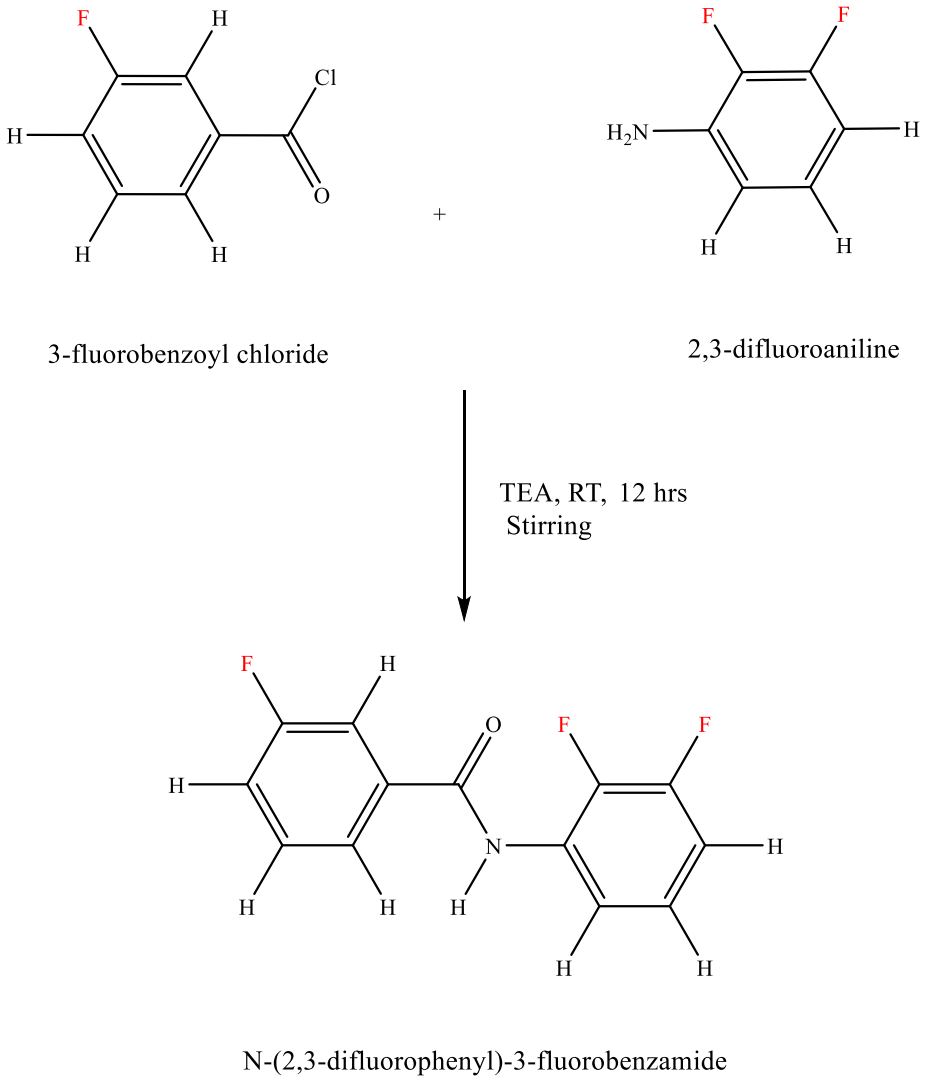

3-fluorobenzoyl chloride

2,3-difluoroaniline

N-(2,3-difluorophenyl)-3-fluorobenzamide

Fig 3.1: reaction scheme for N-(2,3-difluorophenyl)-3-fluorobenzamide:

The reaction proceeds via the Schotten-Baumann Reaction, which occurs between an acyl chloride (3-Fluorobenzoyl Chloride) and a primary amine (2,3-difluoroaniline), resulting in the formation of an amide bridge and loss of HCl.[9] TEA was required to lower the amount of unwanted side reactions that would have occurred with the release of HCl in the reaction.

3.1.2 Halogen bonding

Halogen bonding is a type of non-covalent interaction between a halogen atom and a negative site on another molecule.[10] The interaction strength increases as the halogen is changed from chlorine to bromine to iodine. Clark *et al*. discusses the existence of an area of positive electrostatic potential, called a σ-hole, that is present on the axis of the halogen X, and the moiety it is bonded to, R.[11] This potential has been described by Murray, Paulsen and Politzer, and can be seen in the visualisation below.[12]

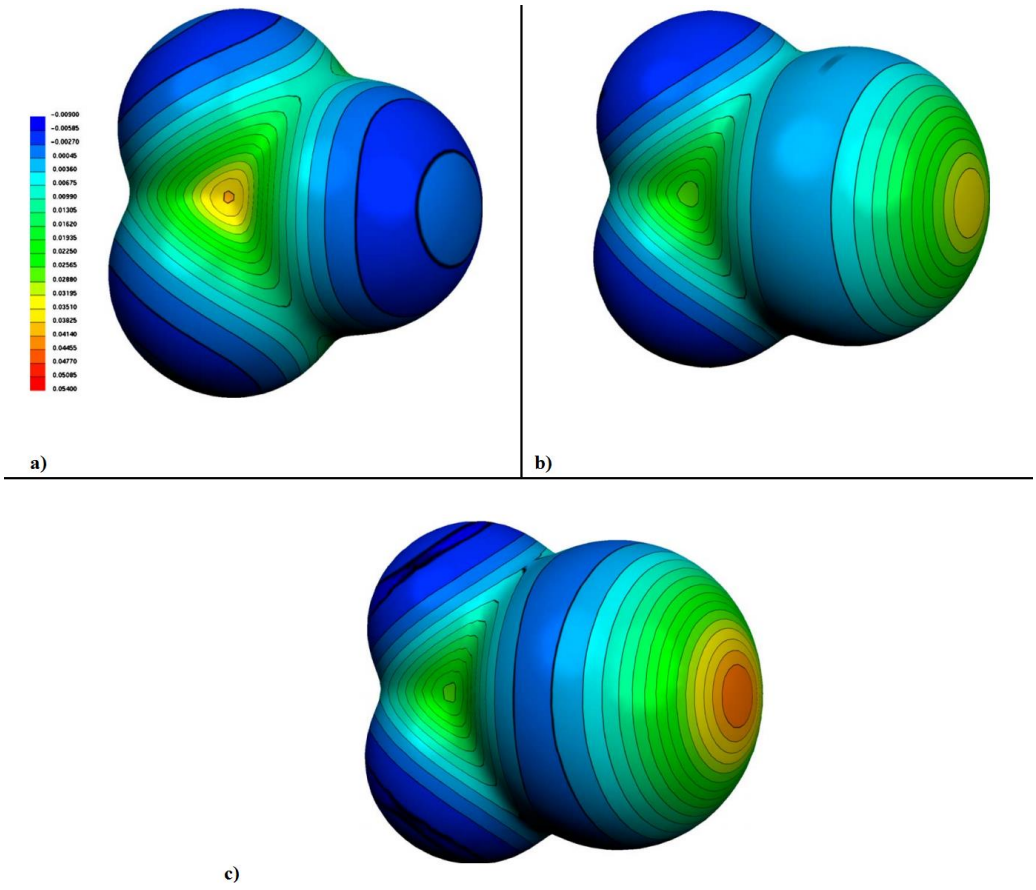

Fig 3.2: Visualisation of σ-hole in isodensity surface of a) CF_4, b) CF_3Cl and c) CF_3Br. Scale in Hartrees, at the 0.001 electrons Bohr^{-3} (adapted from Murray, Paulsen and Politzer).[11]

The relative strength of this potential is affected by the electron-attracting power of the halogen substituent as well as the degree of *sp* hybridization of the *s* unshared electrons present.[13] These interactions can have an effect on packing in the solid state, leading to interesting new structures.[14-16]

3.1.3 Nomenclature

The compounds synthesised were named according to the substitution patterns of the fluorine on the aniline ring. The positions of the fluorine on the benzoyl chloride moiety are not altered in this six compound series. A shorthand method was used to denote the substitution, for example, the *N*-(2,3-difluorophenyl)-3-fluorobenzamide was shortened to **Fm23**. The *m* (x) in this case denotes the *meta*-position of the fluorine on the benzoyl chloride, and the 2,3- (yz) denotes the positions of the difluoro substituents, with one in the *ortho*-, or 2 position and one in the *meta*-, or 3 position. The overall structure abbreviation **Fxyz** and **Mxyz** is used for clarity throughout.

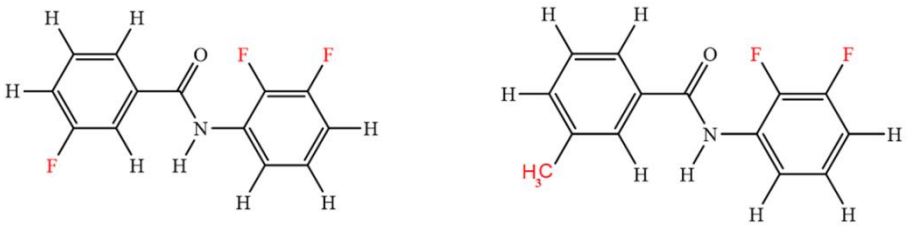

*Fig 3.3: Chapter 3 **Fxyz**/**Mxyz** templates:*

The compounds synthesised were named according to the following tables (Where di F = difluoroaniline and F-benzoyl Cl = fluorobenzoyl Chloride)

*Table 3.1: Nomenclature of **Fxyz** series:*

	2,3 di F	**2,4 di F**	**2,5 di F**	**2,6 di F**	**3,4 di F**	**3,5 di F**
***p*-F-benzoyl Cl**	**Fp23**	**Fp24**	**Fp25**	**Fp26**	**Fp34**	**Fp35**
***m*- F-benzoyl Cl**	**Fm23**	**Fm24**	**Fm25**	**Fm26**	**Fm34**	**Fm35**
***o*- F-benzoyl Cl**	**Fo23**	**Fo24**	**Fo25**	**Fo26**	**Fo34**	**Fo35**

*Table 3.2: Nomenclature of **Mxyz** series:*

	2,3 di F	**2,4 di F**	**2,5 di F**	**2,6 di F**	**3,4 di F**	**3,5 di F**
***p*-Toluoyl Chloride**	**Mp23**	**Mp24**	**Fp25**	**Mp26**	**Mp34**	**Mp35**
***m*-Toluoyl Chloride**	**Mm23**	**Mm24**	**Mm25**	**Mm26**	**Mm34**	**Mm35**
***o*-Toluoyl Chloride**	**Mo23**	**Mo24**	**Mo25**	**Mo26**	**Mo34**	**Mo35**

3.2 Synthetic Procedure

The reactions were carried out in an identical manner to those in Chapter 2 (see section 2.2). Into a 100 mL clean and dry round-bottom flask 30 mL of dichloromethane, 0.005 mol of *N,N* difluoroaniline and a magnetic stirrer were introduced. Into the resulting solution 0.005 mol of the corresponding fluorobenzoyl chloride and 0.005 mol of triethylamine were added. The solution was left to stir overnight. The resulting solution was then washed with 5×30mL of 2% $NaHCO_3$ in a separating funnel. The organic phase was then removed under reduced pressure to remove all traces of solvent, and the product was carefully weighed out.

Table 3.3: Reagents used for fluoro-substituted series:

	Molar mass (g/mol)	**Density (g/mL)**	**Volume(mL)**
2-fluorobenzoyl chloride	158.56	1.328	0.597
3-fluorobenzoyl chloride	158.56	1.304	0.607
4-fluorobenzoyl chloride	158.56	1.342	0.591
2,3-difluoroaniline	129.11	1.274	0.507
2,4-difluoroaniline	129.11	1.282	0.504
2,5-difluoroaniline	129.11	1.283	0.503
2,6-difluoroaniline	129.11	1.277	0.506
3,4-difluoroaniline	129.11	1.302	0.496
3,5-difluoroaniline	129.11	1.295	0.6455

Table 3.4 Reagents used for methyl-substituted series:

	Molar mass (g/mol)	**Density (g/mL)**	**Volume(mL)**
***p*- toluoyl chloride**	158.56	n/a	0.773g
***m*- toluoyl chloride**	158.56	1.173	0.659
***o*- toluoyl chloride**	158.56	1.185	0.652
2,3-difluoroaniline	129.11	1.274	0.507
2,4-difluoroaniline	129.11	1.282	0.504
2,5-difluoroaniline	129.11	1.283	0.503
2,6-difluoroaniline	129.11	1.277	0.506
3,4-difluoroaniline	129.11	1.302	0.496
3,5-difluoroaniline	129.11	1.295	0.6455

3.3 Synthetic Results

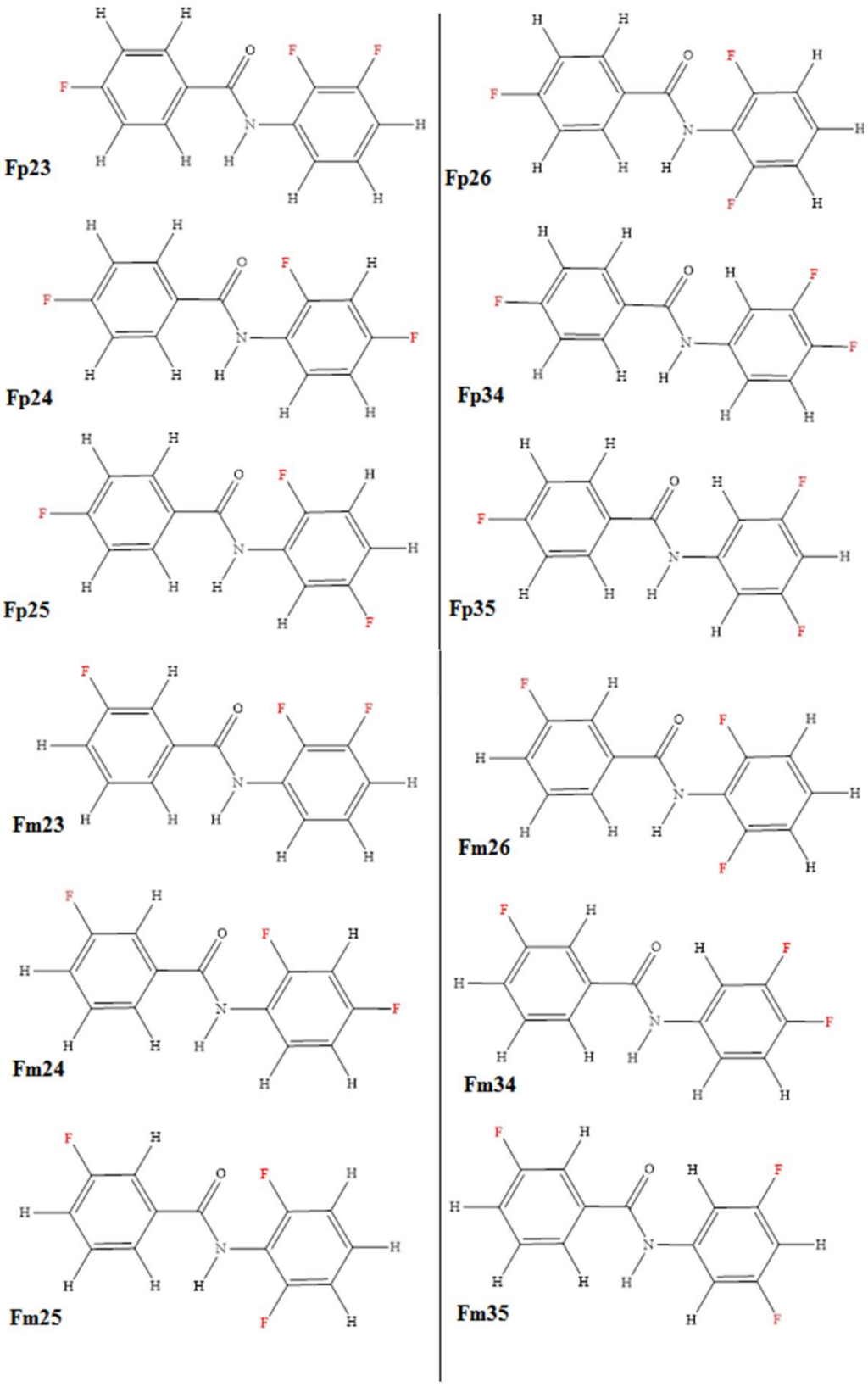

*Fig 3.4: Structures of **Fpxx** series and **Fmxx** series*:

*Table 3.5: Results of **Fpxx** reactions:*

	Melting point (°C)	**Yield (g)**	**N-H Peak DMSO d^6 (ppm)**	**N-H Peak $CDCl_3$ (ppm)**	**Significant IR peaks (cm^{-1})**
Fp23	147-149	0.71 57%	10.39	7.9	3259, 3142, 1932, 1652
Fp24	131-132	0.42 34%	10.18	7.8	3290, 1903, 1644, 1602
Fp25	124-125	0.74 59%	10.28	7.96	3277, 1907, 1660, 1600
Fp26	147-148	0.14 9%	10.20	7.36	3125, 1914, 1664, 1601
Fp34	120-121	0.39 27%	10.48	7.74	3102, 1654, 1601, 1514
Fp35	146-148	0.87 69%	10.60	7.86	3210, 1907, 1649, 1599

*Table 3.6: Results of **Fmxx** reactions:*

	Melting point (°C)	**Yield (g)**	**N-H Peak DMSO d^6 (ppm)**	**N-H Peak $CDCl_3$ (ppm)**	**Significant IR peaks (cm^{-1})**
Fm23	112-115	1.2 94%	10.45	7.94	3309, 1660, 1587, 1468
Fm24	115-117	0.99 80%	10.26	7.84	3296, 1653, 1587, 1527
Fm25	121-122	1.11 89%	10.41	7.99	3320, 1659, 1624, 1478
Fm26	129-130	0.39 31%	10.29	7.47	3362, 1658, 1589, 1519
Fm34	119-121	0.92 74%	10.53	7.83	3319, 1653, 1588, 1511
Fm35	147-149	0.94 75%	10.65	7.89	3306, 1655, 1604, 1438

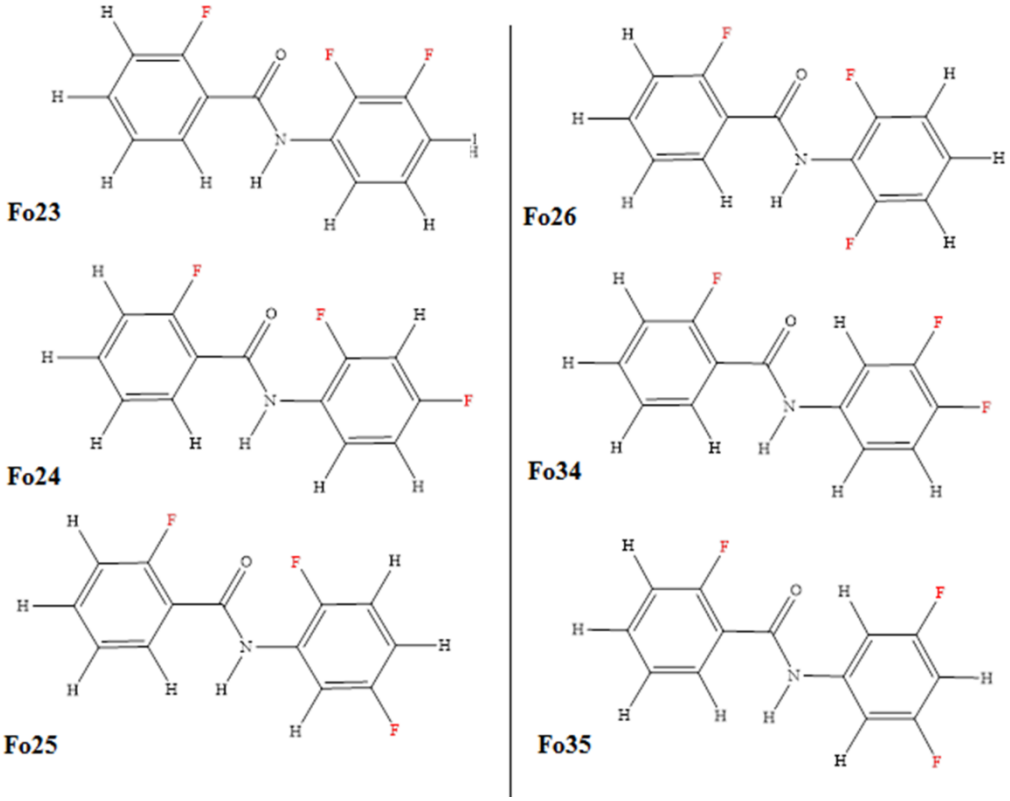

*Fig 3.5: Structures of **Foxx** series:*

*Table 3.7: Results of **Foxx** reactions:*

	Melting point (°C)	**Yield (g)**	**N-H Peak DMSO d^6 (ppm)**	**N-H Peak $CDCl_3$ (ppm)**	**Significant IR peaks (cm^{-1})**
Fo23	100-102	1.14 88%	10.39	8.73	3370, 1661, 1546, 1469
Fo24	110-112	1.09 87%	10.16	8.61	3375, 1656, 1610, 1481
Fo25	63-65	1.1 88%	10.32	8.88	3398, 1669, 1611, 1475
Fo26	112-113	0.37 30%	10.13	8.05	3376, 1666, 1519, 1464
Fo34	126-128	1.1 89%	10.67	8.39	3337, 1661, 1538, 1482
Fo35	130-132	1.15 91%	10.81	8.45	3348, 1660, 1606, 1458

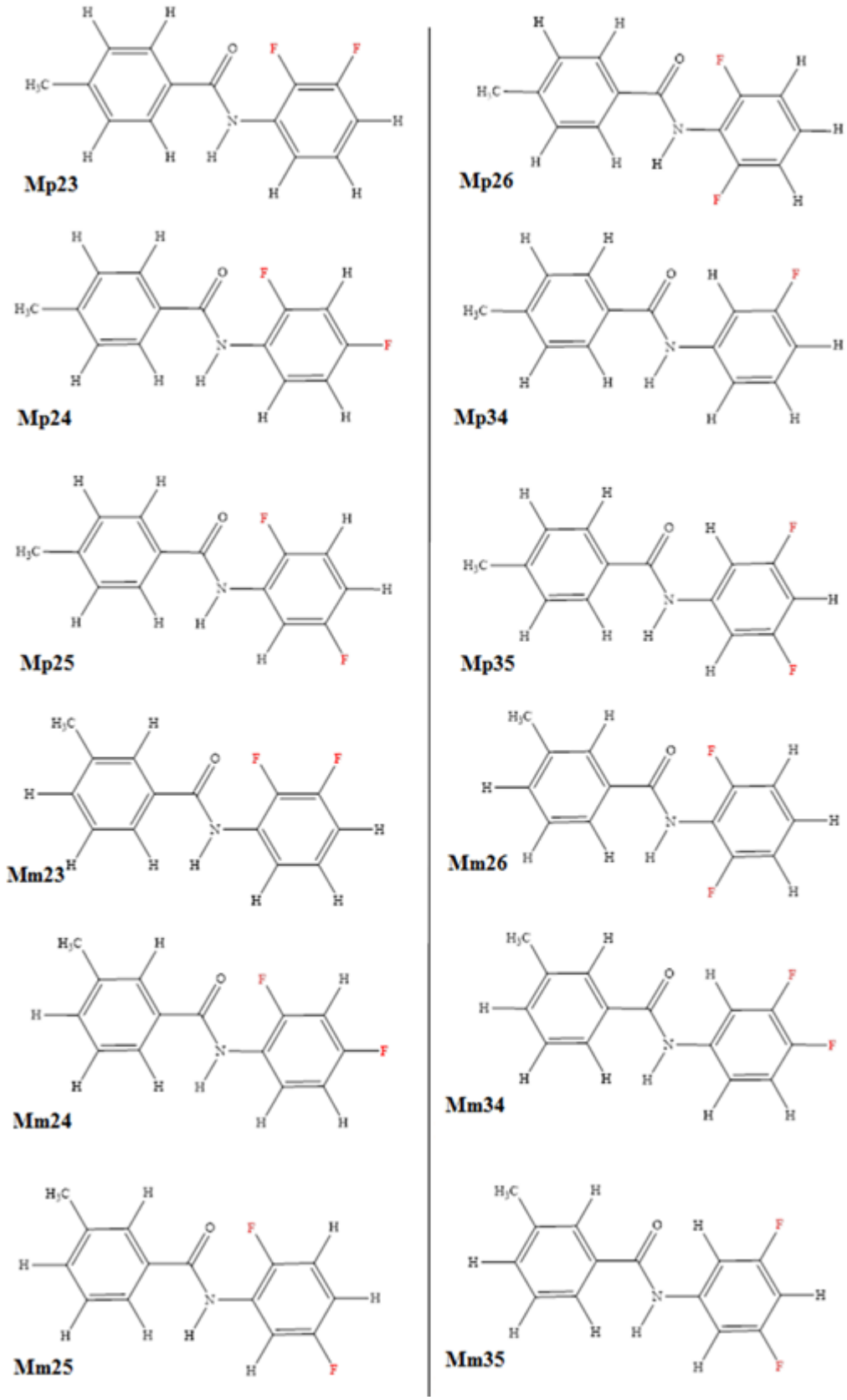

*Fig 3.6: Structures of **Mpxx** and **Mmxx** series:*

*Table 3.8: Results of **Mpxx** reactions:*

	Melting point (°C)	**Yield (g)**	**N-H Peak DMSO d^6 (ppm)**	**N-H Peak $CDCl_3$ (ppm)**	**Significant IR peaks (cm^{-1})**
Mp23	127-128	0.6 48%	10.25	8.06	3259, 1650, 1527, 1497
Mp24	119-120	0.84 68%	10.05	7.94	3288, 1655, 1612, 1500
Mp25	111-112	0.33 27%	10.14	8.09	3299, 1656, 1609, 1476
Mp26	164-165	0.1 2.7%	10.06	7.48	3250, 1658, 1596, 1465
Mp34	157-158	0.43 35%	10.37	7.91	3366, 1657, 1511, 1427
Mp35	166-168	0.42 34%	10.53	7.91	3334, 1649, 1605, 1438

*Table 3.9: Results of **Mmxx** reactions:*

	Melting point (°C)	**Yield (g)**	**N-H Peak DMSO d^6 (ppm)**	**N-H Peak $CDCl_3$ (ppm)**
Mm23	91-92	1.05 85%	10.31	8.06
Mm24	111-112	0.4 33%	10.11	7.84
Mm25	92-93	0.27 22%	10.20	7.99
Mm26	114-115	0.46 37%	10.16	7.68
Mm34	93-94	0.96 78%	10.43	7.79
Mm35	103-105	1.2 97%	10.56	7.84

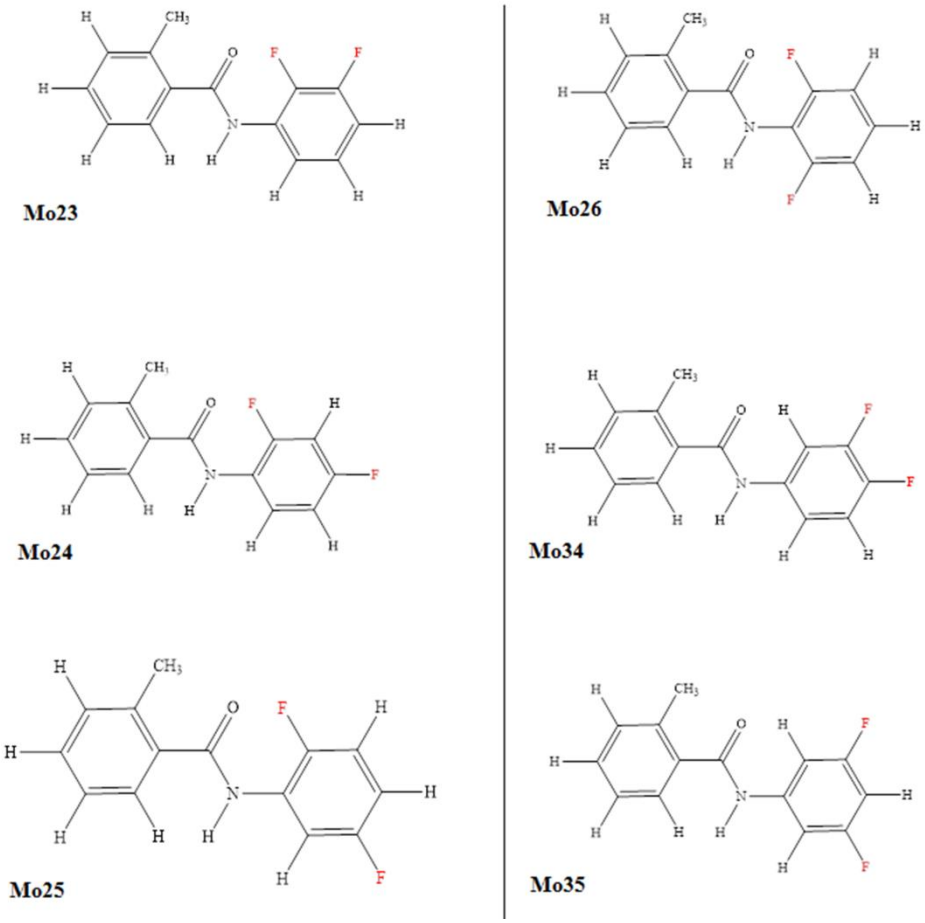

*Fig 3.7: Structures of **Moxx** series:*

*Table 3.10: Results of **Moxx** reactions:*

	Melting point (°C)	**Yield (g)**	**N-H Peak DMSO d^6 (ppm)**
Mo23	101-103	0.95 77%	10.34
Mo24	129-130	0.90 73%	10.12
Mo25	89-90	0.91 74%	10.31
Mo26	137-139	0.72 58%	10.08
Mo34	126-127	0.94 76%	10.57
Mo35	117-118	0.83 67%	10.71

3.4 Discussion

3.4.1 Fxyz series

The yields for the **Fpxx** reactions were all reasonable with the majority found to have around a 50% yield. The number of washings done on each of the compounds could account for some reduced yields. All compounds were analysed by NMR and IR, the data for which can be seen in table 3.5 above. Upon analysis of the N-H proton peak that there seemed to be no major trend in either the DMSO or $CDCl_3$ NMRs. As the fluorines were moved from a position closer to the amide proton to the 2,4- and 2,6- positions, a decrease in chemical shift was observed, the amide proton becomes more shielded when the fluorines are in the 2,4- and 2,6- positions. The highest shift came when the fluorines were in the 3,5- position; the amide proton was considerably more affected by the electron withdrawing tendencies of the fluorine groups and was deshielded as a result.

Melting point were obtained for all series and it was noted that, in general as molecular symmetry increased, so too did the melting points. The highest melting points for the **Fpxx** series were the 2,3-, 2,6- and 3,5-, with melting points in the range of 148°C. The 2,6- and 3,5- were expected to have largest melting points of the series, as both molecules are symmetrical. The 2,3- compound also had a high melting point, this could be due to intermolecular interactions occurring in the solid state, causing a bump in expected M.p.

The **Fmxx** series behaved similarly to the **Fpxx** in regards to both NMR trends and M.p trends. The data for the **Fmxx** series can be seen summarized in table 3.6 above.

Once again we can see an increase in the chemical shift of the amide proton when the fluorine substituents are in the 3,4- and 3,5- positions. The compounds that have the highest M.ps are again seen to be the most symmetrical molecules, **Fm26** and **Fm35**. The **Foxx** series again illustrates the similarities between the three F**xyz** reactions. The chemical shift of the amide proton can be seen to increase when the fluorines are in the 3,4- and 3,5- positions, in this case giving us the highest shift to date, 10.81 ppm. This large jump in chemical shift in the **Foxx** series is due to the proximity of

the fluorine on the benzoyl moiety pulling electron density away from the amide bond and causing a deshielding effect. The results of the **Foxx** reactions can be seen summarized above in table 3.7.

The M.ps observed increase as the molecules become more symmetrical. There is a marked overall reduction in M.p temperature compared to the **Fpxx** and **Fmxx** series, with a drop of 20-30°C. This is due to the *ortho*-fluorine on the benzoyl, which could prevent intermolecular interactions in the solid state because of its proximity to the amide proton.

*Table 3.11: ^{19}F shift for **Fxxx** series:*

Fpxx series	**Fp23**	**Fp24**	**Fp25**	**Fp26**	**Fp34**	**Fp35**
Ppm of significant peaks	-108, -139, -145,	-108, -113, -116,	-108, -118, -127,	-108(1F), -118(2F)	-108, -137, -144,	-108(1F), -109(2F),
Fmxx series	**Fm23**	**Fm24**	**Fm25**	**Fm26**	**Fm34**	**Fm35**
Ppm of significant peaks	-112, -138, -145	-112.5, -113, -116	-108, -113, -122	-113,(1F) -120(2F)	-108, -132, -139	-104(1F), -108(2F)
Foxx series	**Fo23**	**Fo24**	**Fo25**	**Fo26**	**Fo34**	**Fo35**
Ppm of significant peaks	-114, -139, -147	-114, -115, -118	-117, -119, -125	-117(1F), -120(2F)	-118, -139, -142	-110(1F), -115(2F)

^{19}F NMRs were run on the **Fxxx** series, and the results can be seen in table 3.11 above.

The **Fpxx** series showed the expected three signals, with the exception of the two symmetrical molecules **Fp26** and **Fp35**, which showed two signals. The peak at -108 ppm is present in all 6 compounds and is representative of the *para*-fluorine on the benzoyl moiety. More upfield shift is noticed on the fluorines on the aniline ring

when the diF groups are in close proximity to one another. Similar trends can be seen in the **Fmxx** and **Foxx** series. In these series, it was noted that as the two fluorines on the aniline were moved around the aniline ring, their movement caused a slight change in the ppm of the *meta*- and *ortho*-fluorine on the benzoyl moiety. When discussing shielding effects in ^{19}F NMR, the Buckingham equation is used.[17]

It states that the observed shielding (σ_{sample}) results from the additive contributions from the motions of both electrons near the nucleus being looked at (σ_{local}) and electrons in other parts of the molecule ($\sigma_{neighbour}$).[18] Electric fields ($\sigma_{electric}$) or charged parts of the molecule also have an effect on the overall state of the fluorines. Short range contacts can also occur between atoms in close proximity (σ_{sr}). When the diF groups are in close proximity to each other, this could allow for a greater contribution from both short range contacts and $\sigma_{neighbour}$ contributions. In the **Foxx** series, we can see upfield signals again when the diF groups are in the 2,3 and 3,4 positions. As in all the 2,6- and 3,5- compounds, we see only two signals, as the diF groups are accounted for in the peak with integration 2 in the spectra.

3.4.2 Fpxx Crystal structure analysis

Crystals were successfully grown for the **Fpxx** series by slow evaporation at room temperature, again from $CHCl_3$, acetone or ethyl acetate. Full geometry tables and structural information for each elucidated structure can be found in the Appendix. Only the **Fpxx** and **Mpxx** series were successfully resolved the remaining compounds structures were very disordered or did not form sufficiently good single crystals when grown.

3.4.2.1 Fp23 crystal structure analysis

Fp23 crystallises in the space group *C2/c*, and the R factor was 0.060. The major interactions noted in the solid state were C1=O1…H1-N1 hydrogen bonding and F23…H15 short contact interactions with a distance of 2.516 Å. The structure was isomorphous with the previously described structure **Brpp.**

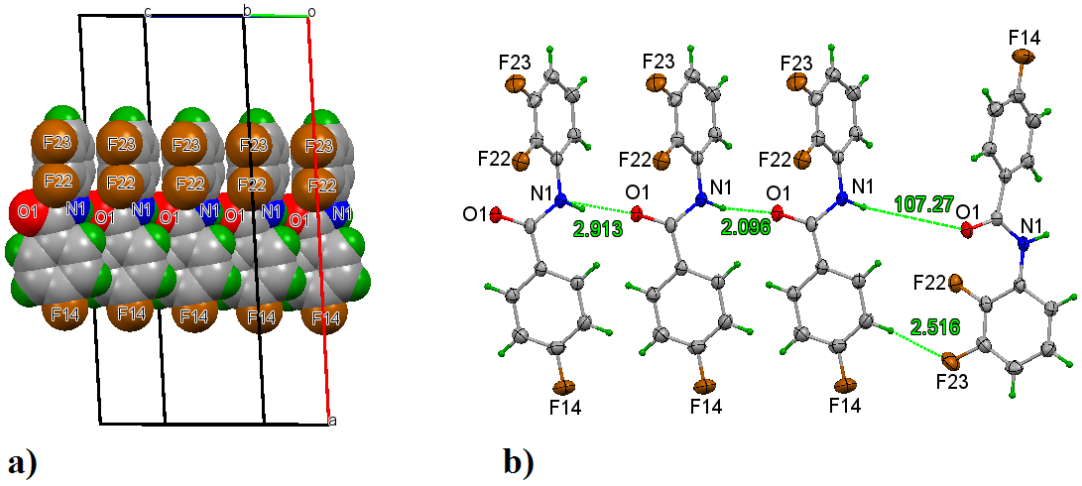

a) **b)**

*Fig 3.8: A) Spacefill diagram showing C1=O1…H1-N1 hydrogen bonding interactions in **Fp23**; B) Ellipsoid diagram showing length of interactions in Å:*

3.4.2.2 Fp24 crystal structure analysis

Fp24 crystallises in the $P2_1$ space group and was found to be quite disordered. The significant interactions in the molecule were C1=O1…H1-N1 hydrogen bonding and F24…H23-C23 interactions.

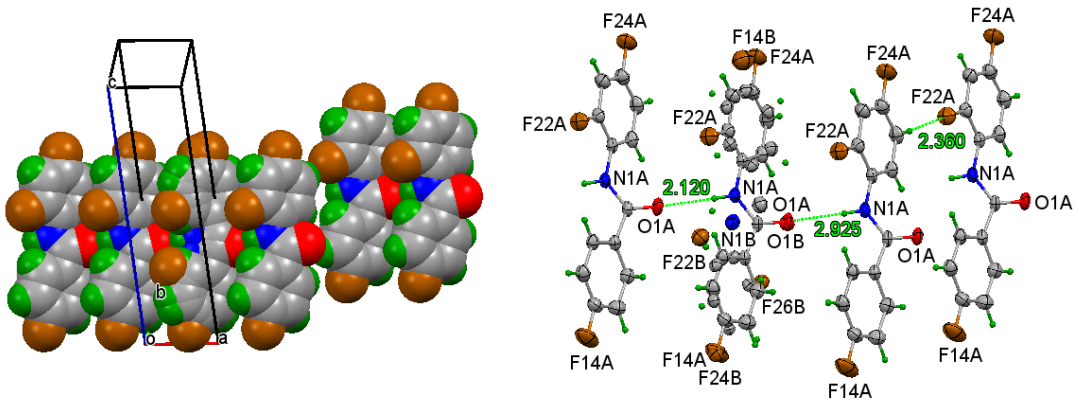

a) **b)**

*Fig 3.9: A) Spacefill diagram showing C1=O1…H1-N1 hydrogen bonding interactions in **Fp24**; B) Ellipsoid diagram showing length of interactions in Å:*

3.4.2.3 Fp25 crystal structure analysis

Fp25 crystallised in the *Pc* space group and the R factor of the structure was found to be 0.033. The interactions noted in the solid state were C1=O1…H1-N1 hydrogen bonding and F25…H15-C15 interactions.

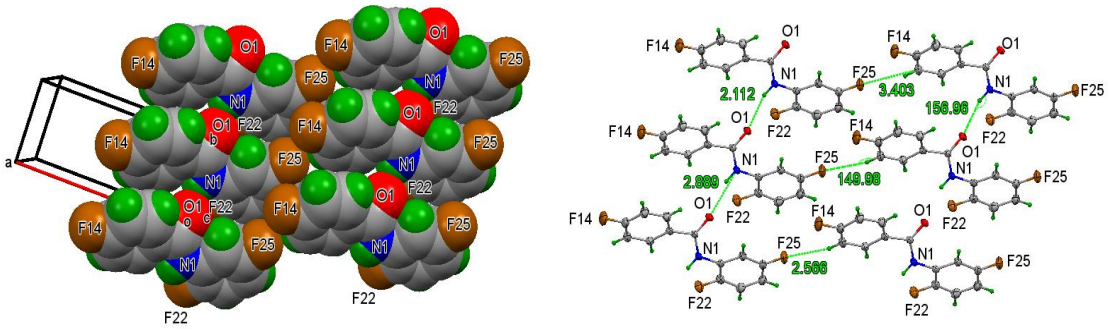

Fig 3.10: A) Spacefill diagram showing C1=O1…H1-N1 hydrogen bonding interactions in ***Fp25****; B) Ellipsoid diagram showing length of interactions in Å:*

3.4.2.4 Fp26 crystal structure analysis

Fp26 was found to crystallise in the $P2_1$ space group and was well resolved with an R factor of 0.033. In addition to C1=O1…H1-N1 hydrogen bonding and F22…H15-C15 interactions, a π…π stacking interaction was noted between C12…C15 with a distance of 3.361 Å.

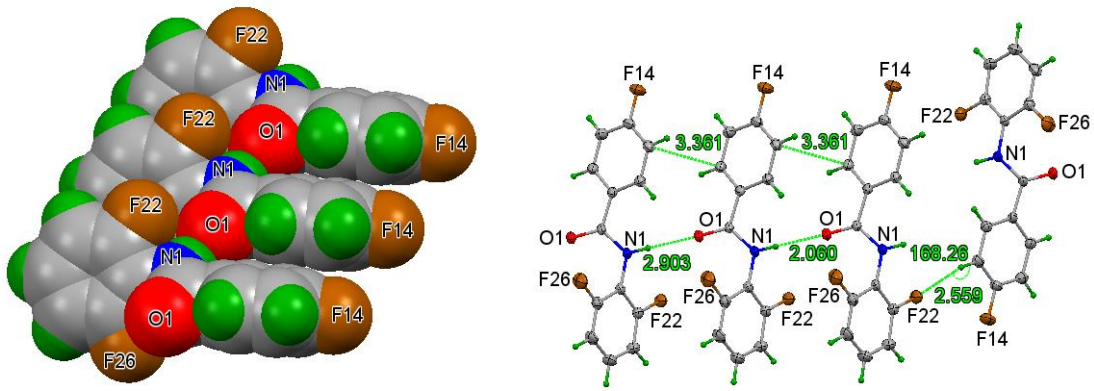

Fig 3.11 A) Spacefill diagram showing pi-pi stacking interactions in ***Fp26*** *solid state; B) ellipsoid diagram of* ***Fp26*** *showing C1=O1…H1-N1 hydrogen bonding interactions and F22…H15-C15 interactions (distances in Å):*

3.4.2.5 Fp34 crystal structure analysis

Fp34 crystallised in the $P2_1/c$ space group with an R factor of 0.045. The main interactions noted wereC1=O1…H1-N1 hydrogen bonding and F23…C14 interactions.

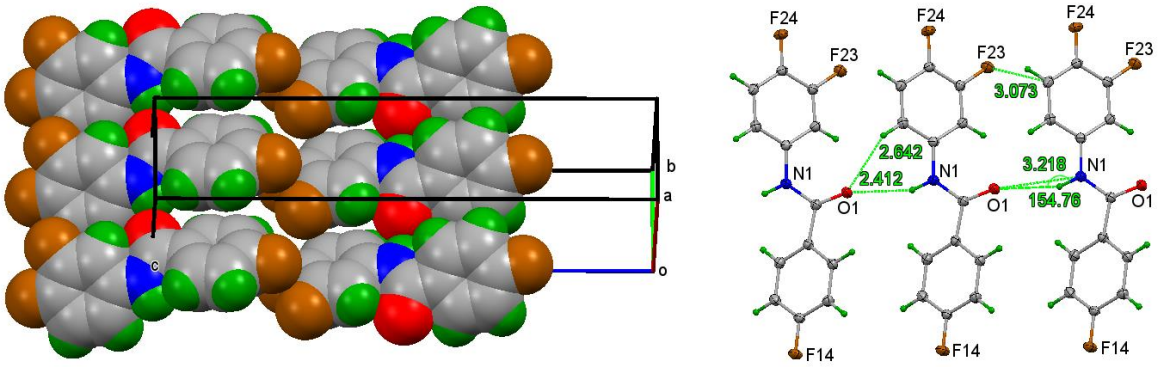

a) **b)**

Fig 3.12: A) Spacefill diagram showing C1=O1…H1-N1 interactions in ***Fp34*** *solid state; B) ellipsoid diagram of* ***Fp34*** *showing length of interactions (distances in Å):*

An interesting F14…F23 interaction also arose in the **Fp34** structure. This intermolecular interaction occurred at a distance of 2.861 Å.

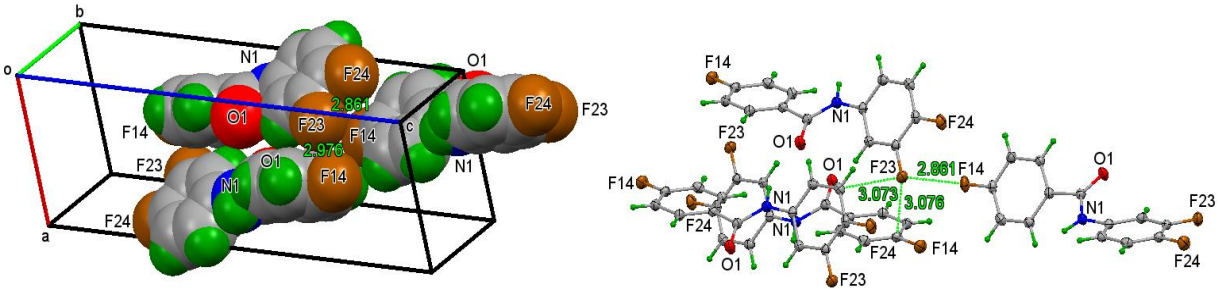

a) **b)**

Fig 3.13: A) Ellipsoid diagram showing F14…F23 interactions in ***Fp34*** *solid state; B) Spacefill diagram of* ***Fp34*** *showing F14…F23 interactions (distances in Å):*

3.4.2.6 Fp35 Crystal structure analysis

Fp35 was found to have crystallised in the $P2_1$ space group, with an R factor of 0.041. The molecule was found to have three main interactions, C1=O1…H1-N1 and O1…H15-C15 hydrogen bonding interactions (as seen in Fig 3.14) along with F23…F23 interactions with an intermolecular distance of 2.91 Å.

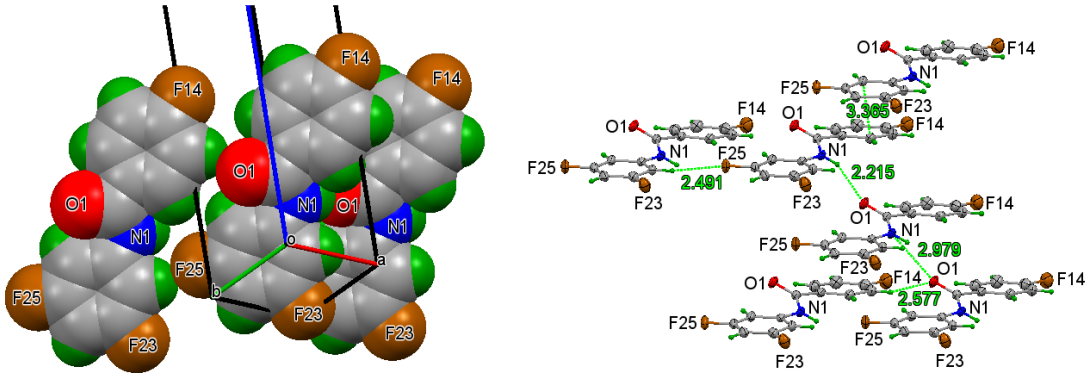

*Fig 3.14: A) Spacefill diagram showing C1=O1…H1-N1 and O1…H15-C15 hydrogen bonding interactions in **Fp35** solid state; B) Ellipsoid diagram of **Fp35** showing hydrogen bonding interactions (distances in Å):*

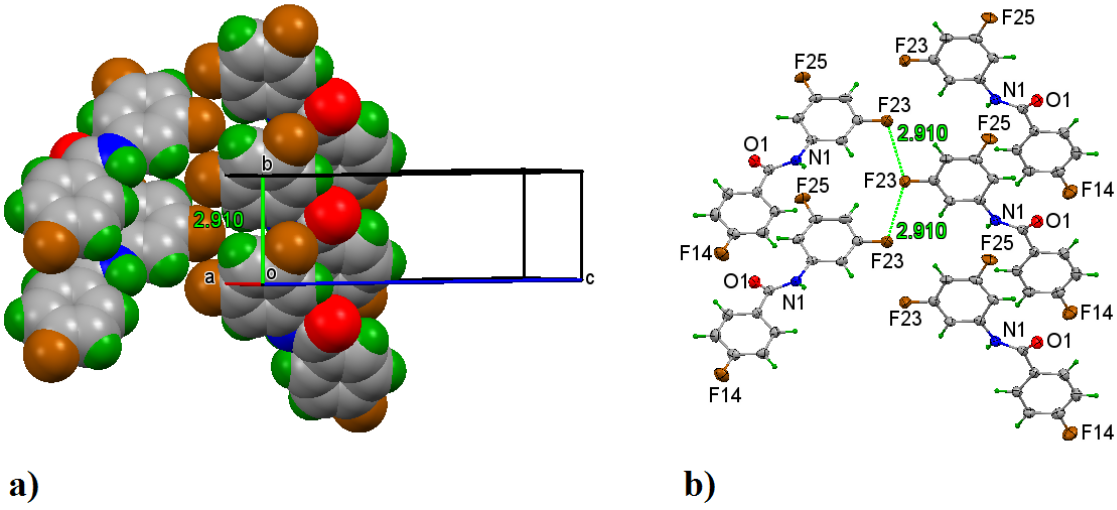

*Fig 3.15 A) Spacefill diagram showing F23…F23 interactions in **Fp35**; B) Ellipsoid diagram showing interactions (distances in Å):*

3.4.3 Mxyz series

The **Mxyz** series gave good yields in all reactions and allowed for characterisation by NMR, IR, M.p and x-ray crystallography. No issues were encountered and with the exception of the **Mp26** reaction, all compounds synthesised gave a yield of around 50%.

The **Mpxx** series showed a number of trends similar to those in the **Fxyz** series of compounds. This similarity is expected as the series differ only by the functional group on the benzoyl backbone, for the **Fxyz** series fluorine, the **Mxyz** series, a methyl group. The NMR data again followed the previous compounds trends of increasing chemical shift as the fluorine substituents moved to the 3,4- and 3,5- positions. The M.ps can be seen to increase as the compounds become more symmetrical. The **Mp26** melting point was not obtained due to a low yielding reaction, all available compound was used up in the running of NMRs, IRs and crystal growth. A summary of the results obtained for the **Mpxx** reactions can be seen above in table 3.8.

The **Mmxx** and **Moxx** series also showed evidence of shared trends with the **Fxyz** series. Both the **Mmxx** and **Moxx** NMR data followed the same path as their fluorinated counterpart, with the largest amide shift noted when the fluorine substituents were in the 3,4- and 3,5- positions. The **Mmxx** series differs in its melting point trends, however. It can be seen below in table 3.8, that the highest melting point was **Mm26**, which was expected, but the next highest is the unsymmetrical **Mm24**, with a melting point only 3°C lower. This could be due to the influence of a number of intermolecular interactions between molecules in the solid state. The positioning of one of the fluorines in the para position could allow for a more closely packed crystal structure, causing a raise in M.p as the more densely packed a crystal the more energy required to break it apart.

The **Moxx** series too differs from the established M.p trends. It can be seen in table 3.9 that the compound with the highest M.p is a symmetrical molecule, **Mo26**, however there are two unsymmetrical molecules that follow closely behind in M.p, **Mo24** and **Mo34**, with M.ps of 129-130°C and 126-127°C respectively. Both of these compounds have fluorine in the *para* position, which lend credence to the fact that this *para* Fluorine is causing better packing in the solid state.

3.4.4 Mpxx Crystallographic analysis

3.4.4.1 Mp23 Crystal structure analysis

Mp23 crystallised in the *Pca2₁* space group and was found to have two major interactions in the solid state, as can be seen in Fig 3.15. C17-H17…C26 interactions and O1…H1-N1 hydrogen bonding were noted, with a distance of 2.891 and 2.099 Å respectively. **Mp23** was found to be isomorphous with **Mp25**.

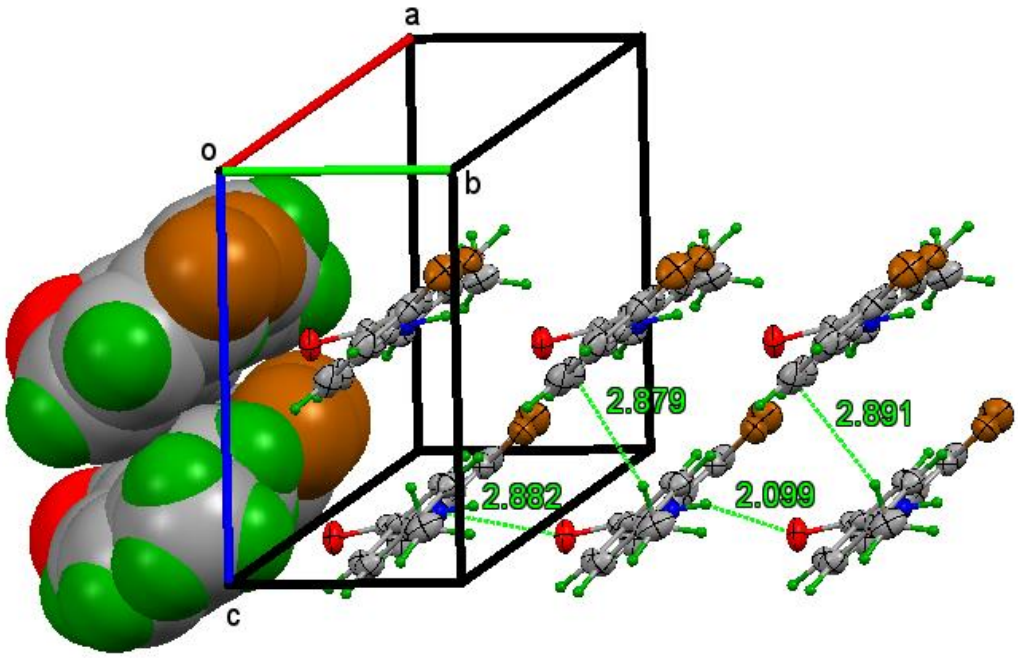

*Fig 3.16: Ellipsoid structure of **Mp23** showing A) H17…C26 interactions B) C1=O1…H1-N1 hydrogen bonding:*

3.4.4.2 Mp24 Crystal structure analysis

Mp24 crystallised in *Pca2₁* space group and has two molecules in its asymmetric unit. It was also found to be isostructural with **Mp23** and **Mp25**. The major interactions of the molecule were found to be C1A=O1A…H1-N1 hydrogen bonding, F24A…H17A-C17A interactions and F22B…H23B-C23B interactions.

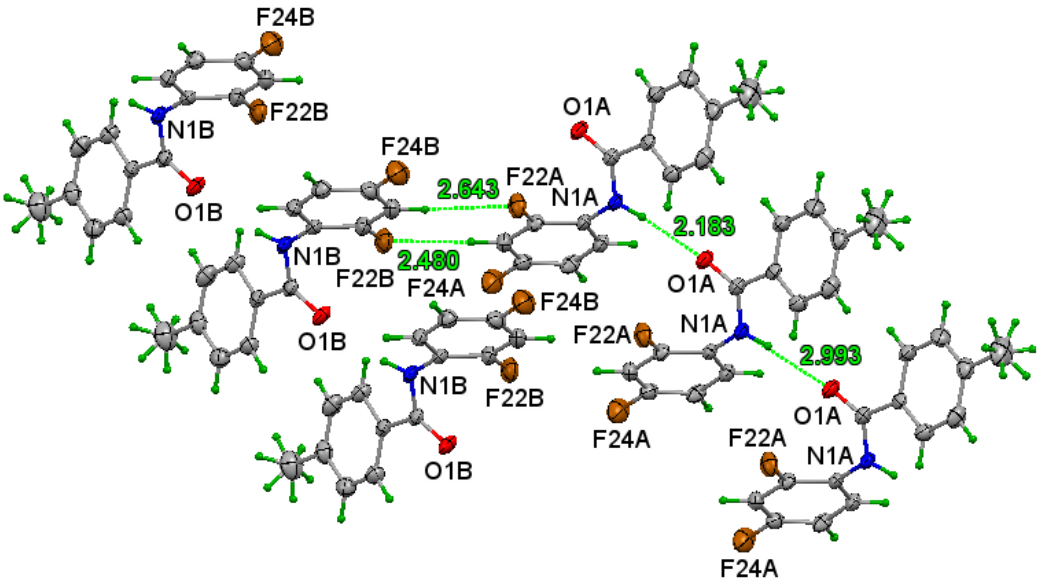

*Fig 3.17: Ellipsoid structure of **Mp24** showing intermolecular interactions:*

3.4.4.3 Mp25 Crystal structure analysis

Mp25 crystallised in the *Pca2$_1$* spacegroup and was found to have two major intermolecular interactions in the solid state. These interactions were a hydrogen bonding interaction between C1=O1...H1-N1 and a F22…H13-C13 interaction. **Mp25** was also found to be isomorphous with **Mp23**.

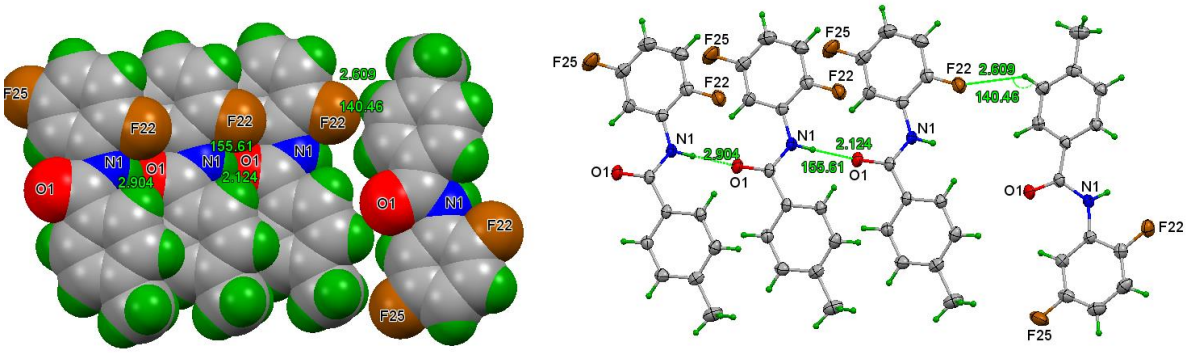

a) **b)**

*Fig 3.18: A) Spacefill structure of **Mp25** showing contact points between C1=O1...H1-N1 and F22…H13-C13. B) Ellipsoid structure showing interaction distances in Å:*

3.4.4.4 Mp26 Crystal structure analysis

Mp26 was found to crystallise in the *P2₁/c* spacegroup and contained two major interactions in the solid state. C1=O1…H1-N1 hydrogen bonding was observed along with a C12-H12…C26 interaction. The molecule was noted to be isostructural with **Mp35.**

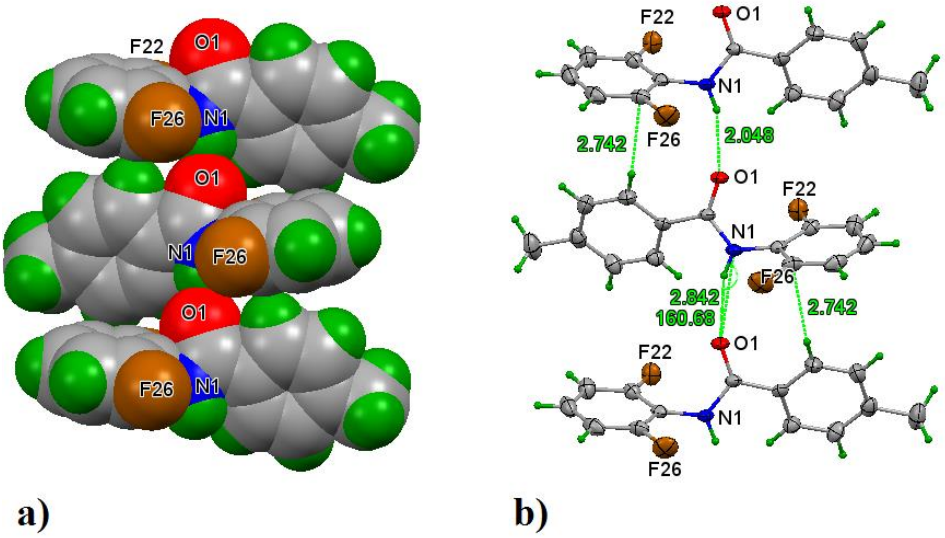

Fig 3.19: A) Spacefill structure showing contact point of C2=O1…H1-N1 hydrogen bonding and C12-H12…C26 interaction. B) Ellipsoid structure of ***Mp26*** *showing interaction distances in Å:*

3.4.4.5 Mp34 Crystal structure analysis

Mp34 was found to have crystallised in the *P-1* spacegroup and contains three intermolecular interactions. O1…H1-N1 hydrogen bonding was observed along with F23…H25-C25 interactions and F24…H17-C17 fluorine to methyl H interactions.

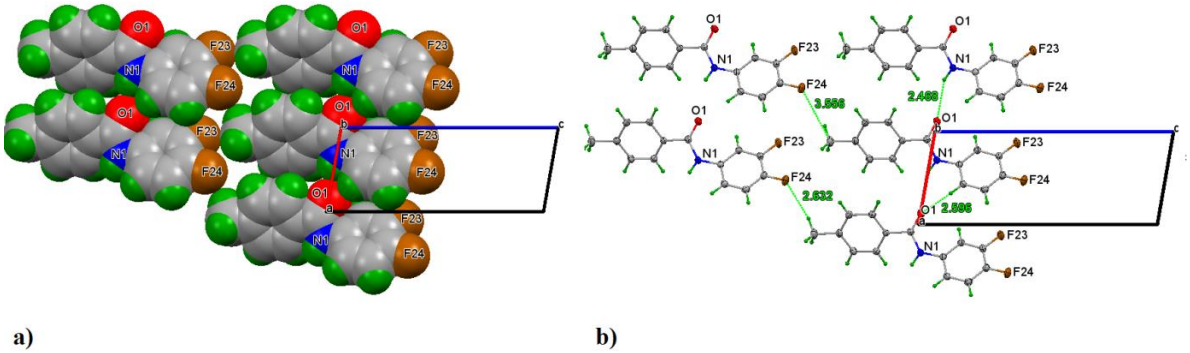

Fig 3.20: A) Spacefill structure of ***Mp34*** *showing contact points of interactions B) Ellipsoid structure showing interaction distances in Å.*

3.4.4.6 Mp35 Crystal structure analysis

Mp35 crystallised in the *P-1* spacegroup and has noted to be isostructural with **Mp26**. The main intermolecular interactions were C1=O1…H1-N1 hydrogen bonding, F23…H24C24 interactions and F25…H23-C23 halogen short contact interactions.

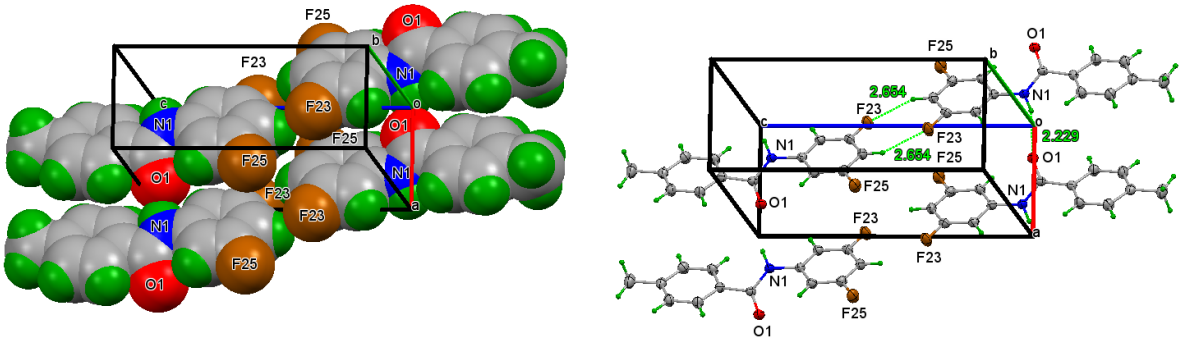

a) **b)**

*Fig 3.21: A) Spacefill structure of **Mp35** showing contact points of interactions. B) Ellipsoid structure showing interaction distances in Å.*

3.5 Conclusion

The synthesis and characterisation of two 3×3 isomer grids, difluorophenyl fluorobenzamides and difluorophenyl methylbenzamides were carried out. All compounds were successfully synthesised in good yield.

^{1}H NMR analysis showed that as the fluorines on the phenyl ring were moved from the 2,3- position to the 2,4- and 2,5- position, a corresponding decrease in chemical shift was observed. When the fluorine substituents were moved to the 3,5- position, a deshielding effect was observed. These observations were also noted with the **Mxyz** series, as expected.

^{19}F NMRs were carried out on the **Fxx** series and showed the expected three signals when analysed, apart from the symmetrical molecules **Fp26** and **Fp35**, which showed two signals. Upfield shift was noticed on the fluorines on the aniline ring when the diF groups were in close proximity to one another, caused by a combination of short range contacts and $\sigma_{neighbour}$ contributions. Melting points for all compounds were run and similar trends were noted in all series. As molecular symmetry increased, so too did melting points.

Mp34 was the one exception to this; its melting point was higher than expected at 157-158°C. This increase in melting point was due to the presence of three intermolecular interactions in the solid state, which allowed for the molecule to pack more tightly in the solid state and thus have a higher melting point than expected.
X-ray crystal structure analysis was carried out for the *para*- series of fluorobenzamide and methylbenzamide series. All structures in the **Fpxx** series were found to have both intermolecular hydrogen bonding interactions and halogen bonding interactions present. **Fp26** was observed to have π…π stacking interactions in addition to the above. The **Mpxx** series again had intermolecular hydrogen bonding and halogen bonding as the prevalent interactions.

3.6 References

1. Danielson M, Falke J. Use of F-19 NMR to probe protein structure and conformational changes. Annu Rev Biophys Biomol Struct 1996;25:163-95.

2. Gerig J. Fluorine nmr of proteins. Prog Nucl Magn Reson Spectrosc 1994;26:293-370.

3. Cobb SL, Murphy CD. F-19 NMR applications in chemical biology. J Fluorine Chem 2009 FEB;130(2):132-43.

4. Battiste J, Newmark R. Applications of F-19 multidimensional NMR. Prog Nucl Magn Reson Spectrosc 2006 MAR 31;48(1):1-23.

5. Mallory F, Mallory C, Butler K, Lewis M, Xia A, Luzik E, Fredenburgh L, Ramanjulu M, Van Q, Francl M, Freed D, Wray C, Hann C, Nerz-Stormes M, Carroll P, Chirlian L. Nuclear spin-spin coupling via nonbonded interactions. 8. the distance dependence of through-space fluorine-fluorine coupling. J Am Chem Soc 2000 MAY 3;122(17):4108-16.

6. Kruk D, Lips O. Field-dependent nuclear relaxation of spins 1/2 induced by dipole-dipole couplings to quadrupole spins: LaF_3 crystals as an example. J Magn Reson 2006 APR;179(2):250-62.

7. Dalvit C, Fagerness P, Hadden D, Sarver R, Stockman B. Fluorine-NMR experiments for high-throughput screening: Theoretical aspects, practical considerations, and range of applicability. J Am Chem Soc 2003 JUN 25;125(25):7696-703.

8. Jackel C, Koksch B. Fluorine in peptide design and protein engineering. Eur J Org Chem 2005 OCT 28(21):4483.

9. Schotten C. Ueber Die oxydation des piperidins. Berichte Der Deutschen Chemischen Gesellschaft 1884;17(2):2544-7.

10. Politzer P, Lane P, Concha MC, Ma Y, Murray JS. An overview of halogen bonding. Journal of Molecular Modeling 2007 FEB;13(2):305-11.

11. Clark T, Hennemann M, Murray JS, Politzer P. Halogen bonding: The σ-hole. Journal of Molecular Modeling 2007;13(2):291-6.

12. Molecular surface electrostatic potentials in the analysis of non-hydrogen-bonding noncovalent interactions. Proceedings of the Indian Academy of Sciences-Chemical Sciences Springer; 1994.

13. Lommerse JP, Stone AJ, Taylor R, Allen FH. The nature and geometry of intermolecular interactions between halogens and oxygen or nitrogen. J Am Chem Soc 1996;118(13):3108-16.

14. Chopra D, Guru Row T. Dimorphic forms in a non-centrosymmetric environment from a prochiral molecule: Cooperative interplay of strong hydrogen bonds and weak intermolecular interactions. Crystal Growth & Design 2005;5(5):1679-81.

15. Prasanna M, Row TG. C–halogen…π interactions and their influence on molecular conformation and crystal packing: A database study. Crystal Engineering 2000;3(2):135-54.

16. Prasanna M, Row TG. Analysis of weak interactions involving fluorine: A comparative study of crystal packing of some benzodiazepinone drug intermediates and their non-fluorinated analogues. CrystEngComm 2000;2(25):134-40.

17. Buckingham A, Schaefer T, Schneider W. Solvent effects in nuclear magnetic resonance spectra. J Chem Phys 1960;32(4):1227-33.

18. Buckingham A. Chemical shifts in the nuclear magnetic resonance spectra of molecules containing polar groups. Can J Chem -Rev can Chim 1960;38(2):300-7.

CHAPTER 4

Investigations Into the Viability of Isomer Grids using Pyrazine and Carbamate Based Backbones

4.1 Introduction

4.1.1 Carbamates

Carbamates and chemicals incorporating the carbamate group are of immense interest in the global agriculture and horticulture industries due to their on-going robust insecticide and herbicide usage. Much of the applications and chemical/ environmental studies in this area stem from the 1960's and 1970's.[1,2] The current drive to find more efficient, safer and more environmentally friendly carbamates for a multitude of applications is on-going and aims to generate by-products and decomposition products that are less harmful to nature. Progressing alongside these studies is research into the biological roles of carbamates and a multitude of new drugs incorporating the carbamate group in drug discovery and design.[3-4]

In contrast with this, research on the structural and supramolecular aspects of carbamates has attracted considerably less attention than other classes of organic molecules to date. Organic carbamates are a category of compounds ripe for systematic studies in crystal engineering, coordination chemistry and material sciences.[5,6]

Until 2013 there were no phenyl-*N*-pyridinylcarbamates reported on the Cambridge Structural Database (CSD) and at that time there were only 33 known phenylcarbamate crystal structures.[5] Therefore, development of aromatic carbamate structural chemistry until very recently was conducted in an irregular/molecule by molecule fashion. There are several factors that have impeded such studies (contrasting with benzamide chemistry) and these include the commercial unavailability of starting chemical building blocks, synthetic and crystallization difficulties and a general lack of stability (with decomposition of the chemical products occurring over days/weeks). Therefore, substituted phenyl-*N*-pyridinylcarbamates represent challenging chemical systems for structural investigations and future studies will facilitate considerable research development into new classes of carbamates and their chemical structure. Of further note is that there are *N*-pyridinylcarbamates that are known to have antifungal, herbicidal and

plant anticytokinin activity.[7,8] These are regarded as significant both in biological and medicinal chemistry research.[9-12]

Mocilac and Gallagher recently reported the first phenyl-*N*-pyridinylcarbamate crystal structures (**CxxOMe**) (where **x** = *para*-, *meta*-, *ortho*) as part of an extensive systematic study of aromatic carbamate isomers.[13]

Isomer grids were synthesised and subsequently characterised by spectroscopic methods, with their solid-state and modelled structures analysed for comparisons.[13-15] These original **CxxOMe** isomers form N-H···N (amide...pyridine) hydrogen bonds as the primary intermolecular interaction, resulting in *C*(5) and *C*(6) chains, dimers with $R^2_2(8)$ rings, or trimers.[13] The isomorphous structures of **CmoM•**H_2O and **CmoBr•**H_2O hydrates have been reported where a monohydrate forms an integral hydrogen bonding component part of the respective crystal structures.[16]

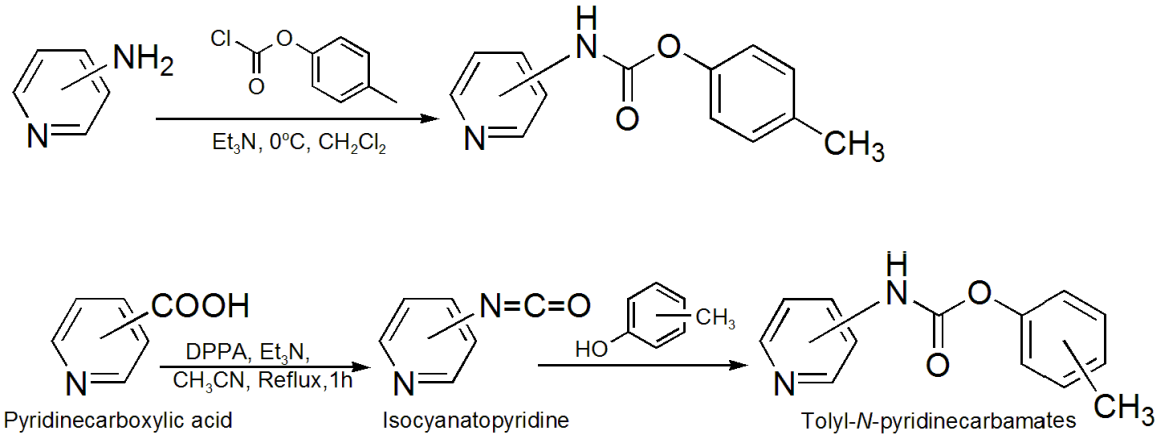

*Fig 4.1: Scheme diagram of Condensation of the 4-/3-/2-aminopyridines with 4-tolylchloroformate for the **CppM, CmpM** derivatives (PhD thesis of P. Mocilac, 2012); with **CopM** under solventless conditions (top) and a general Curtius rearrangement reaction scheme for the six **CxmM** and **CxoM** isomers (bottom):*

In unpublished research work, Mocilac and Gallagher describe the 3 × 3 isomer grid of nine tolyl-*N*-pyridinylcarbamates (**CxxM**) with full characterisation, seven crystal structures and an analysis of the **CxxM** conformations (with **CmoM•**H_2O previously reported).[16] This **CxxM** research builds on their original **CxxOMe** landmark paper published in the journal *Crystal Growth and Design* in 2013.[13] The work on this class of organic linker group and molecule will continue to be an on-going high impact area of research, now and in the future.[3,4 8,17,18] In the scheme above (*Fig 4.1*)

the general approaches taken to synthesise carbamates by using either an acyl or acid starting material are seen. Given the stability (or lack thereof) of carbamates, the fact that the reaction takes place in only one or two steps does not detract from the difficulties in cleaning, separating and purifying the compounds.

4.1.2 Nomenclature

The aim of this chapter of the Thesis was to investigate the viability of a range of different alternative backbone configurations, and to analyse and rationalize their impact on NMR, IR and structure and packing in the solid state. A compound based on the original benzamide backbone was synthesised with the addition of 2-aminopyrazine in place of 2-aminopyridine, as can be seen below in *Fig 4.2.* A series of phenyl carbamate derivatives were also synthesised and analysed, and can also be seen in *Fig 4.2*.

The products synthesized were named based on whether they formed the 1:1 product (**Cxx**) or the 2:1 product (**Cxxd**).The type of diazine used in the reaction was denoted by the following abbreviations in the name, Pyridine(**pyr),** Pyrimidine(**pyrm),** Pyrazine (**pyrz)** *e.g.* **Cxpyr or Cxpyrmd.** The final step was to indicate the position of the amino group ($-NH_2$) on the diazine ring by a red *ortho-*, *meta-* or *para-* e.g. **Copyr or Cmpyrmd.** Formation of a carbonate 2:1 side product was also noted with these reactions, as seen below. Reactions were also carried out with nitrophenyl chloroformate substituted for phenyl chloroformate and these two reactions will be discussed in section 4.4.

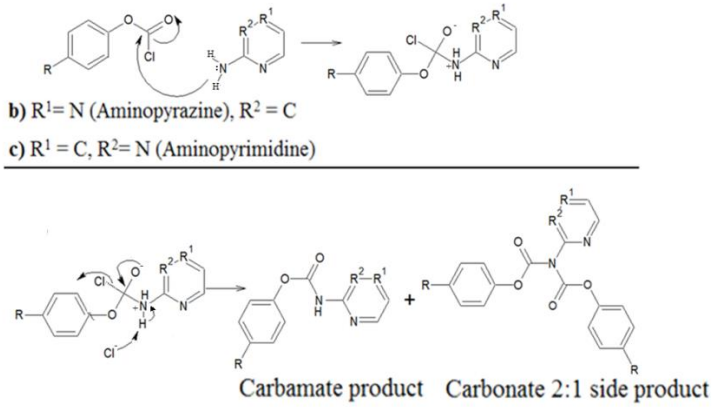

Fig 4.2: Formation of Carbamate and Carbonate side product:

4.2 Synthetic Procedure

A 3-necked 100ml round bottomed flask was equipped with magnetic stirrer and nitrogen bubbler and DCM and Triethylamine were added. This colourless solution was stirred for 5 minutes to allow for a homogenous mixture at room temperature.

Aminopyridine/Aminodiazine was weighed and added, and was stirred until dissolved. Once all solids had dissolved, the reaction mixture was placed on ice before the phenyl chloroformate derivative was added drop-wise into the flask via syringe over 1 minute. The reaction was left to stir overnight before washing. All reactions were run with 10mmol of each starting material.

A 250ml separating funnel was prepared to wash the reaction mixture. 5g of potassium bicarbonate was dissolved in 250ml of deionised water. The reaction mixture was placed into a funnel and washed three times with the $KHCO_3$ solution. The organic layer was separated from the aqueous layer and magnesium sulphate was used to dry the organic layer. The magnesium sulphate was removed via gravity filtration.

The round bottomed flask containing the reaction mixture was placed on a rotary evaporator (set between 30-35°C) to remove any unwanted solvent. The reaction mixture after rotary evaporation usually had an oil-like consistency. This was left overnight and separation was carried out using column chromatography.

Table 4.1: Reagents used for Chapter 4 reactions:

Reagent	Molar Mass (g/mol)	Density (g/ml)	Volume (mL)	Mass (g)	Concentration (mol)
3-Bromobenzoyl Chloride	219.46	1.662	1.32	n/a	0.01
2-Aminopyrazine	95.1	n/a	n/a	0.96	0.01
2-Aminopyrimidine	95.1	n/a	n/a	0.96	0.01
Phenyl Chloroformate	156.57	1.248	1.255	n/a	0.01
4-Nitrophenyl Chloroformate	201.56	1.5	1.344	n/a	0.01
Triethylamine	101.19	0.726	2.78	n/a	0.02

4.3 Synthetic results

The first compounds synthesised were variations on the work done in Chapter 2, with the Aminopyridine moiety replaced with 2-aminopyrazine. a) **Brmozd** and b) **Brmoz** are seen below in *Fig 4.3*:

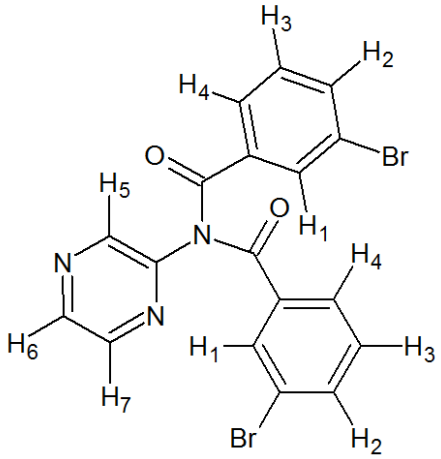

a) 3-bromo-*N*-(3-bromobenzoyl)-*N*-(pyrazin-2-yl) benzamide

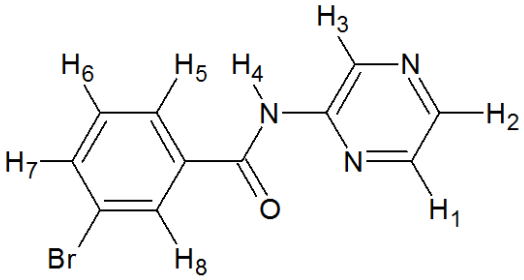

b) 3-bromo-*N*-(pyrazin-2-yl) benzamide

Fig 4.3: Structures of a) ***Brmozd*** *and b)* ***Brmoz****:*

Table 4.2: Results for ***Brmozd/Brmoz*** *reactions:*

	Melting point (°C)	**Yield (g)**	**N-H Peak DMSO d^6 (ppm)**	**N-H Peak $CDCl_3$ (ppm)**	**Significant IR peaks (cm^{-1})**
Brmozd	182-194	0.238 5%	n/a	n/a	3310, 1648, 1508,1267
Brmoz	144-155	0.075 3%	11.28	8.44	n/a

The next reactions attempted were the 7 carbamates, **Copyrz, Copyrm**, **$CopyrzNO_2$**, **$CopyrmNO_2$**, **Copyr, Cmpyr and Cppyr**. Major reactivity issues were encountered during synthesis of these molecules using a condensation reaction. Very little carbamate product was successfully isolated after washing and chromatography.

The majority of the compounds isolated during these reactions were the carbonate by-products. The structures of the carbamates that were attempted can be seen below in fig 4.4:

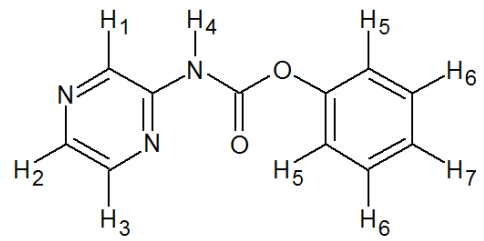

Copyrz

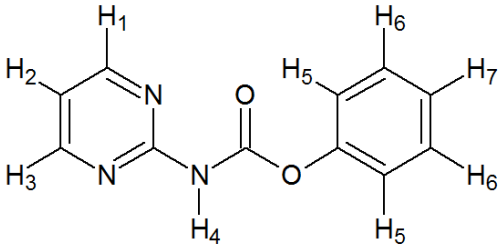

Copyrm

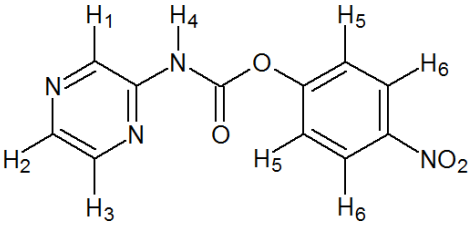

CopyrzNO₂

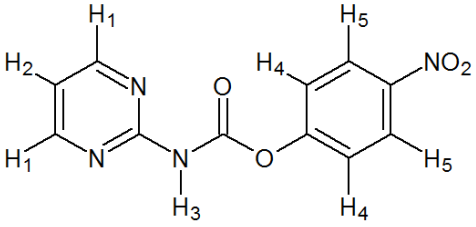

CopyrmNO₂

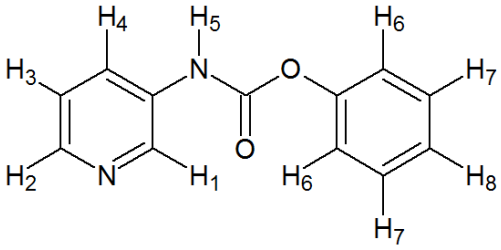

Cmpyr

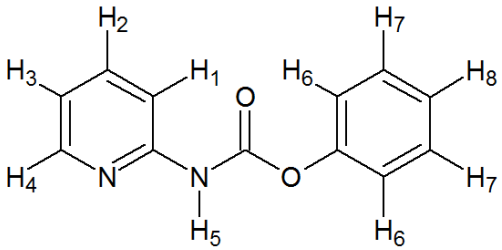

Copyr

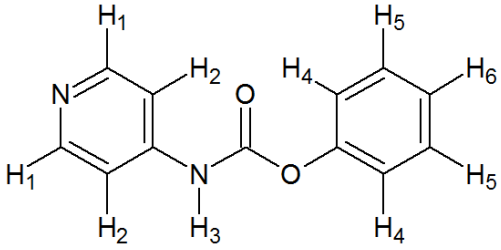

Cppyr

Fig 4.4: Structures of carbamates showing the substitution pattern of nitrogen in pyrazine/pyrimidine/pyridinering in each of the compounds:

Table 4.3: Results for carbamate reactions:

	Melting point (°C)	**Yield (g)**	**N-H Peak DMSO d^6 (ppm)**	**Significant IR peaks (cm^{-1})**
Copyrz	65.0-101.3	0.085 3%	9.33	2924, 1741, 1551, 1188
Copyrm (carbonate by-product)	75.6-81.2	0.06 1%	n/a	2924, 1771, 1488, 1255
CopyrzNO_2	n/a	n/a	n/a	n/a
CopyrmNO_2	n/a	n/a	n/a	n/a
Copyr (carbonate by-product)	75.6-79.4	0.5 mix 22%	n/a	2923, 1763, 1489, 1160
Cmpyr (carbonate by-product)	73.5-79.1	0.037 2%	n/a	2981, 1771, 1488, 1253
Cppyr (carbonate by-product)	140.1-146.2	0.056 3%	n/a	2790, 1752, 1590, 1189

The carbonate side products isolated can be seen below in *fig 4.5.*

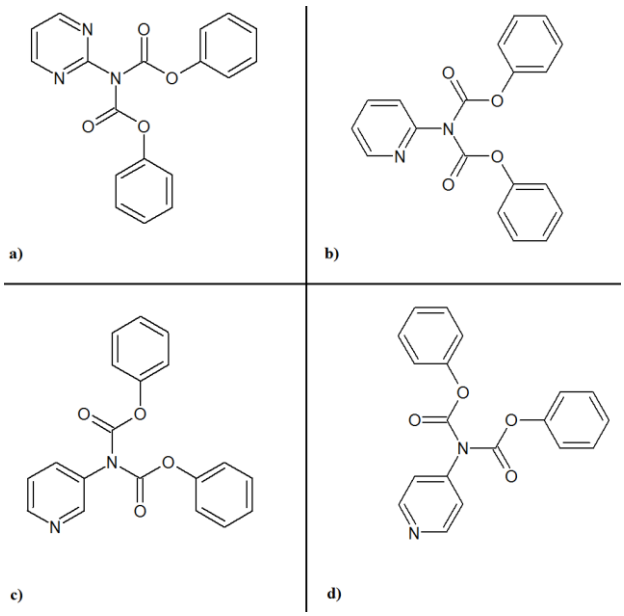

Fig 4.5: structures of a) diphenyl pyrimidin-2-ylimidodicarbonate, b) diphenyl pyridin-2-ylimidodicarbonate, c) diphenyl pyrimidin-3-ylimidodicarbonate and d) diphenyl pyrimidin-4-ylimidodicarbonate:

4.4 Discussion

4.4.1 Brmoz / Brmozd compounds

The yield for **Brmoz** reactions was found to be quite low, with respective yields of 5.2% and 2.7%. Compared to **Brmo,** whose yield was 49%, the alteration between the 2-aminopyridine starting material and the 2-aminopyrazine starting material caused a large change in the overall reactivity of the system. 2-AP acts as a stronger base, with a pK_a of 6.86, compared to its 2-pyrazine counterpart, which has a pK_a of 3.14.[19] The presence of the extra nitrogen in the aromatic ring leads to more inductive effects on the ring itself and thus less available electron density for the lone pair on the amine group.

As with the *ortho*- series on chapter 2, it was observed that formation of an imide moiety had taken place. ^{1}H-NMRs were run in both $CDCl_3$ and DMSO-d_6, the **Brmozd** NMR showed a slight impurity, subsequent analysis was done using the single crystals grown from ethyl acetate. IRs were carried out, the results of which can be seen in *table 4.2*. All functional groups expected were noted in the data.

The melting points collected were significantly higher than those noted for **Brmo** and **Brmod** in chapter 2, **Brmoz** and **Brmozd** were observed to have m.ps of 144-155°C and 181-194°C, compared to m.ps of 115-120°C and 145-147°C for **Brmo** and **Brmod**. This difference is due to the effects of the extra nitrogen in the solid state, allowing for a number of different hydrogen bonding interactions.

4.4.1.1 Brmoz molecular and crystal structure

Single crystals of the **Brmoz** compound were successfully grown from ethyl acetate at room temperature, and it was found to be in the *P-1* spacegroup and had an R factor of 0.044. It was found to have two molecules in its asymmetric unit Z'=2. A number of very interesting interactions can be seen in the solid state of this molecule. As can be seen in *Fig 4.6*, there are three different types of hydrogen bonding interactions side by side. An N1B-H1B…N25A interaction with a distance of 2.38 Å is side by side with an N22B…H26A-C26A interaction with a distance of 2.45 Å. A C1A=O1A…H23B-C23B interaction closes out this closely packed conformation.

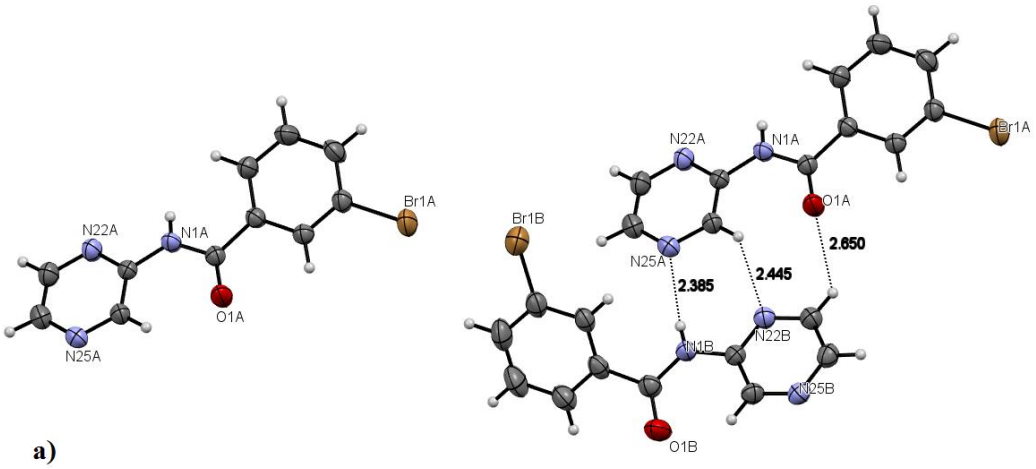

a)

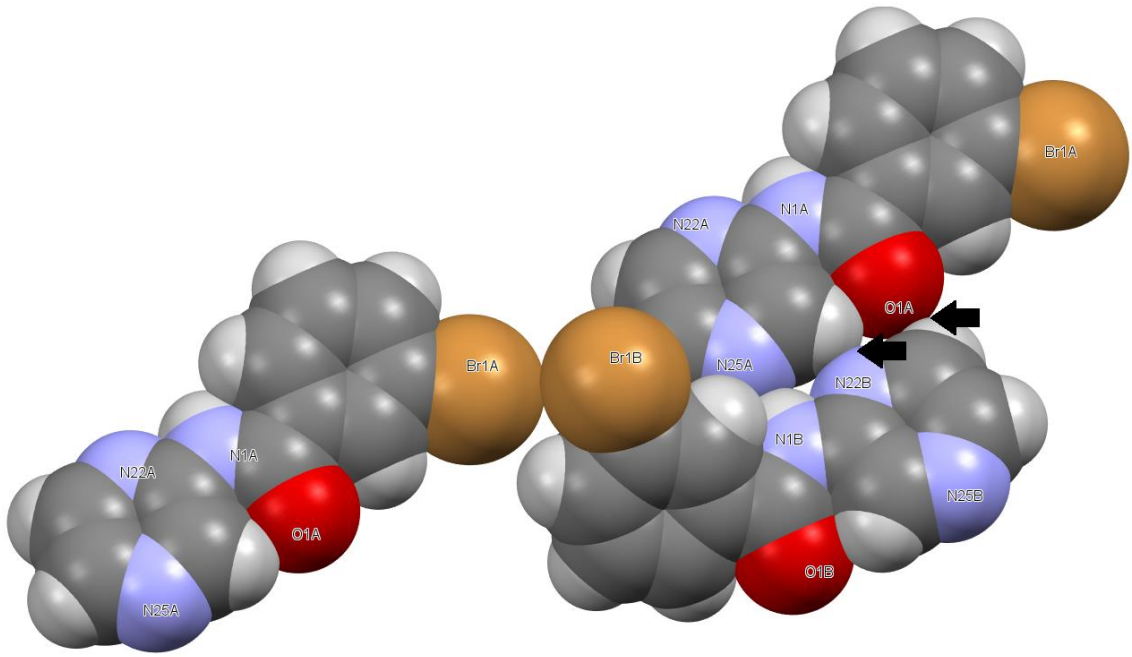

b)

Fig 4.6: Hydrogen bonding interactions in ***Brmoz*** *a) shows 3 unique interactions side by side while b) shows spacefill schematic of the points of contact in the structure:*

Brmoz also contains three weaker interactions, a small C13A-Br1A…Br1B-C13B halogen contact with a distance of 3.68 Å, and a π…π stacking interactions between C12A…C12B and N25B…C24B.

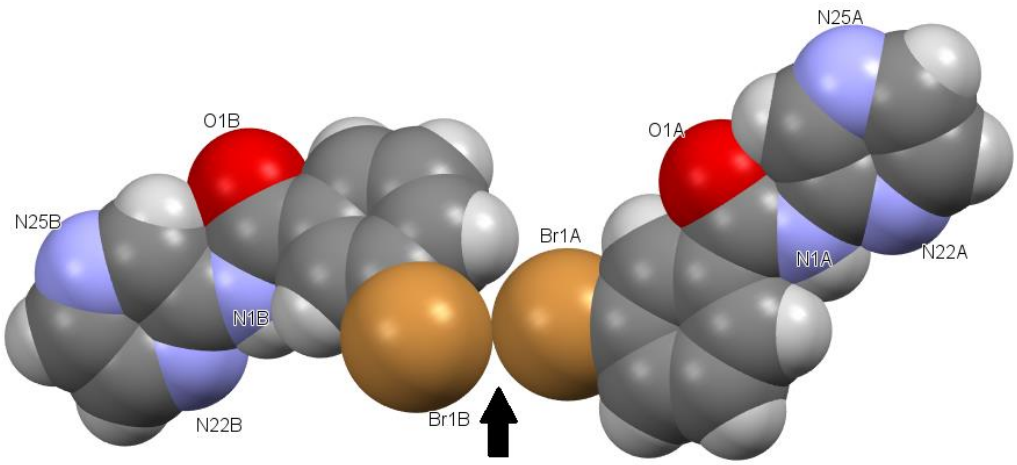

a)

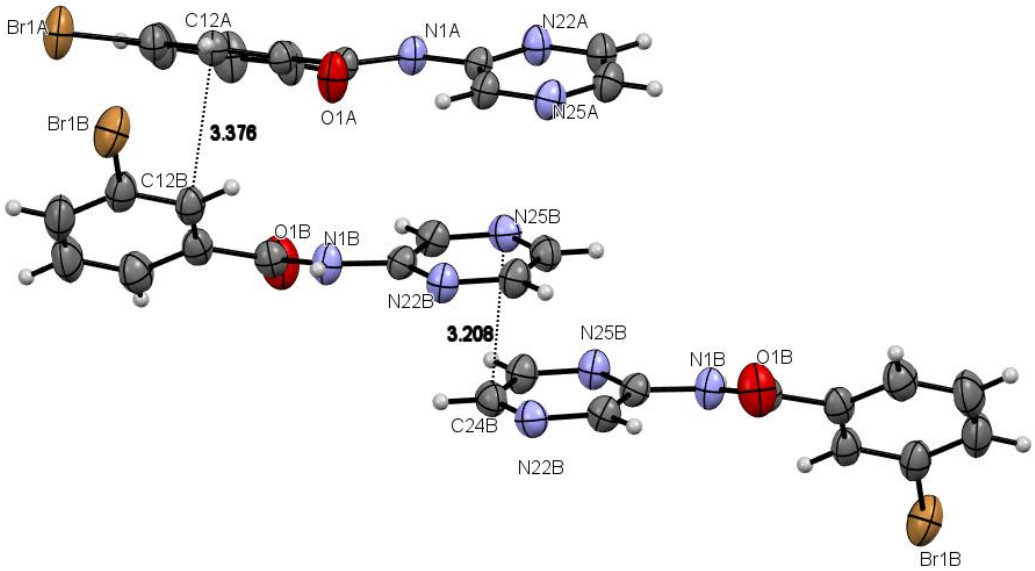

b)

Fig 4.7: a) Spacefill schematic showing C13A-Br1A…Br1B-C13B bromine contact b) Two π…π stacking interactions with distances shown in Å:

4.4.2 Carbamate compounds

The aim of this chapter was to investigate other interesting avenues into the formation of macrocycles and foldamers. Chapter 5 will discuss the compounds successfully made using the benzamide backbone. Seven reactions in total were carried out using phenyl chloroformate and nitrophenyl chloroformate in place of the bromobenzoyl chloride starting material. Along with these alterations, a number of substitutes for aminopyridine, namely aminopyrazines and aminopyrimidines were also investigated.

The yields for these seven carbamate based molecules were found to range from very low to non-existent in the nitrophenyl carbamates case. For the compounds based on aminopyrazines, **Copyrz, CopyrzNO$_2$** and **CopyrmNO$_2$,** this lack of reactivity could be due to the presence of the second nitrogen in the aminopyrazines causing more inductive effects and lowering the amino group's propensity to react. In the nitrophenyl reactions, no carbamates were observed to have formed. The addition of an electron withdrawing group to both the pyrazine and pyrimidine rings further reduced the reactivity of the amine substituent, leading to no reaction.

Another yield reducing element was the formation of a carbonate side product. In four of the reactions, **Copyrm**, **Copyr, Cmpyr** and **Cppyr**, the carbonate was the primary molecule synthesised. These carbonates can be seen in *Fig. 4.5*. The NMR and IR data confirmed the presence of these carbonates. The integration of ^{1}H-NMRs collected showed 14 signals and no characteristic N-H singlet, indicating carbonate formation. The melting points of the carbonate compounds were all in the same range bar one, and melted over ±5°C. The most symmetrical of the four, **Cppyr**, had twice the melting point of the rest, at 140-146°C, compared to **Copyr, Cmpyr** and the pyrimidine molecule **Copyrm**, which had melting points in the range 73-81°C. Four of the carbonates were successfully grown as single crystals and x-ray structures were generated and analysed.

4.4.2.1 Diphenyl pyrimidin-2-ylimidodicarbonate molecular and crystal structure

Diphenyl pyrimidin-2-ylimidodicarbonate was successfully grown from ethyl acetate and crystallized in the *P2$_1$/c* spacegroup. There are both intramolecular and intermolecular interactions in evidence in the molecule. As can be seen in *Fig 4.8*, both an intramolecular N12…O4 interaction and O1…O3 interaction are observed. The intermolecular interactions include a C3=O3…H15-C15 hydrogen bond and N16…H36-C36 interaction.

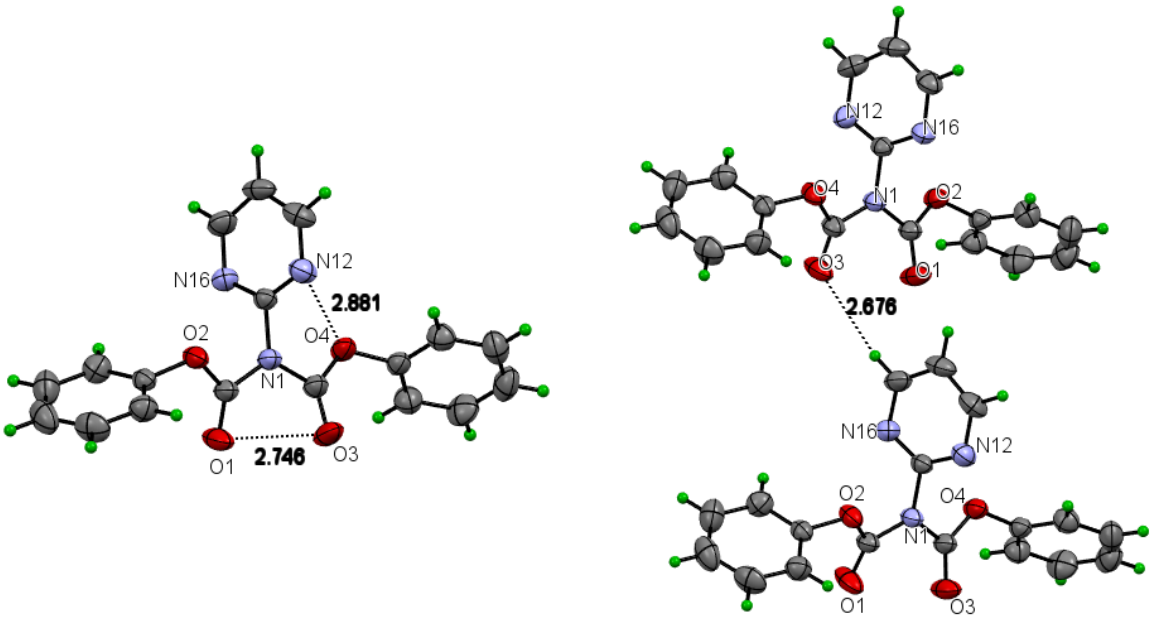

Intramolecular interactions **Intermolecular interactions**

Fig 4.8: Two types of interactions in the solid state of Diphenyl pyrimidin-2-ylimidodicarbonate (distances in Å):

4.4.2.2 Diphenyl carbonate molecular and crystal structure

Diphenyl carbonate was crystallised from ethyl acetate and was found to be in the $P2_12_12_1$ spacegroup. The molecule has been previously published by King *et al*.[20] Its main interaction in the solid state is a C1=O1…H16-C16 hydrogen bonding interaction with a distance of 2.66 Å.

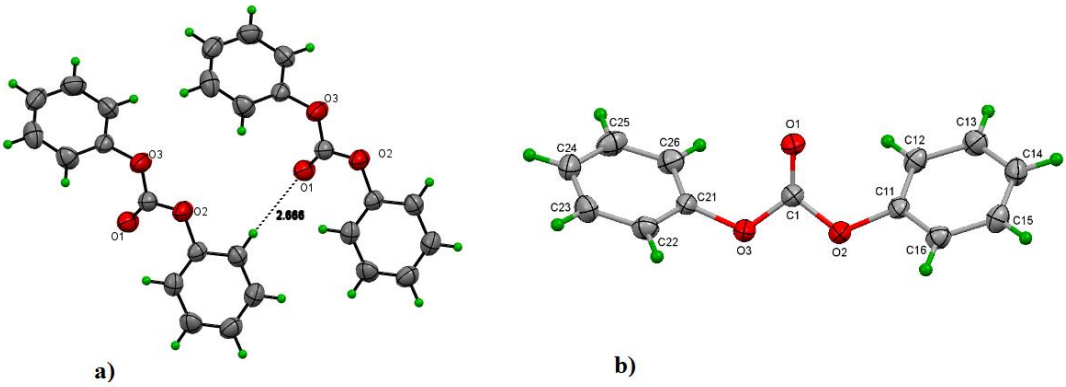

Fig 4.9: a) Structure of diphenyl carbonate: b) previously published structure by King et al.[20]

4.4.2.3 Bis (*p*-nitrophenyl) carbonate molecular and crystal structure

Bis (*p*-nitrophenyl) carbonate was successfully grown from ethyl acetate and was found to be in the *P-1* (No. 2) spacegroup in the solid state. The structure has been previously published by Simon *et al*. with 3 molecules in the asymmetric unit (Z'=3), in $P2_1/c$ with the third being benzene solvate.[21] Our structure has two molecules in the asymmetric unit. The molecule has a number of oxygen interactions in the solid state, an O7A…O7A short contact interaction with a distance of 2.9 Å, and a number of oxygen hydrogen bonding interactions, O3B…H23A-C23A as well as an O6A…C-22B O…π interaction, among others.

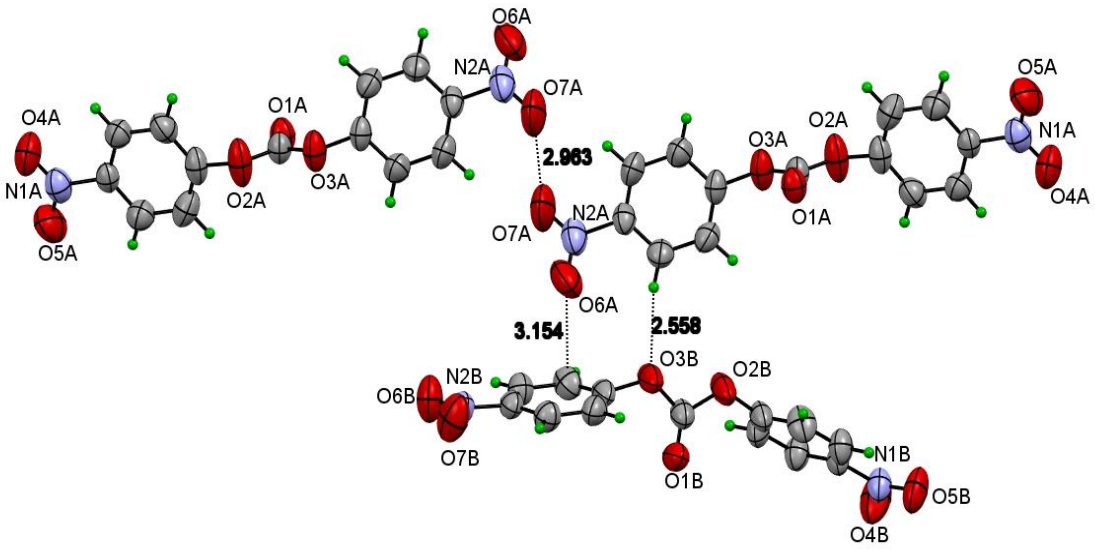

Fig 4.10: Intermolecular interactions in Bis (p-nitrophenyl) carbonate:

4.4.2.4 Diphenyl pyridin-2-ylimidodicarbonate molecular and crystal structure

Diphenyl pyridin-2-ylimidodicarbonate was successfully grown from ethyl acetate and was found to crystallise in the $P2_12_12_1$ spacegroup in the solid state. The molecule was observed to have both intramolecular and intermolecular interactions. The intramolecular interaction is an O3…O1 short contact between the two carbonyl oxygens, while the intermolecular interactions are an O3…H16-C16 hydrogen bond and a N12…H15C15 interaction.

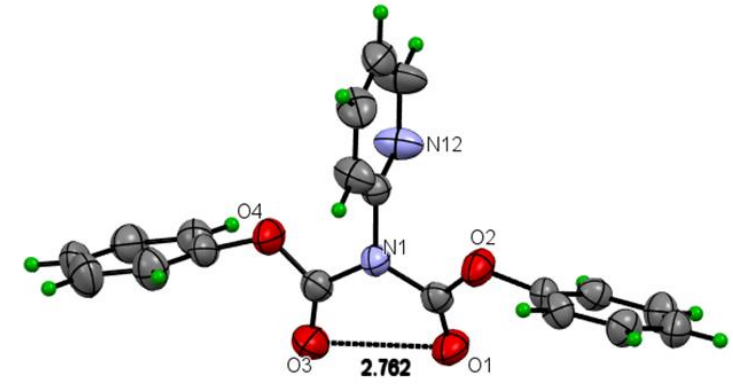

Intramolecular interaction

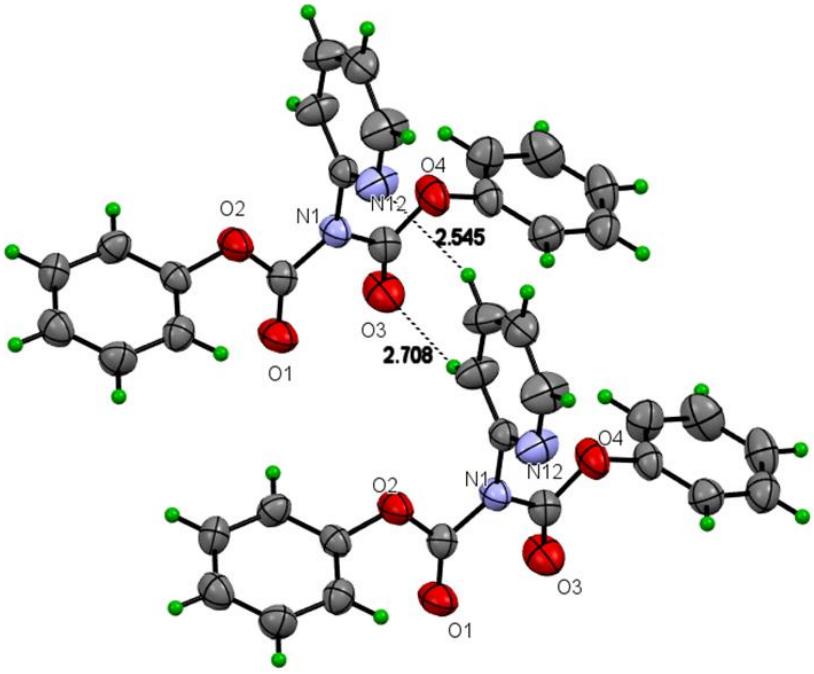

Intermolecular interactions

Fig 4.11: Interactions in the solid state for Diphenyl pyridin-2-ylimidodicarbonate (distances in Å):

4.5 Conclusion

An investigation into the viability of a number of different replacements for the classic benzamide backbone described in Chapter 2 was carried out over a number of different reactions. The substitution of a 2-pyrazine in place of 2-aminopyridine was attempted in the first section of this chapter and results showed low reactivity, with yields at 5%.

The Brmoz compound was successfully grown from ethyl acetate, and was found to have a number of very interesting interactions. Two very short N1B-H1B…N25A and N22B…H26A-C26A interactions allowed for a close packing arrangement. Two π…π stacking interactions were also present in the solid state, leading to a fascinating structure.

The next series of substitutions attempted were the addition of a carbamate into the backbone along with addition of a pyrimidine and a nitro group. These reactions again showed very low yields and in the case of the nitrophenyl chloroformate, no reaction was observed. The combination of the additional nitrogen in the pyrazine and pyrimidine ring that lowered the reactivity of the amide functional group and the formation of a carbonate side product hindered the formation of the desired compounds. A number of crystal structures were grown and analysed above.

We can conclude that using the same synthetic procedure as previous chapters, these reactions are not preferred and in order for the forward reaction to be favoured enough for the formation of foldamers to occur, the benzamide backbone encountered in chapters 1 and 2 is the ideal stable moiety. It gives yields of 50%-70% and has no competing side reactions to lower yields.

There are a number of different ways to form carbamates other than the mechanism that was chosen, and these other synthetic routes could have produced better yields. For this chapter, reactivity using the starting materials at hand was being investigated and as can be seen above it was found that the condensation method was not effective in producing carbamates.[22,23]

4.6 References

1. International Programme on Chemical Safety WHO task group on Carbamate Pesticides. Carbamate pesticides: A general introduction. Carbamate pesticides: A general introduction. 1st ed. Geneva: World Health Organisation; 1986.

2. Mineau P. Cholinesterase-inhibiting insecticides: Their impact on wildlife and the environment. illustrated ed. Elsevier; 1991.

3. O'Donnell S, Mandaro R, Schuster T, Arnone A. X-ray diffraction and solution studies of specifically carbamylated human hemoglobin A. J Biol Chem 1979(254):12204-8.

4. Ray S, Chaturvedi D. Application of organic carbamates in drug design. part 1: Anti-cancer agents-recent reports. Drugs Fut 2004;29(4):343-57.

5. Allen FH, Motherwell WS. Applications of the cambridge structural database in organic chemistry and crystal chemistry. Acta Crystallographica Section B: Structural Science 2002;58(3):407-22.

6. Thomas IR, Bruno IJ, Cole JC, Macrae CF, Pidcock E, Wood PA. WebCSD: The online portal to the cambridge structural database. Journal of Applied Crystallography 2010;43(2):362-6.

7. Lalezari I, Golgolab H, Shafiee A, Wossoughi M. Synthesis and antifungal activity of polyhalophenyl esters of pyridyl-and 4-quinolylcarbamic acids IV. J Pharm Sci 1973;62(2):332-3.

8. Matondo H, Benevides N, Tissut M, Bergon M, De Savignac A, Calmon JP, Lattes A. Synthesis, mechanism of action, and herbicidal activity of new aryl and alkyl N-(4-pyridyl) carbamates. J Agric Food Chem 1989;37(1):169-72.

9. Kopečný D, Briozzo P, Popelková H, Šebela M, Končitíková R, Spíchal L, Nisler J, Madzak C, Frébort I, Laloue M. Phenyl-and benzylurea cytokinins as competitive inhibitors of cytokinin oxidase/dehydrogenase: A structural study. Biochimie 2010;92(8):1052-62.

10. Kapchina-Toteva V, Stoyanova D. Effect of cytokinins and cytokinin antagonists on in vitro cultured gypsophila paniculata L. Biol Plant 2003;46(3):337-41.

11. Somleva M, Kapchina-Toteva V, Alexieva V, Sergiev I, Karanov E. Novel physiological properties of two cytokinin antagonists. J Plant Physiol 2000;156(5):623-7.

12. Somleva M, Kapchina V, Alexieva V, Golovinsky E. Anticytokinin effects on in vitro response of embryogenic and nonembryogenic genotypes of dactylis glomerata L. Plant Growth Regulation 1995;16(2):109-12.

13. Mocilac P, Gallagher JF. The first phenyl-N-pyridinylcarbamate structures: Structural and conformational analysis of nine methoxyphenyl-N-pyridinylcarbamates. Crystal Growth & Design 2013;13(12):5295-304.

14. Gallagher JF, Alley S, Lough AJ. A structural systematic study of semi-rigid ferrocene derivatives as a 3×3 metallocene isomer grid:*p-/m-/o*-(FcC_6H_4)CONH(*p-/m-/o*-C_6H_4)CO_2Et [Fc =η^5-C_5H_5)Fe(η^5-C_5H_4)]. Inorg Chim Acta 2016;444:113-25.

15. Mocilac P, Gallagher JF. Structural systematics and conformational analyses of a 3× 3 isomer grid of nine N-(tolyl) pyridinecarboxamides and three chlorinated relatives. CrystEngComm 2011;13(17):5354-66.

16. Mocilac P, Gallagher JF. Two isostructural carbamates: The o-tolyl N-(pyridin-3-yl) carbamate and 2-bromophenyl N-(pyridin-3-yl) carbamate monohydrates. Acta Crystallographica Section E: Crystallographic Communications 2015;71(11):1366-70.

17. Hay MP, Wilson WR, Denny WA. Design, synthesis and evaluation of imidazolylmethyl carbamate prodrugs of alkylating agents. Tetrahedron 2000;56(4):645-57.

18. Ghosh AK, Brindisi M. Organic carbamates in drug design and medicinal chemistry. J Med Chem 2015;58(7):2895-940.

19. Badger G, Nelson P, Potts K. 1, 2, 4-triazoles. VIII. s-triazolo [2, 3-a] pyrazine Derivatives1a. J Org Chem 1964;29(9):2542-5.

20. King J, Bryant G. Structure of diphenyl carbonate. Acta Crystallographica Section C: Crystal Structure Communications 1993;49(3):550-1.

21. Simon M, Csunderlik C, Jones PG, Neda I, Fischer AK. Bis (p-nitrophenyl) carbonate–benzene (3/1). Acta Crystallographica Section E: Structure Reports Online 2003;59(5):o691-2.

22. Curini M, Epifano F, Maltese F, Rosati O. Carbamate synthesis from amines and dimethyl carbonate under ytterbium triflate catalysis. Tetrahedron Lett 2002;43(28):4895-7.

23. Salvatore RN, Shin SI, Nagle AS, Jung KW. Efficient carbamate synthesis via a three-component coupling of an amine, CO2, and alkyl halides in the presence of Cs2CO3 and tetrabutylammonium iodide. J Org Chem 2001;66(3):1035-7.

CHAPTER 5

Synthesis of Foldamers Based On Benzamide Scaffolds

5.1 Introduction

5.1.1 Aromatic Oligoamide Foldamers

Proteins are biological macromolecules made up of a combination of different amino acids and capable of forming a three dimensional conformation that allow them to carry out myriad functions in the body.[1] Amino acids and proteins use hydrogen bonding interactions to stabilize their secondary and tertiary structures. The secondary structure of a protein refers to its 3D local configuration, and its tertiary structure refers to its specific geometrical arrangement which produces its active site.[2-4] When using unnatural oligoamides to form foldamers, hydrogen bonding is key to foldamer assembly in organic solvents. It has been shown that man-made amide sequences are able to form secondary structures such as helices and sheets.[5]

In aromatic oligoamides, rotation around the Ar-NHCOAr bond must be restricted in order for a secondary structure to form. The stability of an aromatic foldamer is directly related to the strength of the intramolecular hydrogen bonding holding the structure together.[6] Zhang *et al.* gives a number of different hydrogen bonding patterns capable of the restriction of this rotation.[6]

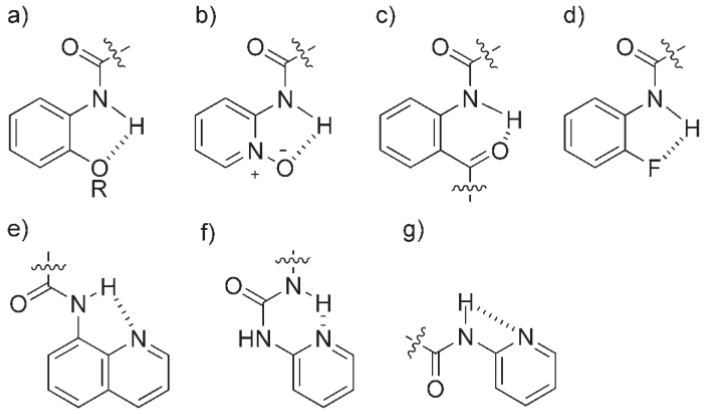

Fig 5.1: Illustration of a number of different intramolecular H-bonding patterns:[6]pg 786

In derivatives of 2-aminopyridine and 2,6 diaminopyridine, which our group has done previous work on, we see the formation of N-HN hydrogen bonds.[7] This

attraction between the amide H and the pyridine N, allows for an *anti*-conformation. The follow on to this work has been discussed in detail in Chapter 2 (section 2.5.4).

Aromatic oligomers can serve a variety of different roles in foldamer chemistry. Nowick *et. al* have used these oligomers as intramolecular templates to stabilize the formation of β sheets.[8] Research into the uses of these foldamers as a framework to allow for the storage and possible transport of small organic molecules has yielded a number of promising preliminary results. Zhang has presented oligomers where molecules such as zinc coordinated porphyrins and linked macrocycles (catenane) are bound in the cavities of their foldamer construct.[9]

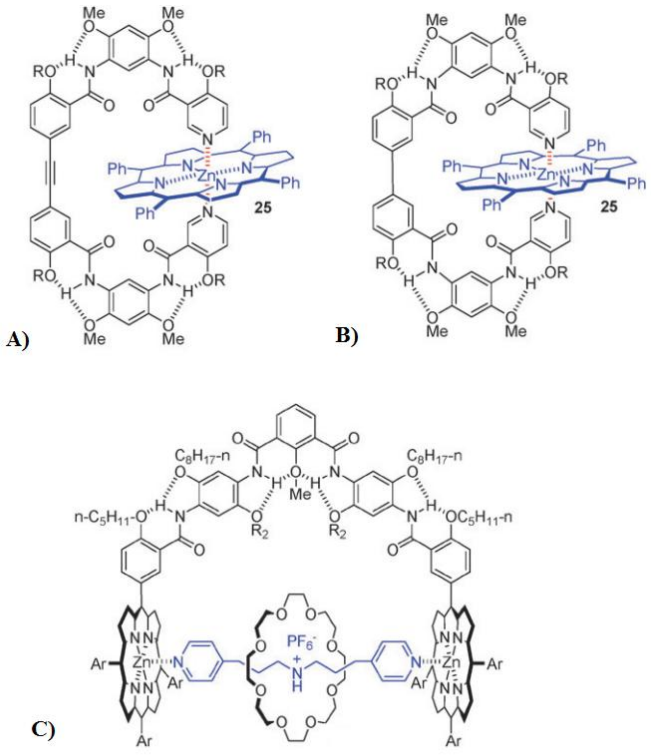

Fig 5.2: A) and B) illustrates zinc coordinated porphyrins held inside foldamer cavity; C) shows formation of catenane between two bonded porphyrins rings:[9] adapted

As more and more foldamer backbones are synthesised, the possibilities for protein mimicry for use in medicine and protein research will continue to grow, and lead to new understanding of the human body and the proteins that control its functions.

5.1.2 Nomenclature

The goal of Chapter 5 was to attempt to synthesise a range of different foldamer-like structures based on our previous experiments with benzamides. The Gallagher group recently published work in which a number of macrocycles were successfully formed from reactions between 2-aminopyridine and isophthaloyl dichloride.[10,11] The original drive of this chapter was to expand on this macrocyclic synthesis and construct macrocycles with cavities in the solid state to explore the storage and possible transport of small organic molecules.[12] By the addition of an inward facing nitrogen, it was hoped to create a stable cavity with available hydrogen bonding possibilities in the solid state. A series of foldamer like molecules were successfully synthesised and fully characterised and are presented in the chapter below. The compound names were simplified for ease of discussion, and were named according to the number of halogens and pyridinedicarbonyl linkages each compound contained, for example, the compound seen below, was shorthanded to **F_3N_2**, due to the three *fluoro-* functional groups and the two pyridinedicarbonyl moieties present in the molecule.

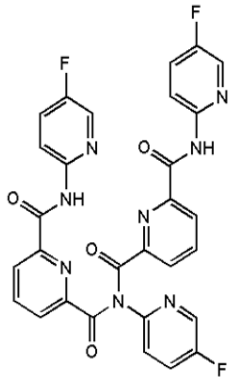

Fig 5.3: structural schematic of ***F_3N_2****, full name N2,N6-bis(5-fluoropyridin-2-yl)- N2 -(6-((5-fluoropyridin-2-yl)carbamoyl)picolinoyl)pyridine-2,6-dicarboxamide:*

The reaction proceeds via the Schotten-Baumann reaction, which between an acyl chloride (2,6-pyridinedicarbonyl dichloride) and a primary amine (2-amino,5-fluoropyridine), resulting in the formation of an amide bridge and loss of HCl. DMAP was added to the reaction in a catalytic amount and the TEA was required to lower the amount of unwanted side reactions that would have occurred with the release of HCl in the reaction.

5.2 Synthetic procedure

5.2.1 FxNx Reactions

Reaction media was prepared by dissolving DMAP (10 mg, 0.08 mmol) and triethylamine (4 ml, 29.8 mmol) in 80 ml of dry dichloromethane (DCM). The 2-amino-5-fluoropyridine (1.0986 g, 9.8 mmol) was dissolved in 20 ml of dry DCM and left with occasional stirring on a warm (25°C) bath. The 2,6-pyridinedicarbonyl dichloride (1.9992 g, 9.8 mmol) was dissolved in 80 ml of dry DCM in a 250 ml round bottom flask, under N_2 on an ice bath. The ice bath was cooled to approximately -20°C, using a combination of ice, salt, ammonium chloride and ethanol. The 2-amino-5-fluoropyridine solution was quickly and quantitatively added to the cooled flask containing dissolved 2,6-pyridinedicarbonyl dichloride, TEA and DMAP. The reaction mixture was stirred overnight.

A colour change was observed over about twenty minutes after addition of the 2-amino-5-fluoropyridine. The solution got a progressively darker off-yellow/red colour as the temperature of the reaction warmed slowly back to room temperature and the reaction began to proceed towards completion.

After 24 hours the reaction was taken off the stirring plate and any precipitate was removed by filtration. At this stage, any precipitate that was in suspension was due to the formation of insoluble polymers and oligomers. These were removed and stored in vials and may be analysed and purified at a later stage. At this point, the major goal of these reactions was to isolate the macrocycles that were hoped to have been formed, so the polymer/oligomers were left aside for the time being. The reaction mixture was diluted with technical grade DCM up to 200 ml and washed with aqueous solution of NH_4Cl (~pH=5) (3 × 200 ml) and dried over magnesium sulphate for an hour. The washed and dried reaction mixture was left overnight protected from light and the next day, the DCM was reduced in vacuo to leave a resin. A short column was set up to remove any remaining oligomers, then the obtained resin was immediately purified by column chromatography on silica gel (70 um, 82 g of silica, dimension of the silica column: h = 25 cm, d = 3 cm). Column mobile phase was run in 5:1 CHF:EA, and was found to give good separation. Three fractions were collected, $\mathbf{F_2N_1}$ (215.1 mg), $\mathbf{F_3N_2}$ (89.3 mg), $\mathbf{F_4N_3}$ (35.2 mg).

Table 5.1: Reagents used in synthesis of fluoro- series:

Reagent	Molar Mass (g/mol)	Density (g/cm^3)	Volume (ml)	Mass (g)	Concentration (mol)
2-amino-5-fluoropyridine	112.11	n/a	n/a	1.099	0.01
2,6-pyridinedicarbonyl dichloride	204.01	n/a	n/a	1.99	0.01
DMAP	122.17	n/a	n/a	0.01	0.00008
Triethylamine	101.19	0.726	4	n/a	0.03

In *Fig 5.4*, the three compounds separated in the fluoro- series of the foldamer synthesis can be seen.

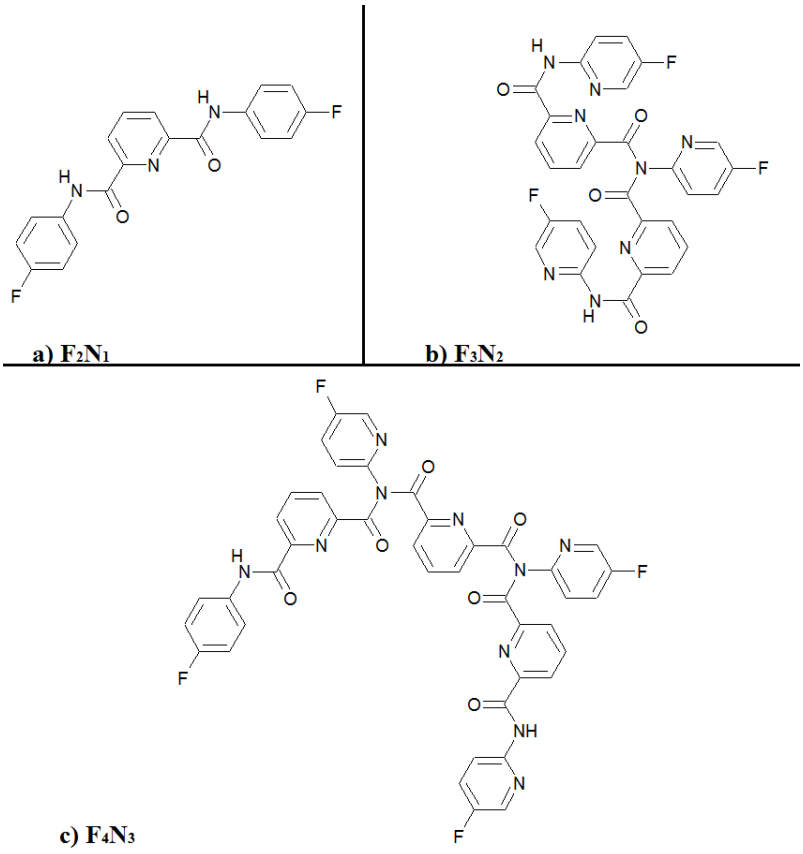

*Fig 5.4: Schematic structures of 3 compounds synthesised in fluoro- series***:**

5.2.2 Chloro and Bromo reactions

The same synthetic procedure was used for the synthesis of the *chloro*- and *bromo*- variants of the series. For the *chloro*- reaction, the reaction media was prepared by dissolving DMAP (10 mg, 0.08 mmol) and triethylamine (4 ml, 29.8 mmol) in 80 ml of dry dichloromethane (DCM). The 2-amino-5-chloropyridine (1.259888 g, 9.8 mmol) was dissolved in 20 ml of dry DCM and left with occasional stirring on a warm (25°C) bath. The 2,6-pyridinedicarbonyl dichloride (1.9992 g, 9.8 mmol) was again dissolved in approx. 80 ml of dry DCM, and the 2-amino-5-chloropyridine was added quantitatively into the reaction vessel.

The *bromo*- reaction was done exactly the same as the above reactions with the only difference being the addition of 1.6758g (9.8mmol) 2-amino 5-bromopyridine.

5.2.3 Separation issues (Major problems and Difficulties)

During the chromatography stage, it was observed that both the chloro- and bromo- compounds had issues with solubility in organic solvents. This made the selection of a mobile phase for column chromatography more difficult than normal as a compromise had to be made between solubility and separation. During both the short column to separate the oligomers and second optimized to separate the different foldamers, it was noted that some precipitation occurred in the column as the mobile phase moved downwards. This precipitation and subsequent slow redissolution of product led to mixing of fractions and poor separation. Preparative TLC was also attempted as a way around this solubility issue, but it led to the same precipitation issues. In the interest of time, it was decided to take these mixed fractions and grow single crystals from a wide range of different solvents for x-ray analysis. This crystal growth was successful and the structures for both $\mathbf{Cl_4N_3}$ and $\mathbf{Br_4N_3}$ were elucidated and analysed fully.

Table 5.2: Reagents used in synthesis of chloro- and bromo- series:

Reagent	Molar Mass (g/mol)	Density (g/cm^3)	Volume (ml)	Mass (g)	Concentration (mol)
2-amino-5-chloropyridine	128.56	n/a	n/a	1.26	0.01
2-amino-5-bromopyridine	173.01			1.68	0.01
2,6-pyridinedicarbonyl dichloride	204.01	n/a	n/a	1.99	0.01
DMAP	122.17	n/a	n/a	0.01	0.00008
Triethylamine	101.19	0.726	4	n/a	0.03

In *Fig 5.5*, the two compounds successfully grown for x-ray analysis can be seen.

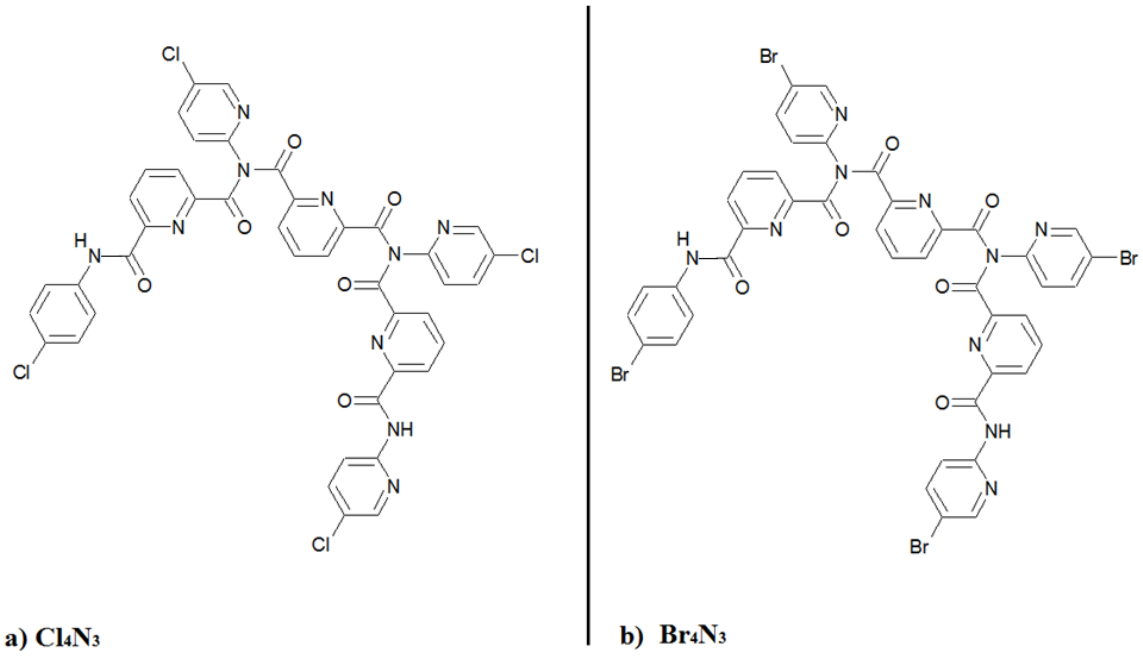

Fig 5.5: Schematic structures of ***Cl_4N_3*** *and* ***Br_4N_3****:*

5.3 Synthetic results

Results for the 3 fluoro- compounds can be seen below, along with the ^{1}H NMR for the foldamers. Additional data (including ^{1}H NMR, IR and full x-ray geometry tables) can be found in full in Appendix 5. X-ray crystal structure analysis of Cl_4N_3 and Br_4N_3 can be found in section 5.5.3.

Table 5.3: Results for fluoro- series:

	Melting point (°C)	**Yield (mg)**	**Significant IR peaks (cm^{-1})**
F_2N_1	198.6-200.1	215.1 12%	n/a
F_3N_2	262.8-264.1	89.3 2.3%	3350, 1709, 1390, 1231, 836
F_4N_3	224.6-225.7	35.2 0.5%	3270, 1691, 1539, 1392, 1232, 834

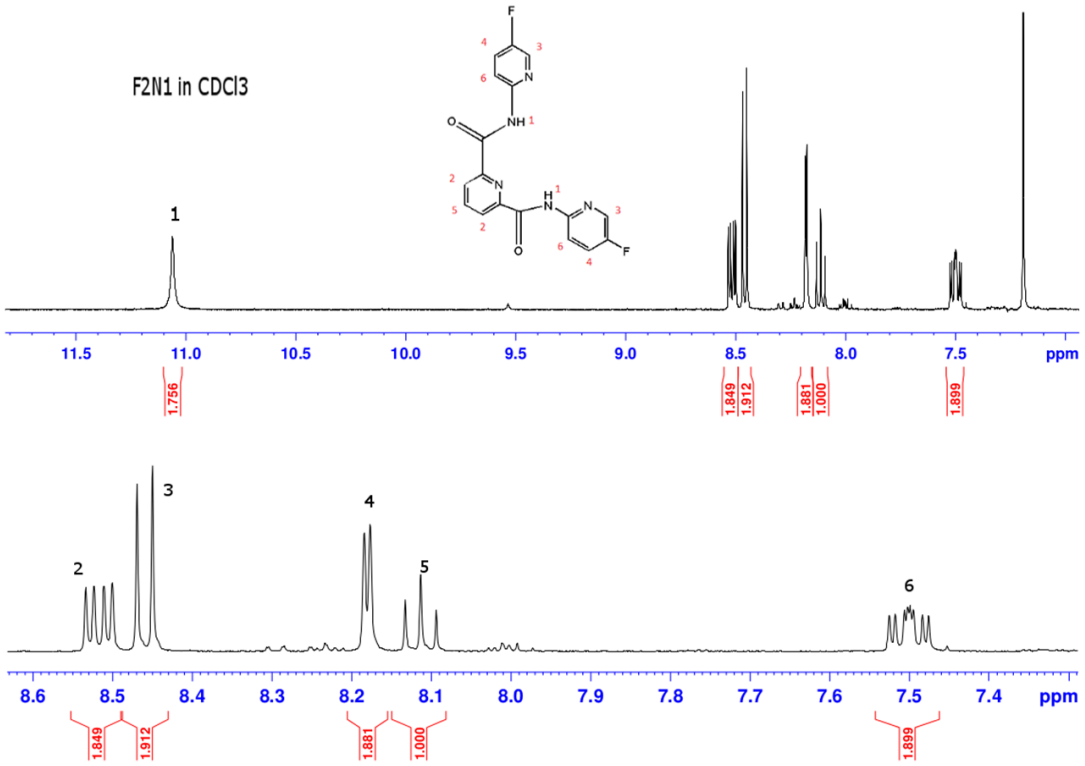

*Fig 5.6: ^{1}H NMR of **F_2N_1** in $CDCl_3$:*

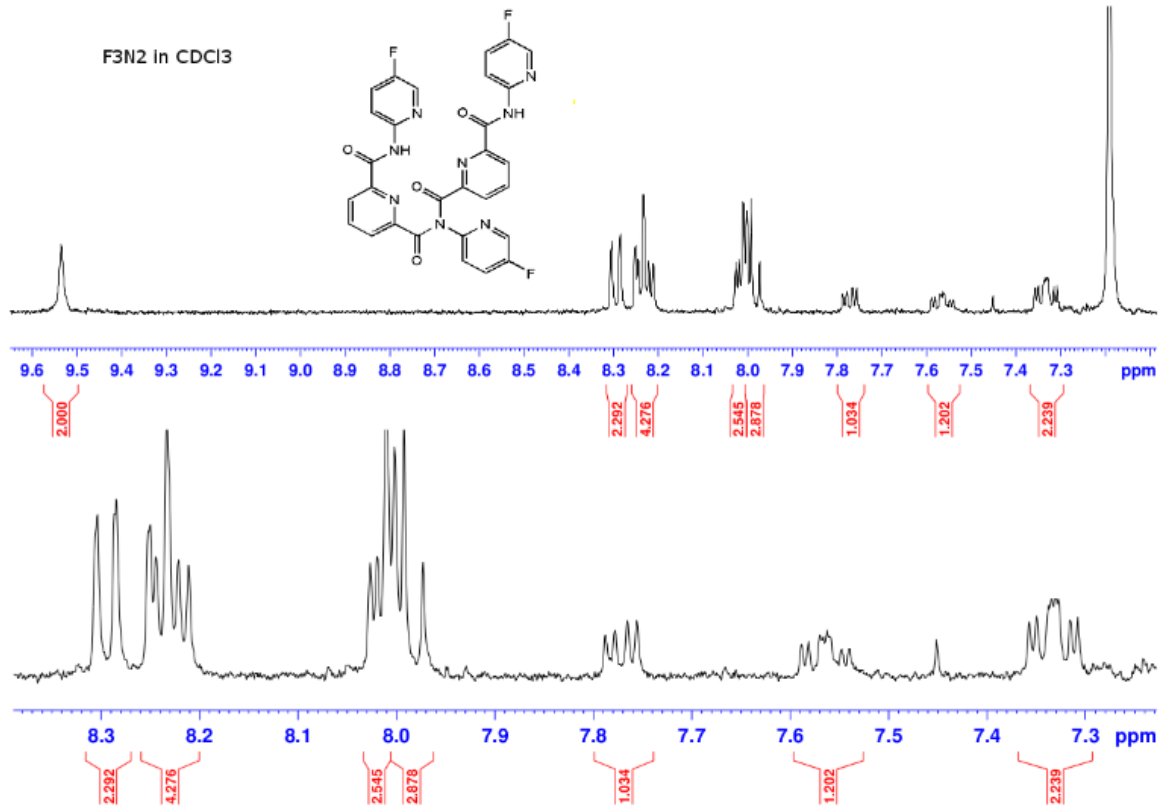

Fig 5.7: ^{1}H NMR of $\boldsymbol{F_3N_2}$ in $CDCl_3$:

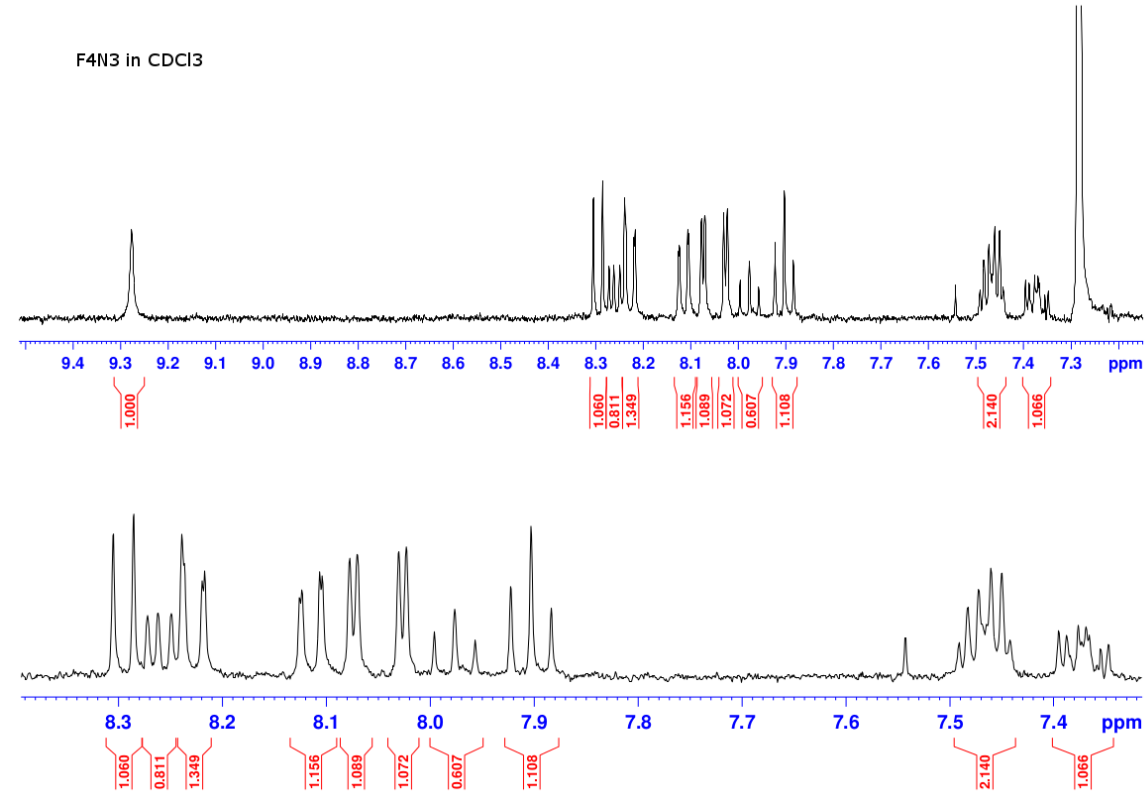

Fig 5.8: ^{1}H NMR of $\boldsymbol{F_4N_3}$ in $CDCl_3$:

5.4 Discussion

5.4.1 F_xN_x compounds

Three compounds were successfully separated in the F_xN_x reaction. No issues were encountered with separation, with both the precolumn to remove oligomers and polymers and the long column optimised to separate the foldamers running without problem. The reaction was run at -20°C during the first few hours of reaction to reduce the amount of polymer/oligomer formed and allow for the formation of the desired foldamers. Despite this, a large amount of the starting materials continued to react and polymerise during the course of the reaction, lowering the yields of the foldamers significantly. The two to one compound **F_2N_1**, was found to have a yield of 12% and the other foldamers had even lower yields. The **F_3N_2** compound had a yield of 2.3% and the **F_4N_3** compound a yield of 0.5%. These small amounts of product were nevertheless enough to characterize the compounds by NMR, IR and collect x-ray crystal structures.

^{1}H NMRs were run and the spectra can be seen in Figs *5.6-5.8*. All spectra point towards the formation of both foldamers, with the integration fitting in both cases. In both cases a chloroform peak[13] at 7.3ppm was observed, as the column mobile phase that gave separation was a mix of chloroform and ethyl acetate in a 5:1 ratio. As the peak was not obscuring any vital parts of the spectra, the compounds were not dried further and the compounds were split into vials for crystal growth by slow room temperature evaporation. Melting points were run for the three compounds and **F_3N_2** was found to have the highest melting point at 262.8-264.1°C. This was 40°C higher than the **F_4N_3** molecule, and was likely caused by the formation of a closely packed dimer in the solid state (see *Fig 5.9*). The molecule adopts an interesting conformation with two of its three pyridine rings forming an almost 90 degree angle, with the third ring sitting in the cavity between them. This tight configuration allows a number of interactions to take place in the solid state such as C3=O3…C15A interaction, which hold the dimer together.

5.4.2 F_xN_x series crystal structure analysis

Crystals were successfully grown for both compounds by slow evaporation at room temperature, again from $CHCl_3$, acetone or ethyl acetate. Full geometry tables and structural information for each elucidated structure can be found in **Appendix 5**.

5.4.2.1 F_3N_2 crystal structure analysis

F_3N_2 crystallised in the space group P1 and is an excellent example of a mixed imide/amide compound. It contains an intramolecular contact between C2=O2…N12 with a distance of 2.9Å. A number of intermolecular interactions act to allow formation of a hydrogen bonded dimer in the solid state. The interaction between C2=O2…H26-C26 with a distance of 2.42Å seems to be the key factor in the assembly of this dimer. A N22A…H16-C16 interaction was also noted. In *Fig 5.9*, the molecule and dimer formation can be seen.

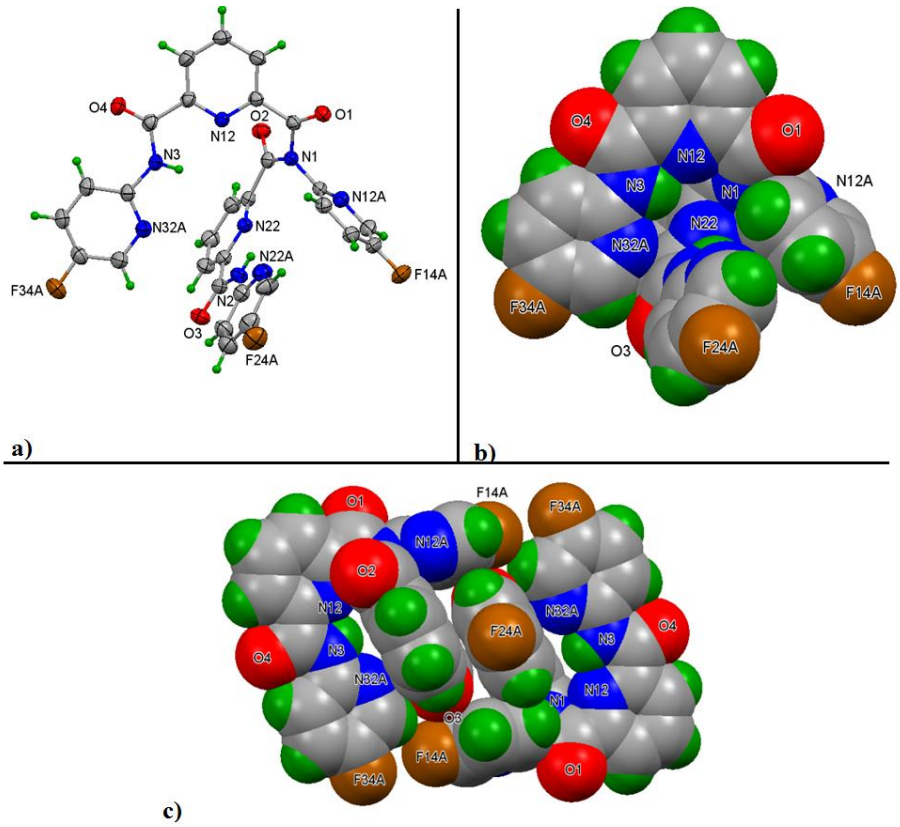

*Fig 5.9: a) **F_3N_2** structure as an ORTEP diagram (displacement ellipsoids at 30%); b) Spacefill structure of **F_3N_2**; c) hydrogen bonded dimer structure:*

5.4.2.2 F_4N_3 crystal structure analysis

F_4N_3 crystallised in the $P2_1/c$ space group and has a number of interesting interactions in the solid state. An intramolecular interaction between N32A…O4=C4 was observed, along with a number of hydrogen bonding interactions, O1…H43A-C43A, O6…H24-C24, O4…H15-C15 and O5…H26-C26.

Halogen bonding interactions were also noted in the **F_4N_3** structure. Three different fluorine interactions were observed, F14A…C15, with a distance of 2.9Å, F44A…H36-C36, with a distance of 2.34Å, and F24A…H26-C26, with a distance of 2.43Å. The C-H…F interactions lead to a 1D chain forming along the b axis in the solid state as can be seen in *Fig 5.11*.

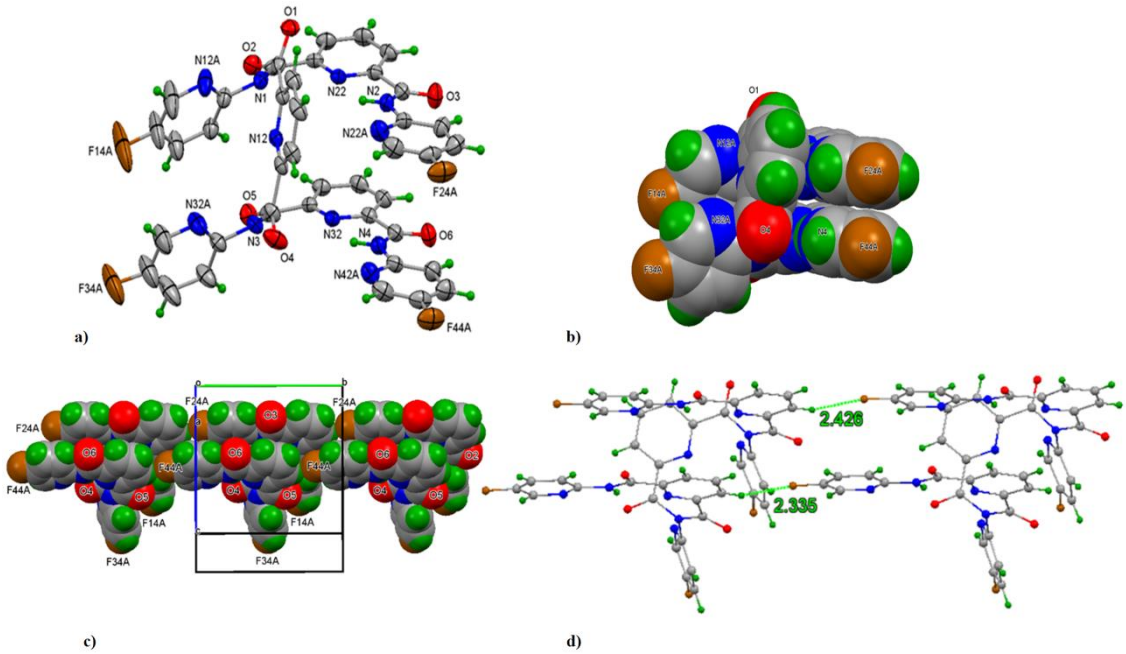

Fig 5.10: a) ***F_4N_3*** *structure as an ORTEP diagram (displacement ellipsoids at 30%); b) Spacefill structure of* ***F_4N_3****, c)* ***F_4N_3*** *structure as an ORTEP diagram (displacement ellipsoids 30%) and d) Spacefill drawing; the hydrogen bonding as C-H…F interactions at F24A and F44A depicted as a 1-D chain along the b-axis direction and a ball and stick diagram with H…F distances:*

5.4.3 Cl_4N_3 crystal structure analysis

Cl_4N_3 crystallised in the P2/n space group and contained a molecule of dichloromethane in the asymmetric unit. Three different hydrogen bonding interactions were observed, C2=O2…H26-C6 with a distance of 2.54Å, C1=O1…H25A-C25A with a distance of 2.52Å, and a dichloromethane interaction, C3=O3…H1S-C1S with a distance of 2.23Å, leading to chain formation along the c axis in the solid state (*see Fig 5.11*).

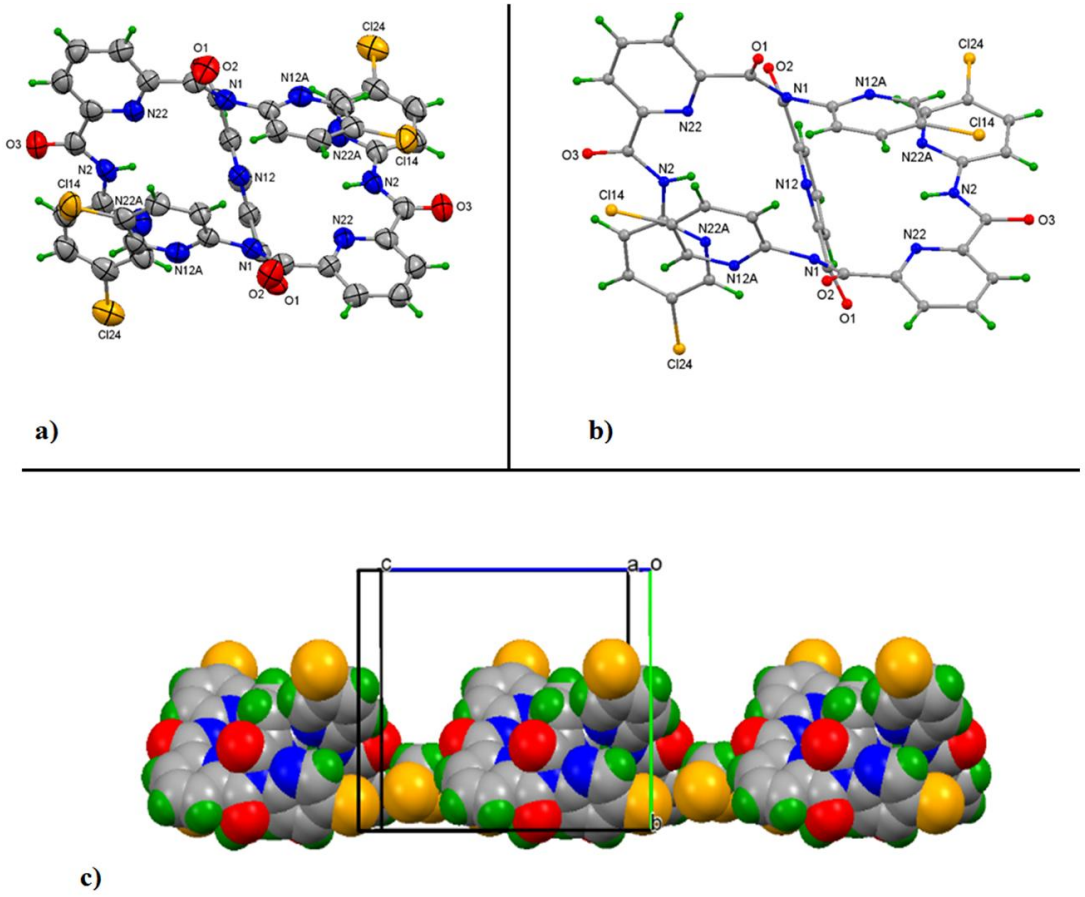

Fig 5.11: a) ***Cl_4N_3*** *structure as an ORTEP diagram (displacement ellipsoids 30%) and b) ball and stick structure; c) ORTEP schematic with a spacefill view of Cl_4N_3 together with a chain of molecules linked by dichloromethane (C-H…O interactions) along the c-axis direction.*

5.4.4 Br_4N_3 crystal structure analysis

Br_4N_3 crystallised in the space group P2/n and also was found to contain a molecule of dichloromethane in the asymmetric unit. **Br_4N_3** was found to be isomorphous with **Cl_4N_3**. Two hydrogen bonding interactions were noted, C1=O1…H25A-C25A and a dichloromethane interaction C3=O3…H1S-C1S. Two bromine interactions were also observed, Br24…H12-C12 with a distance of 3.01Å, and Br24…C24 with a distance of 3.53Å. The differences in conformation of the three 4:3 molecules (**F_4N_3**, **Cl_4N_3** and **Br4N_3**) were quite evident in their solved structures. The **F_4N_3** molecule ring systems layer on top of one another, causing a plane of interactions to form, while the **Cl_4N_3** and **Br4N_3** molecules adopted a twisted configuration, wrapped around a central pyridinedicarbonyl moiety.

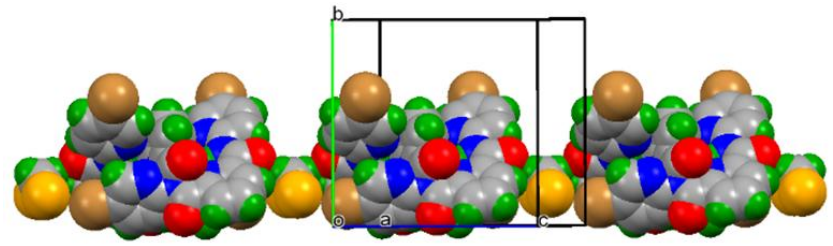

a)

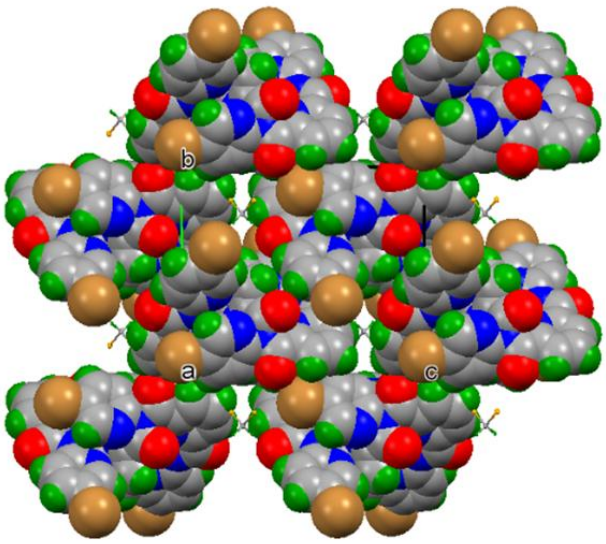

b)

*Fig 5.12: a) Spacefill structure of **Br_4N_3** showing a chain of molecules linked by CH_2Cl_2 (C-H…O interactions) along the c-axis direction with atoms depicted as their van der Waals spheres. b) A view of the solvents sites in the lattice.*

5.5 Conclusion

Five compounds in total were successfully synthesised and characterised for chapter 5 of this thesis. Four foldamer compounds were synthesised despite major chromatography issues and single crystals of each were characterised fully by X-ray crystallography. Yields were found to be very poor for all reactions, as polymer/oligomer synthesis was favoured over the formation of the desired foldamers. ^{1}H NMR analysis confirmed the formation of two types of foldamer based on the benzamide backbone, a 3:2 variant, **F_3N_2**, and a 4:3 variant, **F_4N_3**.

Full spectroscopic analysis was carried out for the **F_3N_2** and **F_4N_3** compounds and crystal structures were completed for **Cl_4N_3** and **Br4N_3** molecules. The melting point analysis of the **F_xN_x** compounds showed **F_3N_2** was found to have the highest melting point due to the formation of a closely packed dimer in the solid state. The conformation of the **F_3N_2** molecule facilitates a number of interactions to take place in close proximity on the molecule, causing a large increase in the forces holding the compound together in the solid state.

The X-ray analysis showed a number of interesting interactions in the structures of the foldamers in the solid state. **F_3N_2** had C2=O2…H26-C26 hydrogen bonding leading to the formation of a tightly packed dimer. The presence of F44A…H36-C36 and F24A…H26-C26 interactions in **F_4N_3** led to the formation of 1D chain along the *b* axis in the solid state. **Cl_4N_3** contained an interaction with DCM that allowed for chain formation along the *c* axis. The **Br4N_3** structure showed the presence of bromine interactions, Br24…H12-C12 and Br24…C24, allowing for a compact twisted conformation in the solid state, unlike the **F_4N_3** structure which aligned in a stacked conformation.

5.6 References

1. Nelson DL, Lehninger AL, Cox MM. Lehninger principles of biochemistry. Macmillan; 2008.

2. Dill K. Dominant forces in protein folding. Biochemistry (N Y) 1990 AUG 7;29(31):7133-55.

3. Dobson C. Protein folding and misfolding. Nature 2003 DEC 18;426(6968):884-90.

4. Gething M, Sambrook J. Protein folding in the cell. 1992.

5. Seebach D, Overhand M, Kuhnle FNM, Martinoni B, Oberer L, Hommel U, Widmer H. Beta-peptides: Synthesis by arndt-eistert homologation with concomitant peptide coupling. structure determination by NMR and CD spectroscopy and by X-ray crystallography. helical secondary structure of a beta-hexapeptide in solution and its stability towards pepsin. Helv Chim Acta 1996 1996;79(4):913-41.

6. Zhang D, Zhao X, Hou J, Li Z. Aromatic amide foldamers: Structures, properties, and functions. Chem Rev 2012 OCT 2012;112(10):5271-316.

7. Mocilac P, Tallon M, Lough AJ, Gallagher JF. Synthesis, structural and conformational analysis of a 3 x 3 isomer grid based on nine methyl-N-(pyridyl)benzamides. Crystengcomm 2010;12(10):3080-90.

8. Nowick JS. Exploring beta-sheet structure and interactions with chemical model systems. Acc Chem Res 2008 OCT 2008;41(10):1319-30.

9. Zhang D, Zhao X, Li Z. Aromatic amide and hydrazide foldamer-based responsive host-guest systems. Acc Chem Res 2014 JUL;47(7):1961-70.

10. Mocilac P, Gallagher JF. Trezimides and tennimides: New imide-based macrocycles. J Org Chem 2013 MAR 15;78(6):2355-61.

11. Mocilac P, Gallagher JF. Halogen bonding directed supramolecular assembly in bromo-substituted trezimides and tennimides. Crystengcomm 2014;16(10):1893-903.

12. Mocilac P, Gallagher JF. Halogenated tennimides and trezimides: Impact of halogen bonding and solvent role on porous network formation and inclusion. Crystengcomm 2016;18(13):2375-84.

13. Gottlieb HE, Kotlyar V, Nudelman A. NMR chemical shifts of common laboratory solvents as trace impurities. J Org Chem 1997;62(21):7512-5.

Papers in preparation for submission in 2016/2017

A number of papers are currently being worked on based the work of this thesis, below are the working titles and journals to which the papers will be aimed in late 2016/2017.

1 Structural systematics and conformational analyses of two 3 × 3 isomer grids of brominated benzamides as nine bromo-*N*-(pyridyl)benzamides and nine *N*-(bromobenzene)pyridinecarboxamides: physicochemical correlations, polymorphism and isomorphous relationships, by **Niall Hehir** and **John F. Gallagher** for *CrystEngComm*.

2 Hydrogen bonded Tetramer formation in Iodinated pyridinecarboxamides: Comparisons and structural implications, by **Niall Hehir** and **John F. Gallagher** for *Acta Crystallographica Section B.*

3 Structural systematic studies of twelve difluorinated fluoro and methylbenzamides by **Niall Hehir**, **Marion Lefebvre**, **Marie Beliard** and **John F. Gallagher** for *CrystEngComm* in 2017.

4 Further progress in the structural chemistry of carbamate derivatives by **Niall Hehir** and **John F. Gallagher.**

5 Halogenated open chain mixed amide-imide oligomers as models for the structural aggregation of polyamideimides by **Niall Hehir** and **John F. Gallagher**.

There may be some additional papers in *Acta Crystallographica sections C and E*.

Future perspectives

The work conducted in this research project spans halobenzamide and halocarboxamide chemistry in Chapters 2 and 3, through initial tests on some carbamate chemistry in Chapter 4, towards exciting and promising research work in 'foldamer' chemistry in Chapter 5. Benzamide derivatives appear as promising drug candidates and have even found applications in materials science with 'kevlar' being one of the most interesting examples.[1-5]

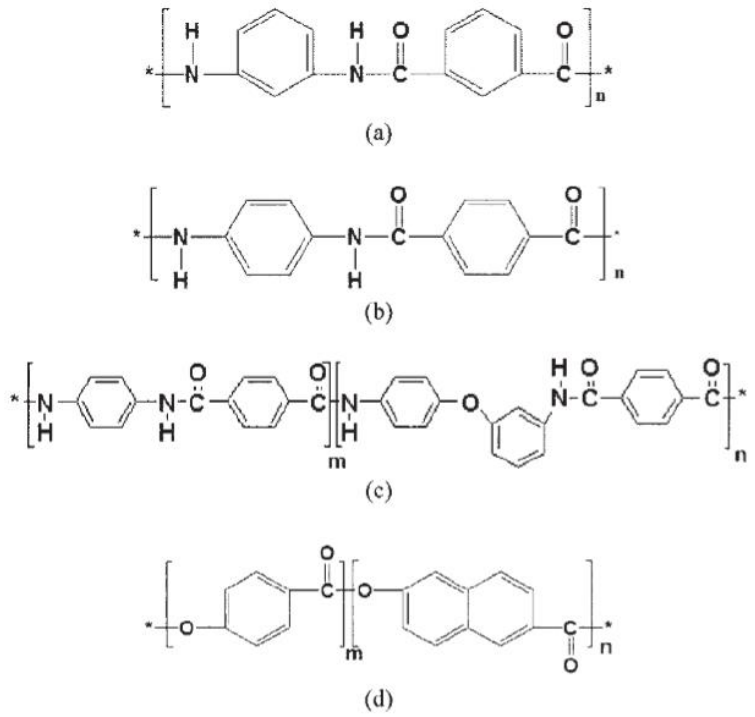

Fig 6.1: Repeating structures of commonly used high temperature resistant rigid rod polymers.[6] *a)* ***Nomex****, b)* ***Kevlar****, c)* ***Technora*** *and d) a copolyester fiber* ***Vectran:*** [6-9]

The halobenzamide and halocarboxamide chemistry adds to our knowledge of a relatively straightforward organic type compound with results that greatly benefits our on-going quest for information on amide...amide or amide...pyridine interactions. Alongside this benzamide research is the important work and recent developments in halogen bonding interactions and contacts and their influence on molecular aggregation.[10-12]

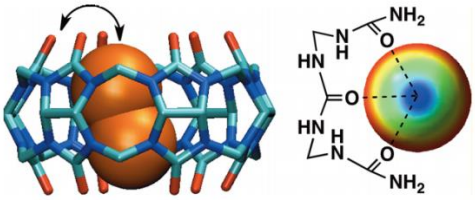

Fig 6.2: synthetic macrocycle cucurbit[6]uril forms host−guest inclusion complexes with molecular dibromine and diiodine.[12] *adapted:*

While the carbamate research was difficult given problems with solubility, separations and overall stability, the importance of organic carbamates in herbicide and insecticide research should not be underestimated.[13] Finally, an exciting area for future development and one that has evolved in the past two decades is that of foldamer chemistry which promises to bring about exciting breakthroughs in both materials sciences and biological sciences with applications as diverse as liquid crystals, drug delivery systems, and unnatural biosystems. [14-16] Fundamental questions can be asked as to how foldamers aggregate and their conformations and folding in comparison with research work conducted on natural biological systems. Our amide:imide foldamers (oligomers) are at the interface between simple organic molecules, oligomers and plastics such as polyamideimides. Nadrian Seeman and co-workers have spent a considerable amount of research effort in manipulating artificial DNA, forming complex nanoparticle template DNA bonds that can be used to construct proteins at the nanoscale.[17-19]

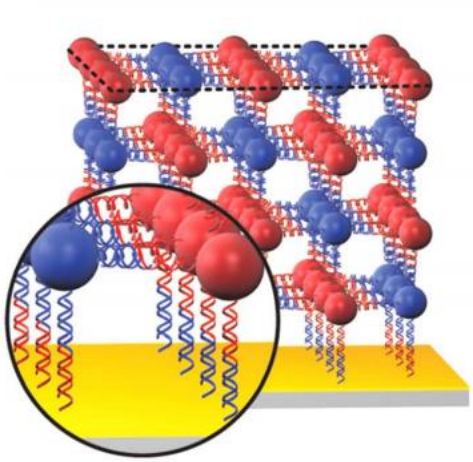

Fig 6.3: DNA superlattices grown from a substrate with a preferred orientation, allowing for texture nanoparticle films adapted from Seeman et. al.[17]

Research into the uses of foldamers to both imitate and construct vital biological building blocks is continuing and may have wide ranging implications in the treatment of a number of disease states, and aid in developing useful self-assembled systems.[20-22]

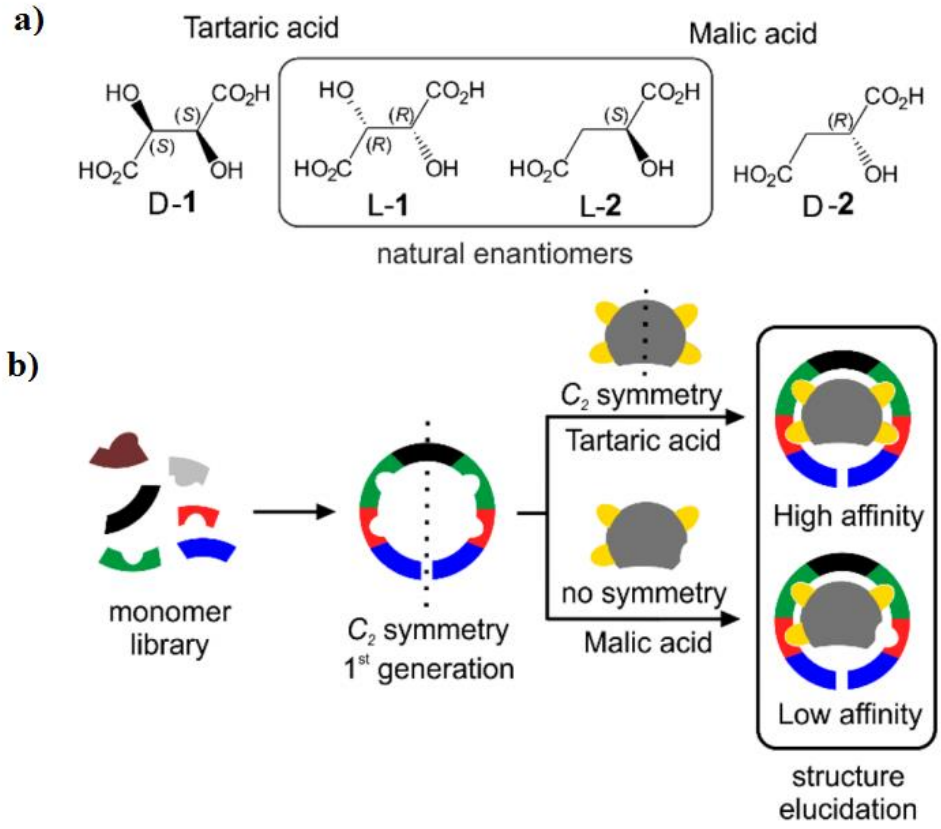

Fig 6.4: a) *Stereochemical configurations of D/L tartaric acid and malic acid, along with b) Schematic of the preparation of 1st generation of symmetrical foldamer receptor for selective recognition of tartaric acid.*[21]

References

1. Horio T, Hamasaki T, Inoue T, Wakayama T, Itou S, Naito H, Asaki T, Hayase H, Niwa T. Structural factors contributing to the Abl/Lyn dual inhibitory activity of 3-substituted benzamide derivatives. Bioorg Med Chem Lett 2007;17(10):2712-7.

2. Moradei OM, Mallais TC, Frechette S, Paquin I, Tessier PE, Leit SM, Fournel M, Bonfils C, Trachy-Bourget M, Liu J. Novel aminophenyl benzamide-type histone deacetylase inhibitors with enhanced potency and selectivity. J Med Chem 2007;50(23):5543-6.

3. Narayana B, Raj KV, Ashalatha B, Kumari NS, Sarojini B. Synthesis of some new 5-(2-substituted-1, 3-thiazol-5-yl)-2-hydroxy benzamides and their 2-alkoxy derivatives as possible antifungal agents. Eur J Med Chem 2004;39(10):867-72.

4. Saleem M, Saeed A, Atia-tul-Wahab, Khan A, Abbasi S, Khan W, Khan SB, Choudhary MI. Benzamide sulfonamide derivatives: Potent inhibitors of carbonic anhydrase-II. Medicinal Chemistry Research 2016 MAR;25(3):438-48.

5. Li L, Allard L, Bigelow W. On the morphology of aromatic polyamide fibers (kevlar, kevlar-49, and PRD-49). Journal of Macromolecular Science, Part B: Physics 1983;22(2):269-90.

6. Chae H, Kumar S. Rigid-rod polymeric fibers. J Appl Polym Sci 2006 APR 5;100(1):791-802.

7. Foo CC, Chai GB, Seah LK. Mechanical properties of nomex material and nomex honeycomb structure. Composite Structures 2007;80(4):588-94.

8. Dobb M, Johnson D, Saville B. Supramolecular structure of a high-modulus polyaromatic fiber (kevlar 49). Journal of Polymer Science: Polymer Physics Edition 1977;15(12):2201-11.

9. Cageao R, Schneider A, Biswas A, Blackwell J. Chain conformation of the technora copolyamide. Macromolecules 1990 MAY 28;23(11):2843-8.

10. Metrangolo P, Neukirch H, Pilati T, Resnati G. Halogen bonding based recognition processes: A world parallel to hydrogen bonding. Acc Chem Res 2005;38(5):386-95.

11. Metrangolo P, Resnati G, Pilati T, Liantonio R, Meyer F. Engineering functional materials by halogen bonding. Journal of Polymer Science Part A: Polymer Chemistry 2007;45(1):1-15.

12. El-Sheshtawy HS, Bassil BS, Assaf KI, Kortz U, Nau WM. Halogen bonding inside a molecular container. J Am Chem Soc 2012;134(48):19935-41.

13. Smith JA, Witkowski PJ, Fusillo TV. Manmade organic compounds in the surface waters of the united states: A review of current understanding. 1990.

14. Marcos M, Martín-Rapún R, Omenat A, Serrano JL. Highly congested liquid crystal structures: Dendrimers, dendrons, dendronized and hyperbranched polymers. Chem Soc Rev 2007;36(12):1889-901.

15. Bautista AD, Craig CJ, Harker EA, Schepartz A. Sophistication of foldamer form and function in vitro and in vivo. Curr Opin Chem Biol 2007;11(6):685-92.

16. Checco JW, Lee EF, Evangelista M, Sleebs NJ, Rogers K, Pettikiriarachchi A, Kershaw NJ, Eddinger GA, Belair DG, Wilson JL. α/β-Peptide foldamers targeting intracellular Protein–Protein interactions with activity in living cells. J Am Chem Soc 2015;137(35):11365-75.

17. Jones MR, Seeman NC, Mirkin CA. Nanomaterials. programmable materials and the nature of the DNA bond. Science 2015 Feb 20;347(6224):1260901.

18. Seeman NC. An overview of structural DNA nanotechnology. Mol Biotechnol 2007 NOV;37(3):246-57.

19. Aldaye FA, Palmer AL, Sleiman HF. Assembling materials with DNA as the guide. Science 2008 SEP 26;321(5897):1795-9.

20. Fisher BF, Guo L, Dolinar BS, Guzei IA, Gellman SH. Heterogeneous H-bonding in a foldamer helix. J Am Chem Soc 2015 MAY 27;137(20):6484-7.

21. Lautrette G, Wicher B, Kauffmann B, Ferrand Y, Huc I. Iterative evolution of an abiotic foldamer sequence for the recognition of guest molecules with atomic precision. J Am Chem Soc 2016 AUG 17;138(32):10314-22.

22. Brioche J, Pike SJ, Tshepelevitsh S, Leito I, Morris GA, Webb SJ, Clayden J. Conformational switching of a foldamer in a multicomponent system by pH-filtered selection between competing noncovalent interactions. J Am Chem Soc 2015 MAY 27;137(20):6680-91.